

AD-A012 810

EVALUATION OF HOLOGRAM OPTICAL ELEMENTS

John N. Latta, et al

Environmental Research Institute of Michigan

Prepared for:

Aeronautical Systems Division
Defense Advanced Research Projects Agency

June 1975

DISTRIBUTED BY:

NTIS

National Technical Information Service
U. S. DEPARTMENT OF COMMERCE

dc
194500-8-F
ADA012810

217089

Final Technical Report

EVALUATION OF HOLOGRAM OPTICAL ELEMENTS

20 October 1972 — 30 September 1973

J.N. LATTA and R.C. FAIRCHILD
Radar and Optics Division

JUNE 1975

D D C
RECORDED
JUL 31 1975
REGISTERED
B

Prepared for:

Defense Advanced Research Projects Agency
1400 Wilson Boulevard
Arlington, Virginia 22209
ARPA Order No. 1957

and

Aeronautical Systems Division
(Directorate of Reconnaissance Engineering)
Air Force Systems Command
Wright-Patterson Air Force Base
Ohio 45433

Reproduced by
NATIONAL TECHNICAL
INFORMATION SERVICE
US Department of Commerce
Springfield, VA. 22151

ENVIRONMENTAL
RESEARCH INSTITUTE OF MICHIGAN
FORMERLY WILLOW RUN LABORATORIES, THE UNIVERSITY OF MICHIGAN
BOX 618 • ANN ARBOR • MICHIGAN 48107

DISTRIBUTION STATEMENT A

Approved for public release
Distribution Unlimited

NOTICES

Sponsorship. The work reported herein was conducted by the Environment Research Institute of Michigan (formerly the Willow Run Laboratories of The University of Michigan) for the Advanced Research Projects Agency of the Department of Defense and was monitored by the Air Force Avionics Laboratory under Contract No. F33615-73-C-2039, ARPA Order No. 1957. Contracts and grants to the Institute for the support of sponsored research are administered through the Office of Contracts Administration.

Disclaimer. The views and conclusions contained in this document are those of the authors and should not be interpreted as necessarily representing the official policies, either expressed or implied, of the Advanced Research Projects Agency or the U.S. Government.

Distribution. Initial distribution is indicated at the end of this document.

DDC Availability. Qualified requesters may obtain copies of this document from:

Defense Documentation Center
Cameron Station
Alexandria, VA 22314

Final Disposition. After this document has served its purpose, it may be destroyed. Please do not return it to the Environmental Research Institute of Michigan.

ACCESSION for	
NTIS	White Section <input checked="" type="checkbox"/>
DDC	Buff Section <input type="checkbox"/>
UNANNOUNCED	<input type="checkbox"/>
JUSTIFICATION	
BY	
DISTRIBUTION/AVAILABILITY CODES	
DELT.	AVAIL. 200/01 SP. CIAL
A	

per letter Gmfels

Unclassified

SECURITY CLASSIFICATION OF THIS PAGE (When Data Entered)

REPORT DOCUMENTATION PAGE		READ INSTRUCTIONS BEFORE COMPLETING FORM
1 REPORT NUMBER <i>F13M</i> 194500-8-F	2 GOVT ACCESSION NO.	3 RECIPIENT'S CATALOG NUMBER <i>AD-A012 810</i>
4 TITLE (and Subtitle) Evaluation of Hologram Optical Elements		5 TYPE OF REPORT & PERIOD COVERED Final Technical Report 20 Oct. '72-30 Sept. '73
		6 PERFORMING ORG REPORT NUMBER 194500-8-F
7 AUTHOR(s) John N. Latta and Ronald C. Fairchild Radar and Optics Division (313) 483-0500, Ext. 286		8 CONTRACT OR GRANT NUMBER (s) F33613-73-C-2039 ARPA Order No. 1957
9 PERFORMING ORGANIZATION NAME AND ADDRESS Environmental Research Institute of Michigan P. O. Box 618, Ann Arbor, Michigan 48107		10 PROGRAM ELEMENT, PROJECT, TASK AREA & WORK UNIT NUMBERS Program Code No. 3M10
11 CONTROLLING OFFICE NAME AND ADDRESS Defense Advanced Research Projects Agency 1400 Wilson Boulevard Arlington, Va. 22209		12 REPORT DATE June 1975
14 MONITORING AGENCY NAME AND ADDRESS (if different from Controlling Office) Aeronautical Systems Division (Directorate of Reconnaissance Engineering) Air Force Systems Command, Wright-Patterson AFB, Ohio 45433		13 NUMBER OF PAGES <i>175</i>
		15 SECURITY CLASS (of this report) Unclassified
16 DISTRIBUTION STATEMENT (of this Report) See distribution list at the end of this document		15a DECLASSIFICATION/DOWNGRADING SCHEDULE
<p>DISTRIBUTION STATEMENT A</p> <p>Approved for public release Distribution Unlimited</p>		
17 DISTRIBUTION STATEMENT (of the abstract entered in Block 20, if different from Report)		
18 SUPPLEMENTARY NOTES Principal Investigator: John N. Latta		
19 KEY WORDS (Continue on reverse side if necessary and identify by block number) Holography Computer Design Optics Hologram Optical Elements Telescope Infrared Optics		
<p style="text-align: right;">PRICES SUBJECT TO CHANGE</p> <p>20 ABSTRACT (Continue on reverse side if necessary and identify by block number) This report is the third in a series that cover the investigation of the properties and applications of holographic optics. This type of optics is relatively new in that the techniques of holography are being applied to the fabrication of optical elements. These elements can be combined into lens systems and several are considered in this report. A major focus of this effort was on large aperture (10") holographic optics, the application of wavelength shift techniques to the holographic telescope, and infrared optics. One of the more promising results of the</p>		

DD FORM 1473 EDITION OF 1 NOV 65 IS OBSOLETE
1 JAN 73

Unclassified
SECURITY CLASSIFICATION OF THIS PAGE (When Data Entered)

Unclassified

SECURITY CLASSIFICATION OF THIS PAGE (When Data Entered)

study were designs that utilize holographic optics in the infrared. A two element telescope was designed using wavelength shift techniques where the elements were made in the visible spectrum and reconstructed at 10.6 μ . Further a single element was thoroughly tested which was designed for operation at 1.15 μ . The agreement with theory was quite close. High quality holographic telescopes were fabricated based on the design techniques developed during this and the earlier studies. An advantage of holographic optics is the relatively simple fabrication process; this becomes important in larger aperture optics. Both transmission and reflection elements were fabricated during this contract. In the reflection case a subcontract was let to Radiation, Inc. for the fabrication and an assessment of its producibility. Their report is an appendix to this report.

Several other areas were also addressed: wide angle reflection holographic optics and the development of facilities for producing high quality elements. The wide angle problem was found to be a very difficult one because of severe mechanical constraints. As a part of our overall effort the techniques for producing high quality elements were developed. Much of this was found to be dependent upon the precision and flexibility of equipment available.

Holographic optics have some very attractive features and attributes. These are illustrated in the promising applications in the infrared. Further, the producibility of large aperture elements illustrates another advantage of holographic optics.

Unclassified

SECURITY CLASSIFICATION OF THIS PAGE (When Data Entered)

FOREWORD

This report was prepared by the Radar and Optics Division of the Environmental Research Institute of Michigan. The work was sponsored by the Defense Advanced Research Projects Agency under ARPA Order 1957 and the Aeronautical Systems Division (Directorate of Reconnaissance Engineering), Air Force Systems Command, under Contract F33615-73-C-2039, which began on October 20, 1972.

This final report covers work performed between 20 October 1972 and 30 September 1973. The contract monitor is Dennis A. Ingebretsen, ASD/ENRSC, Wright-Patterson Air Force Base, Ohio, 45433. The principal investigator is John N. Latta.

This work was only possible with the support and efforts of Kenneth Perko at ASD/ENRSC and Col. W. Kirlin of the Defense Advanced Research Projects Agency.

SUMMARY

This report is the third in a series that cover the investigation of the properties and applications of holographic optics. This type of optics is relatively new in that the techniques of holography are being applied to the fabrication of optical elements. These elements can be combined into lens systems and several are considered in this report.

A major focus of this effort was on large aperture (10") holographic optics, the application of wavelength shift techniques to the holographic telescope, and infrared optics. One of the more promising results of the study were designs that utilize holographic optics in the infrared. A two element telescope was designed using wavelength shift techniques where the elements were made in the visible spectrum and reconstructed at 10.6μ . Further a single element was thoroughly tested which was designed for operation at 1.15μ . The agreement with theory was quite close. High quality holographic telescopes were fabricated based on the design techniques developed during this and the earlier studies. An advantage of holographic optics is the relatively simple fabrication process; this becomes important in larger aperture optics. Both transmission and reflection elements were fabricated during this contract. In the reflection case a subcontract was let to Radiation, Inc. for the fabrication and an assessment of its producibility. Their report is an appendix to this report.

Several other areas were also addressed: wide angle reflection holographic optics and the development of facilities

for producing high quality elements. The wide angle problem was found to be a very difficult one because of severe mechanical constraints. As a part of our overall effort the techniques for producing high quality elements were developed. Much of this was found to be dependent upon the precision and flexibility of equipment available.

Holographic optics have some very attractive features and attributes. These are illustrated in the promising applications in the infrared. Further, the producibility of large aperture elements illustrates another advantage of holographic optics.

TABLE OF CONTENTS

Foreword	3
Summary	5
List of Illustrations.	10
List of Tables	14
1. Introduction	15
2. Two Element Wavelength Shift Hologram Telescope. .	19
2.1. Telescope Design #1.	19
2.1.1. Design	19
2.1.2. Implementation	29
2.2. Telescope Design #2.	41
2.2.1. Design	41
2.2.2. Implementation and Testing	47
2.3. Telescope Design #3.	54
2.3.1. Design	56
2.4. Conclusions.	60
3. Three Element Wavelength Shift Hologram Telescopes	61
3.1. Telescope Design #1.	62
3.1.1. Design	62
3.1.2. Implementation and Testing	66
3.2. Telescope Design #2.	68
3.2.1. Design	68
3.3. Conclusions.	70

4.	Infrared Hologram Optical Elements	74
4.1.	Single Element Lens - 1.15 microns	74
4.1.1.	Design	75
4.1.2.	Implementation and Testing	75
4.2.	Two Element Telescope - 10.6 microns	81
4.2.1.	Design	81
4.3.	Conclusions	82
5.	Wide Angle Imaging Lens Design	86
5.1.	Design and Implementation.	86
6.	Large Aperture Hologram Optical Elements	97
6.1.	Design	97
6.2.	Fabrication.	97
7.	Single Hologram Element Properties	101
7.1.	Selection of Study Parameters.	101
7.2.	Case 1: $Q = 1, \nu = 1$	105
7.3.	Case 2: $Q = 1, \nu = 1.23$	108
7.4.	Case 3: $Q = 2, \nu = 1$	111
7.5.	Case 4: $Q = 2, \nu = 1.23$	115
7.6.	Large Wavelength Shifts.	115
8.	Description of Facilities.	121
9.	Summary and Conclusions.	131
Appendix A.	Final Report, "Large Aperture Holographic Optical Elements," Subcontractor, Radia- tion, Inc.	135

Appendix B. Publication, "New Developments in the
Design of Holographic Optics," by John
N. Latta and Ronald C. Fairchild. 154

References 177

Distribution List. 178

LIST OF ILLUSTRATIONS

1.	Construction Geometries for First Telescope Design (#1) a) Objective Element and b) Eyepiece Element . . .	21
2.	Reconstruction Geometry for First Telescope Design (#1).	24
3.	Exit Wavefront Total Aberrations as a Function of Input Field Angle for Telescope #1	26
4.	Point Focus Test Geometry for Individual Hologram Elements	30
5.	Point Focus of Objective Element at a) 5145A and b) 6328A for Telescope #1.	31
6.	Point Focus of Eyepiece Element at a) 5145A and b) 6328A for Telescope #1.	32
7.	Point Focus Test Geometry for Assembled Telescope #1	34
8.	Point Focus of Telescope #1 at a) 5145A and b) 6328A	35
9.	Interferogram Test Geometry for Assembled Telescope #1	36
10.	Interferogram of Wavefront Aberrations for Telescope #1 at a) 5145A and b) 6328A.	37
11.	Resolution Target Test Geometry for Assembled Telescope.	39
12.	Resolution Target at a) 5145A and b) 6328A for Telescope #1	40
13.	Construction Geometries for Second Telescope (#2) Design a) Objective Element and b) Eyepiece Element. . .	43
14.	Reconstruction Geometry for Second Telescope Design.	44
15.	Exit Wavefront Total Aberrations as a Function of Input Field Angle for Telescope #2	46
16.	Point Focus of Objective Element at a) 5145A and b) 6328A for Telescope #2.	48

17.	Point Focus of Eyepiece Element at a) 5145A ^o and b) 6328A for Telescope #2.	49
18.	Diffraction Limited Point Focus at 6328A ^o for a) Objective Element and b) Eyepiece Element for Telescope #2	51
19.	Point Focus of Assembled Telescope at 6328A ^o for a) Four Inch Aperture and b) 2.8 Inch Aperture	52
20.	Resolution Target at a) 5145A ^o and b) 6328A ^o with Four Inch Aperture for Telescope #2.	53
21.	Resolution Target at a) 5145A ^o and b) 6328A ^o with 2.8 Inch Aperture for Telescope #2	55
22.	Construction Geometries for Telescope Design #3 a) Objective Element and b) Eyepiece Element	57
23.	Reconstruction Geometry for Telescope Design #3.	58
24.	Exit Wavefront Total Aberrations as a Function of Input Field Angle for Telescope #3	59
25.	Construction Geometries for Telescope Design #1 a) Objective Element, b) Field Element and c) Eyepiece Element	63
26.	Reconstruction Geometry for Telescope Design #1.	64
27.	Exit Wavefront Total Aberrations as a Function of Input Field Angle for Telescope #1	67
28.	Resolution Target at 6328A ^o for a) Field Element Located as Designed and b) Displaced 1 cm with Telescope Design #1.	69
29.	Construction Geometries for Telescope Design #2 a) Objective Element, b) Field Element and c) Eyepiece Element	71
30.	Reconstruction Geometry for Telescope Design #2.	72
31.	Exit Wavefront Total Aberrations as a Function of Input Field Angle for Telescope Design #2.	73

32.	Construction and Reconstruction Geometries of Infrared Holographic Lens at $\lambda_C = 1.15 \mu$	76
33.	Point Focus Test Geometry for Infrared Holographic Element at $\lambda_C = 1.15 \mu$	77
34.	Point Focus at 1.15μ of Infrared Holographic Element	79
35.	Computer Generated Point Plot a) at Hologram Surface and b) at Plane of Best Focus	80
36.	Construction Geometries for Infrared Telescope a) Eyepiece Element and b) Objective Element at $\lambda_C = 10.6 \mu$	83
37.	Reconstruction Geometry of Infrared Telescope at $\lambda_C = 10.6 \mu$	84
38.	Exit Wavefront Total Aberrations as a Function of Input Field Angle at $\lambda_C = 10.6 \mu$	85
39.	Construction Geometries for the Two Element Wide Angle Imaging Lens.	87
40.	Reconstruction Light Ray Paths for the Two Element Holographic Wide Angle Lens at a) $\alpha_C = 0^\circ$, b) $\alpha_C = 10^\circ$, and c) $\alpha_C = -15^\circ$	89
41.	Image Location Z_I For the Two Element Lens as a Function of a) α_C and b) β_C	92
42.	Wavefront Aberrations, $ \Delta_C $, for the Two Element Wide Angle Imaging Lens as a Function of a) α_C and b) β_C	94
43.	Construction Geometry for Large Aperture Holographic Element	98
44.	Photograph of Large Aperture Element.	100
45.	Representative Construction Geometries for $Q = 1$ and a) $\phi = -10^\circ$, b) $\phi = +10^\circ$, and c) $\phi = +30^\circ$	103
46.	Maximum Total Aberrations Across a $+5^\circ$ Field for $Q = 1$, and $\mu = 1$	107

47.	Total Aberrations for Case 2, $Q = 1$ and $\mu = 1.23$.	.109
48.	Optimum Case 2 a) Construction and b) Reconstruction Geometries Showing Increased Reconstruction Angle α_C .	.110
49.	Component Aberrations for Case 2.	.112
50.	Total Aberrations for Case 3, $Q = 2$ and $\mu = 1$.	.113
51.	Component Aberrations for Case 3.	.114
52.	Total Aberrations for Case 4, $Q = 2$ and $\mu = 1.23$.	.116
53.	Component Aberrations for Case 4.	.117
54.	Total Aberrations for Large Wavelength Shift.	.119
55.	Component Aberrations for Large Wavelength Shift.	.120
56.	Photograph of 8' x 16' Stable Table with Two Lasers and Associated Optical Components on the Table. All Parts of the Table Cover Have Been Raised.	.123
57.	Photograph of a Large Aperture Off-Axis Collimator Including Mount	.124
58.	Photograph of a Medium Aperture Off-Axis Collimator	.125
59.	Holographic Optics Alignment and positioning Equipment with Three Element Holders	.127
60.	A Single Holographic Element-Holder Table	.128
61.	A Single Holographic Element Holder Table with Positioning Rods and Micro Positioner	.129

LIST OF TABLES

1.	Two Element Telescope #1 Design Parameters	25
2.	Two Element Telescope #2 Design Parameters	45
3.	Two and Three Element Diameters for Two Element Design #2 and Three Element Design #1 as a Function of the Field-of-View.	65
4.	Wide Angle Imaging Lens Construction and Reconstruction Geometry Parameters	88
5.	List of the Important Cases to be Analyzed in the Single Hologram Element Properties Study. . .	106

1
INTRODUCTION

This report covers the second period of investigation into holographic optical elements which has been funded by ARPA at ERIM. The actual contract period for the work described here was from 20 October 1972 to 30 September 1973. The contract under which this was conducted was extended into a third phase which will be described in a separate report. The contract ended on 15 July 1974.

The three phases of ARPA support can best be put into perspective by outlining the thrust of the activities encompassed within the first two phases. In the first, which is discussed in a previous final report, there was little attempt to study specific application areas. The intent, rather, was to consider the overall potential of holographic optics and outline as many areas which did show potential for using these elements. Fundamentally, an important output of the study was a direction in which further work could be focused. The details of this study are contained in the previous final report. At the end of this study it was decided to focus the activities into large aperture elements and systems with as high a performance as can be achieved. A direct outgrowth of this approach was the requirement to improve the facilities for hologram

element construction. To achieve this a large stable table was purchased along with high quality large aperture off-axis collimators. Some special lens construction and fabrication equipment was designed and built to permit very accurate alignments. The facilities are described in Section 8 of this report. Another important question to be addressed by this study was the producibility of large aperture elements. To implement this ERIM let a contract to Radiation, Inc. for the fabrication of a large element that had reflective properties.

An important distinction which characterized this work was the requirement that wavelength shift compensation techniques be used as much as possible in all designs. This requirement had some very interesting and potentially significant results. To satisfy the wavelength shift needs we undertook both the telescope designs and a single hologram element property study. As a direct outgrowth of the latter some important insights were gained into the domain over which wavelength shift compensation may be applied. This is described in Section 7. Specific results are given in Section 4 where we undertook designs at both 1.15μ and 10.6μ . These systems were designed for use at the long wavelength,

however, they were to be constructed in the visible spectrum.

The report has nine sections. The second section is directed at wavelength shift two element telescopes and is a direct extension of work which was carried out under the earlier phase of the ARPA support. As an extension of the work to obtain high quality imaging with wavelength shift techniques, we describe two designs of three element telescopes in Section Three. Some of the most significant results from this study are contained in Section Four which applies the results of Sections Two, Three, and Seven to the problem of infrared optics using holographic elements. On the opposite end of the holographic optics spectrum a wide-angle reflective optics design is considered in Section Five. The results of the fabrication and testing of a glass substrate large aperture element are contained in Section Six. Underlying much of the wavelength shift results presented in Sections Two, Three, and Four is the study of hologram optics wavelength shift properties in Section Seven. The facilities which were used during this work are discussed in Section Eight. Two appendices are included. The first is a copy of the report submitted by Radiation Inc. which discusses

their work on fabricating a large aperture element with photoresists. The second appendix is a copy of a paper which outlines the design tools that we used during the course of this effort.

2
TWO ELEMENT TELESCOPES

It is only natural that in considering two element optical systems one should think of the basic telescope. Two simple lenses, one of a short focal length and another of a long focal length, when placed in a confocal arrangement, will produce an image at infinity with an angular magnification equal to the ratio of the long focal length to the short focal length. Inasmuch as holograms may be used as simple lenses, it is of interest to consider using them to form a simple telescope and to assess their relative advantages or disadvantages. Such an investigation was performed to a limited extent in a preceding ARPA Contract¹. It is the intent here to extend that investigation and, in particular, to consider the case in which the reconstruction wavelength may be quite different from the construction wavelength.

2.1 TELESCOPE #1 - DESIGN

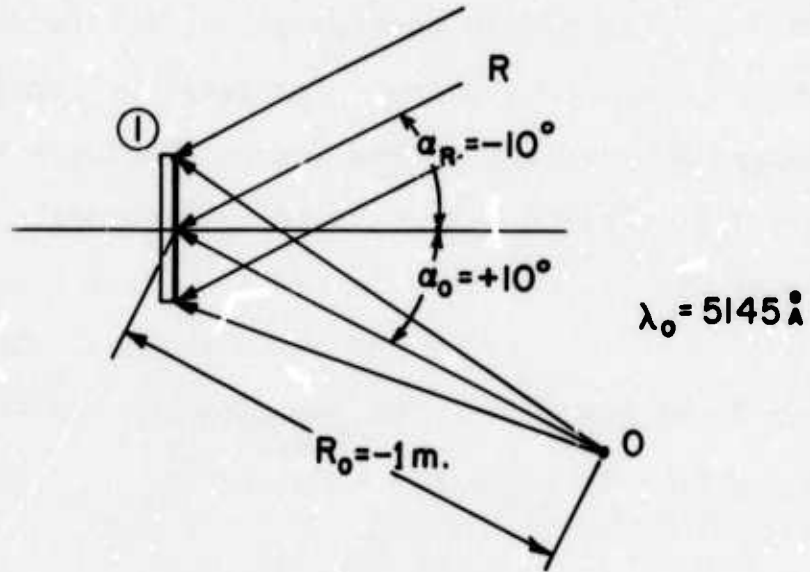
2.1.1. DESIGN

The first task undertaken was the design of a two element telescope with a construction wavelength of

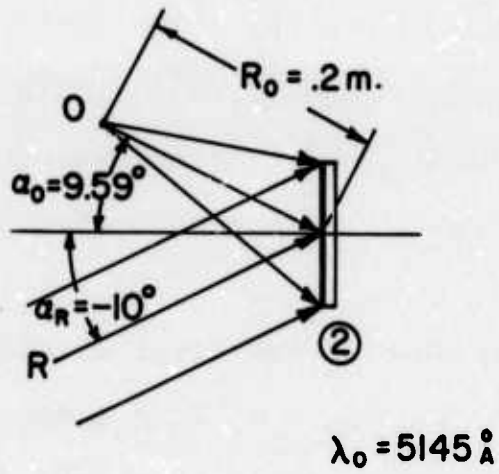
¹Latta, J. N., "Evaluation of Hologram Optical Elements," Final Report 197400-1-F, Willow Run Laboratories, The University of Michigan, August 1973.

5145⁰Å and a reconstruction wavelength of 6328⁰Å, such laser wavelengths being readily available. The hologram elements were specified to have four-inch diameter clear apertures and to be recorded on five-inch square micro-flat glass substrates. In addition, construction focal lengths of 1.0 meter and 0.2 meters were specified, resulting in an angular magnification of five.

At this point all the parameters necessary for construction of a system have been specified except for the offset angles of the construction and reconstruction beams. Drawing from past experience, it was decided to start by making the normal to the hologram surface bisect the angle formed by the object and reference beams during construction. Referring to Figure 1, this implies that $\alpha_0 = -\alpha_R$ for both hologram elements. Such a condition was found to have the least amount of aberrations in the previously studied case of a telescope with no wavelength shift. From a materials standpoint, such a condition also insures that distortions due to nonuniform emulsion shrinkage will be minimal, since the fringes will generally lie perpendicular to the surface of the emulsion. For convenience, α_0 and α_R were chosen to be ten degrees.



(a) Objective Element



(b) Eyepiece Element

FIGURE 1. CONSTRUCTION GEOMETRIES FOR FIRST TELESCOPE DESIGN (#1). $\lambda_0 = 5145 \text{ \AA}$.

It is now possible to specify an initial reconstruction geometry based on the above parameters. Recalling that a change in wavelength when reconstructing a hologram element produces a change in both image angle and focal length, it is necessary to use the first order imaging equations to correct for these changes. The changes in focal length for the two elements can be computed immediately using the equation

$$\frac{1}{R_I} = \frac{1}{R_C} + \mu \left(\frac{1}{R_O} - \frac{1}{R_R} \right)$$

where R_O and R_R are the object and reference beam focal lengths, respectively, R_I and R_C are the image and reconstruction beam focal lengths, respectively, and $\mu = \lambda_C / \lambda_O$ is the ratio of the reconstruction and construction wavelengths.

In the case of the first elements $\lambda_C = 6328\overset{\circ}{\text{A}}$, $\lambda_O = 5145\overset{\circ}{\text{A}}$, $R_R = R_C = \infty$, $R_O = 1$ meter and thus $R_I = .81305$ meters. Likewise, for the second element $R_I = .16261$ meters. From these results it can be seen that a radial separation of $.81305 + .16261 = .97566$ meters is needed to provide a confocal arrangement.

The change in angular location of the image beam with a change in wavelength presents more of a problem. At this point the first element alone was optimized to determine the best angle of the reconstruction beam. The best angle in this case is the angle for which the exit wavefront has a minimum of aberrations. Having chosen the reconstruction angle, the image angle and hence the angular separation of the two elements is determined by the equation

$$\sin \alpha_I = \sin \alpha_C + \mu (\sin \alpha_O - \sin \alpha_R).$$

Solving this equation with $\alpha_C = -14.9^\circ$, $\alpha_O = +10^\circ$ and $\alpha_R = -10^\circ$ we find that $\alpha_I = +9.7889^\circ$. A holographic telescope with wavelength shift can now be specified in detail. From here on it is just a matter of using the hologram ray tracing programs to optimize the various parameters for peak performance. A diagram of the completed telescope is given in Figure 2 along with the final parameter values given in Table 1.

Figure 3 is a graph of the predicted exit wavefront aberrations as a function of input field angle. The

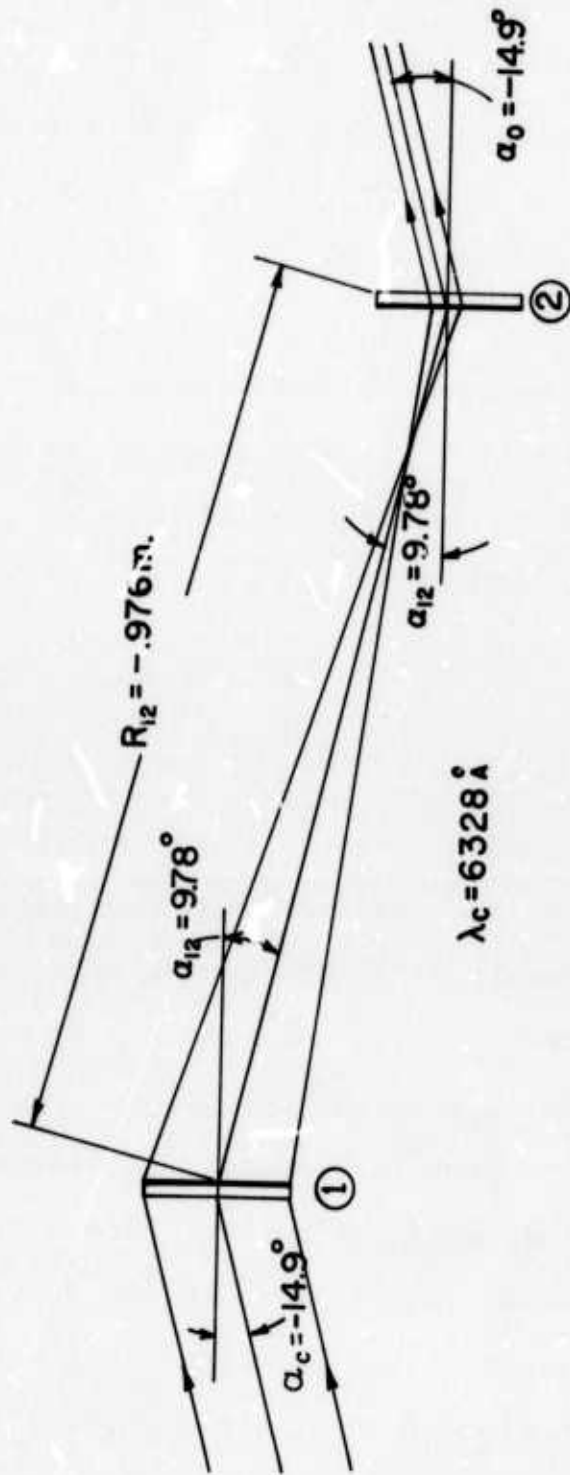


FIGURE 2. RECONSTRUCTION GEOMETRY FOR FIRST TELESCOPE DESIGN (#1). $\lambda_c = 6328 \text{ \AA}$.

TABLE 1. TWO ELEMENT TELESCOPE
#1 DESIGN PARAMETERS

HOLOGRAM 1

$$\alpha_O = 10^\circ, R_O = -1 \text{ m.}$$

$$\alpha_R = -10^\circ, R_R = \infty$$

HOLOGRAM 2

$$\alpha_O = 9.59^\circ, R_O = .2\text{m}$$

$$\alpha_R = -10^\circ, R_R = \infty$$

$$\alpha_{12} = 9.78^\circ, R_{12} = -.9762 \text{ m}$$

$$\alpha_C = -14.9^\circ, R_C = \infty$$

$$\alpha_I = -14.9^\circ, R_I = \infty$$

$$\lambda_O = 5145\overset{\circ}{\text{A}}, \quad \lambda_C = 6328\overset{\circ}{\text{A}}$$

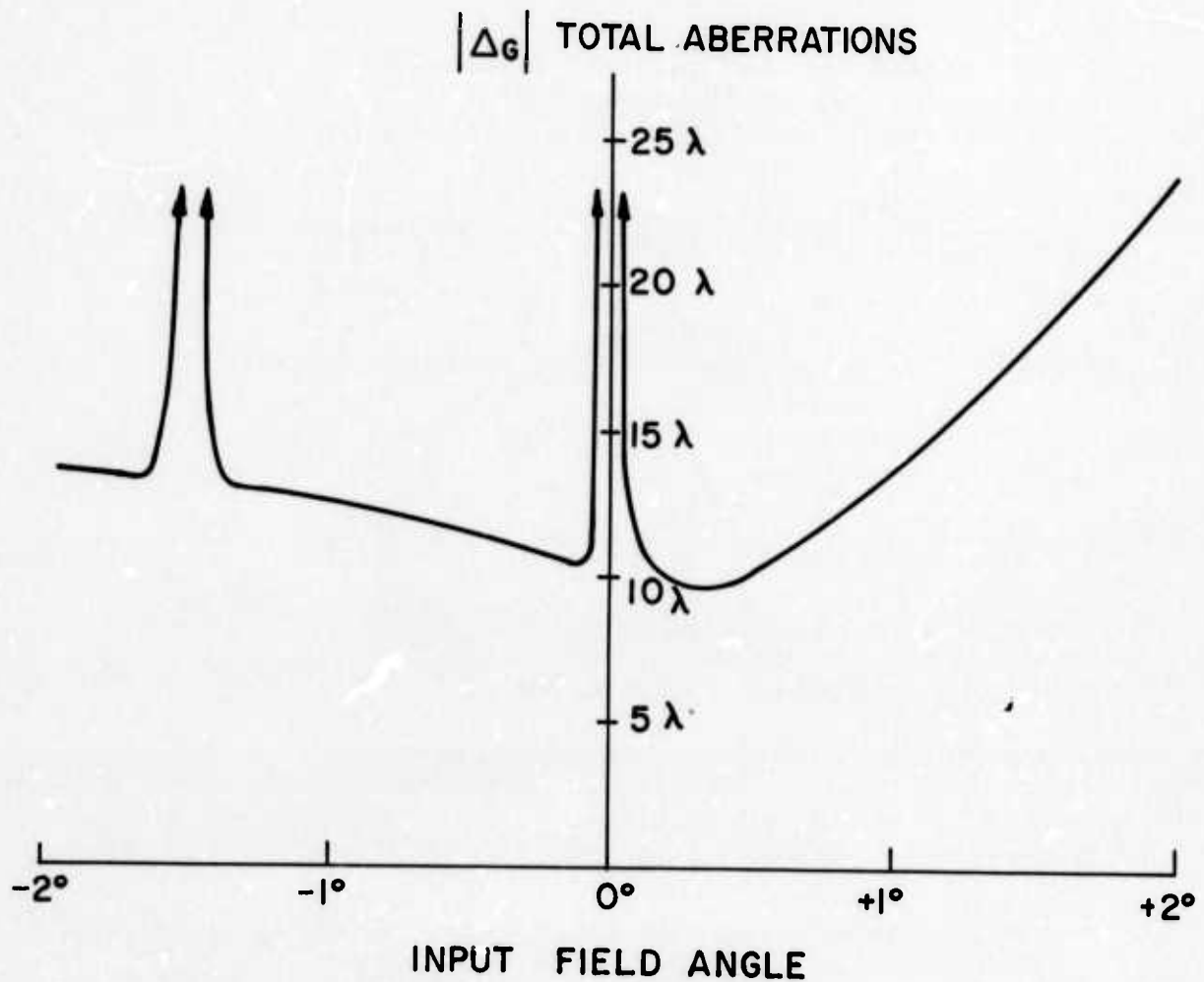


FIGURE 3. EXIT WAVEFRONT TOTAL ABERRATIONS AS A FUNCTION OF INPUT FIELD ANGLE FOR TELESCOPE #1

input field angle has been normalized such that an input field angle of zero corresponds to a reconstruction angle of -14.9° on the first element of the telescope. It is apparent upon inspection that the aberrations are not symmetrical, being relatively flat for negative field angles and increasing rapidly for positive field angles. In addition, two significant anomalies occur at zero and -1.5° field angles; the exact source of these anomalies is unclear. Considering that holographic optical systems rely heavily on the aberrations of one hologram offsetting or compensating for the aberrations in another hologram, these anomalies may be cases in which the aberrations are instead compounded. Certainly such anomalies are undesirable, and, as we shall see in later designs, they can be eliminated.

An important parameter in evaluating a telescope design is the field-of-view. This is a fairly straightforward calculation if we assume the projected input aperture on the second hologram to be of constant size. From geometry it can be seen that in the on-axis case the projected aperture is $1/5$ the input aperture, or .8 inches for telescope #1 (see Figure 2). Taking

the limiting case to be when the projected aperture is at the edge of the second hologram aperture, it can be calculated that the angle of the exit beam of the first hologram must be within the range 7.418° to 12.117° . In other words

$$7.418^\circ \leq \alpha_I \leq 12.117^\circ$$

for the first hologram element. Using this range in the previous grating equation we find that the input field angle has the range

$$-12.547^\circ \leq \alpha_C \leq -17.340^\circ$$

or that the field-of-view is approximately $\pm 2.4^\circ$. Depending upon the application this may or may not be an adequate field-of-view. Certainly if a larger field-of-view were desired, the second element could be made larger, however, not without a corresponding increase in aberrations around the periphery of the image. Of more interest is the technique of employing a field lens element between the two elements for increased field-of-view. Such a technique has been studied and will be discussed in detail in Section Three.

2.1.2 TELESCOPE #1 - IMPLEMENTATION & TESTING

The two hologram elements shown in Figure 1 were constructed on five-inch square microflat plates with a thickness one quarter inch. The construction wavelength was $5145\overset{\circ}{\text{A}}$ from an argon laser and the reconstruction wavelength was either $5145\overset{\circ}{\text{A}}$ or $6238\overset{\circ}{\text{A}}$, the latter provided by a helium-neon laser. Each hologram was then individually tested at each wavelength. Figure 4 shows the geometry used for testing the elements. Basically it consisted of a four-inch diameter collimated beam illuminating the hologram at angle α_C and a microscope-camera assembly positioned to record the point focus of the hologram element. Figures 5a and 5b show point focus photographs of the first hologram element at each wavelength. The angle α_C of the test geometry was 10° for the $5145\overset{\circ}{\text{A}}$ case and 14.9° for the $6328\overset{\circ}{\text{A}}$ case. As predicted and expected, the performance at $6328\overset{\circ}{\text{A}}$ is significantly degraded. Test photographs for the second element are shown in Figures 6a and 6b. Although these point foci are worse because of the higher f-number of the second element when operated at full aperture, note that this element is only used at 1/5 the full aperture for any given field angle.

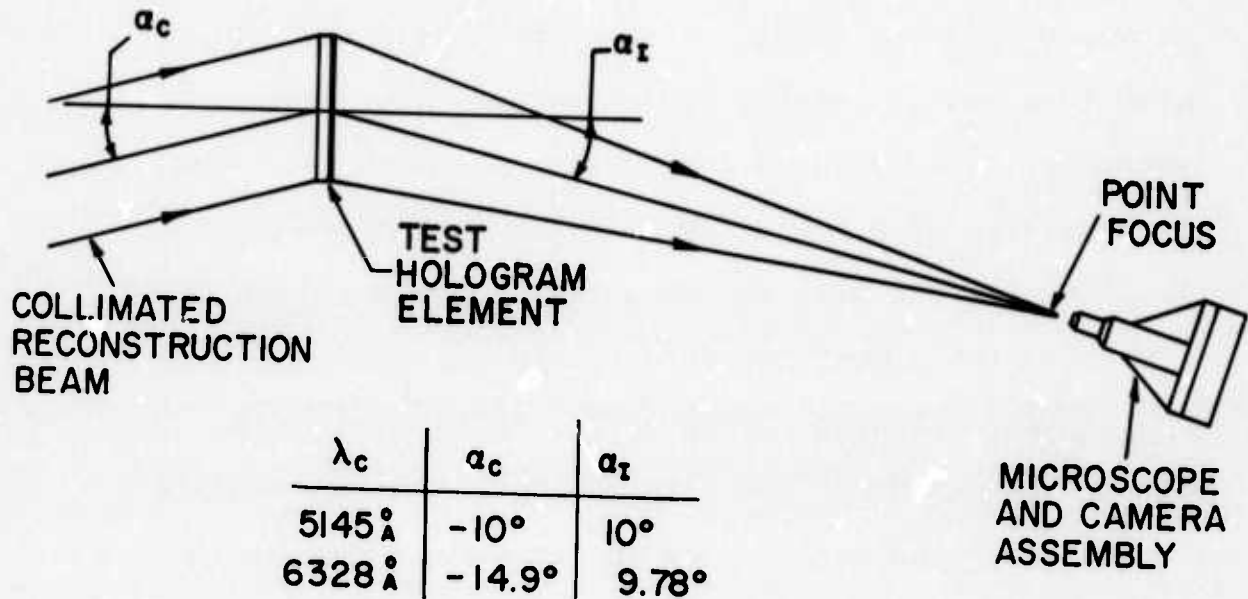
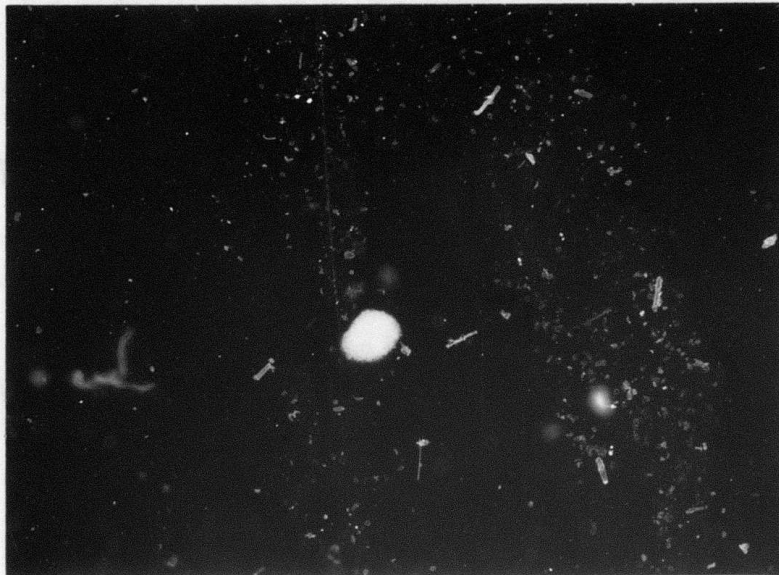
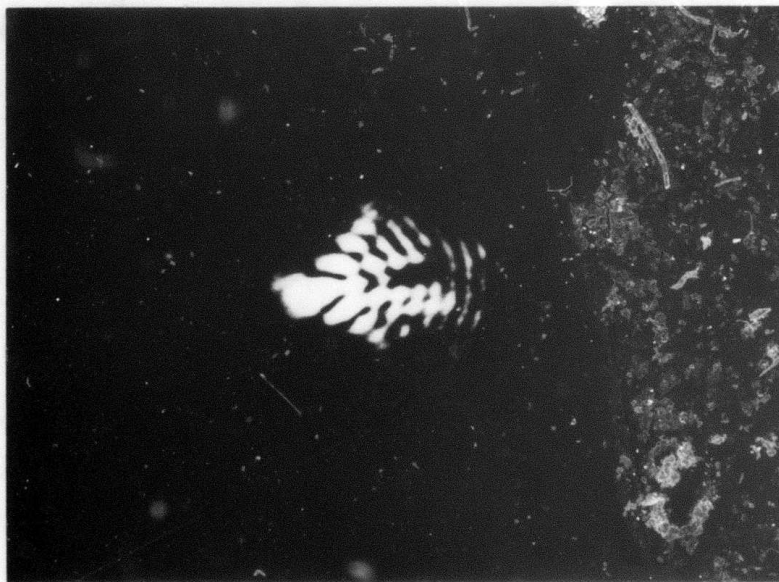


FIGURE 4. POINT FOCUS TEST GEOMETRY FOR INDIVIDUAL HOLOGRAM ELEMENTS



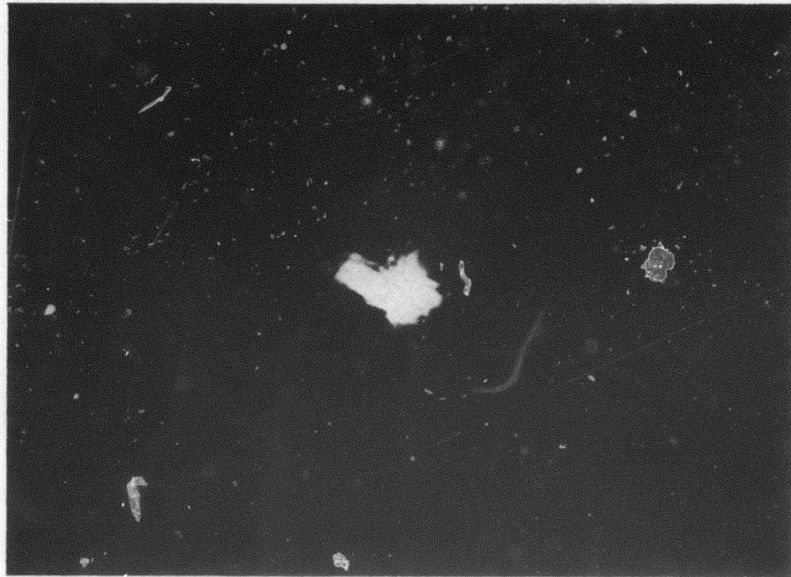
Reproduced from
best available copy.

(a) 5145 Å

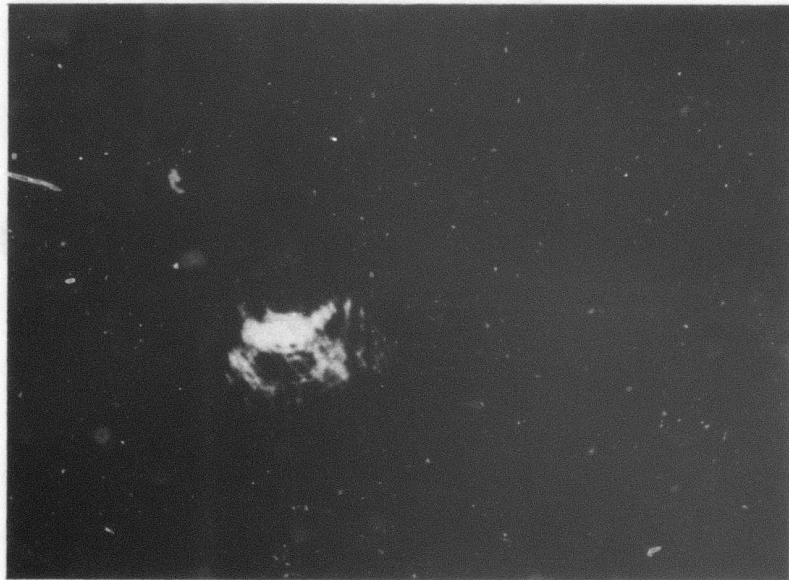


(b) 6328 Å

FIGURE 5. POINT FOCUS OF OBJECTIVE ELEMENT FOR TELESCOPE #1



(a) 5145 Å



(b) 6328 Å

FIGURE 6. POINT FOCUS OF EYEPIECE ELEMENT FOR TELESCOPE #1

The assembled telescope was tested in several manners. First, a test geometry as shown in Figure 7 was implemented at both wavelengths. The telescope was illuminated by a collimated four-inch diameter beam at the appropriate angle α_C and the resulting collimated image beam was brought to focus by a high quality imaging lens. Photomicrographs of the point focus may be seen in Figure 8, and as anticipated, there is a significant degradation in the point focus as a result of wavelength shift.

A second test was made using the geometry shown in Figure 9. In this test a reference plane wave was extracted from the illumination source and subsequently interfered with the telescope exit beam. Such a condition will produce an interferogram or fringe plot indicating the relative phase differences of the two beams. It can be seen from the photographs in Figure 10 that at $5145\overset{\circ}{\text{A}}$ there is little phase change across the exit pupil, while at $6328\overset{\circ}{\text{A}}$ there are approximately 8 fringes, corresponding well with the predicted value of 10 wavelengths.

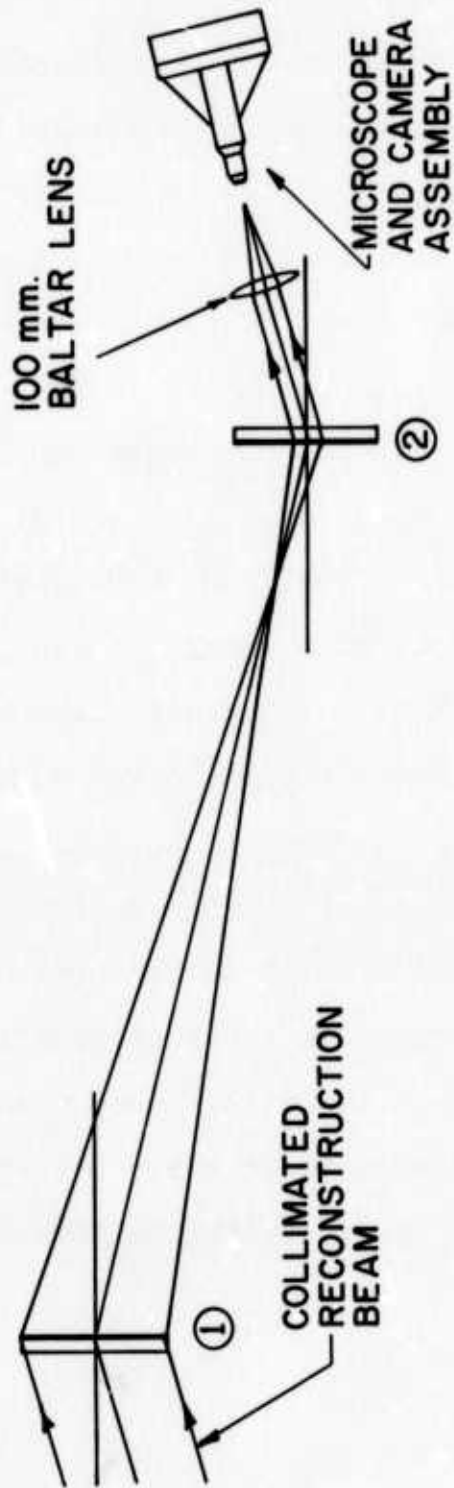
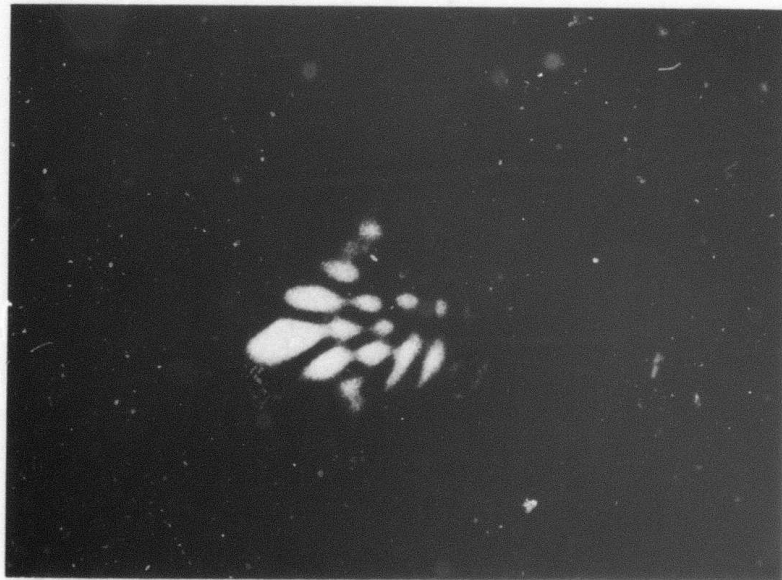


FIGURE 7. POINT FOCUS TEST GEOMETRY FOR ASSEMBLED TELESCOPE #1



(a) 5145 Å



(b) 6328 Å

FIGURE 8. POINT FOCUS OF TELESCOPE #1

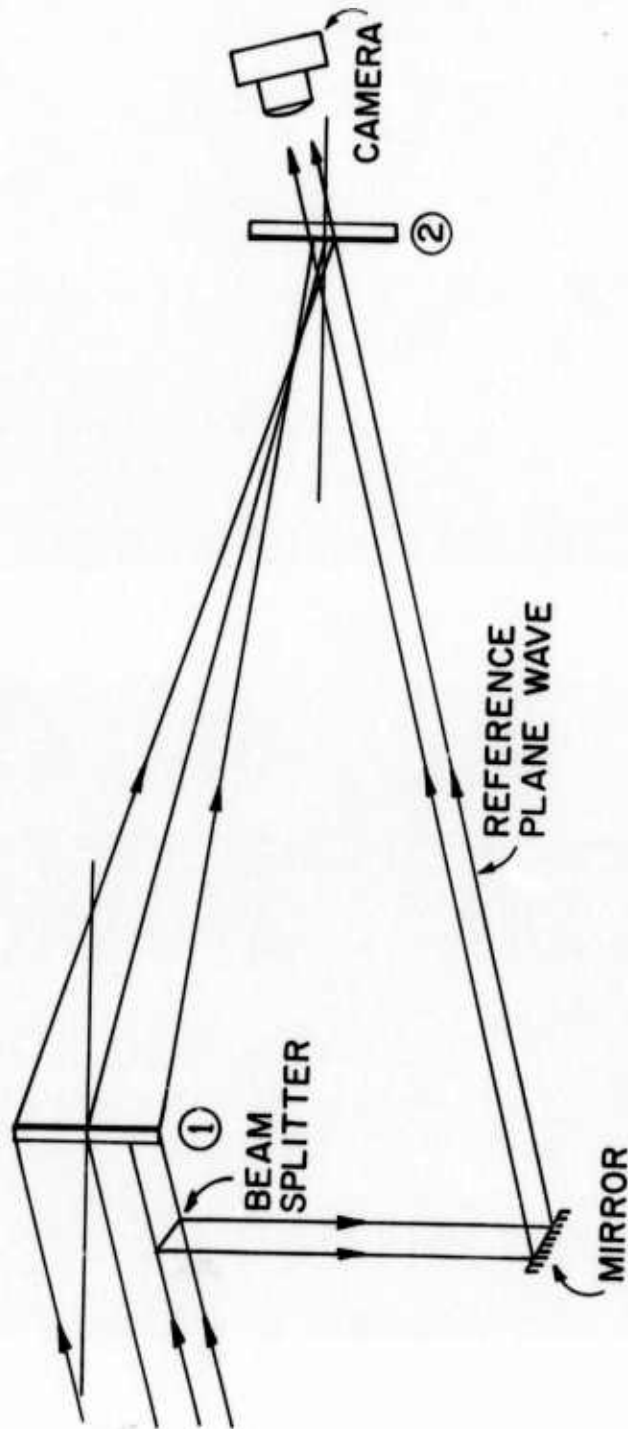
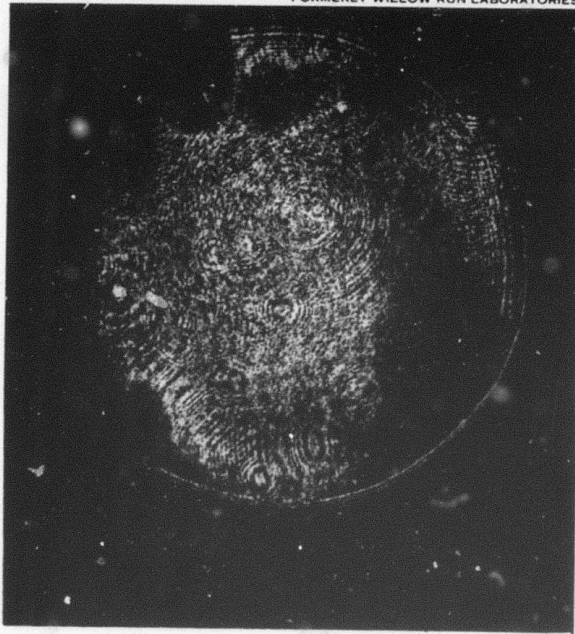
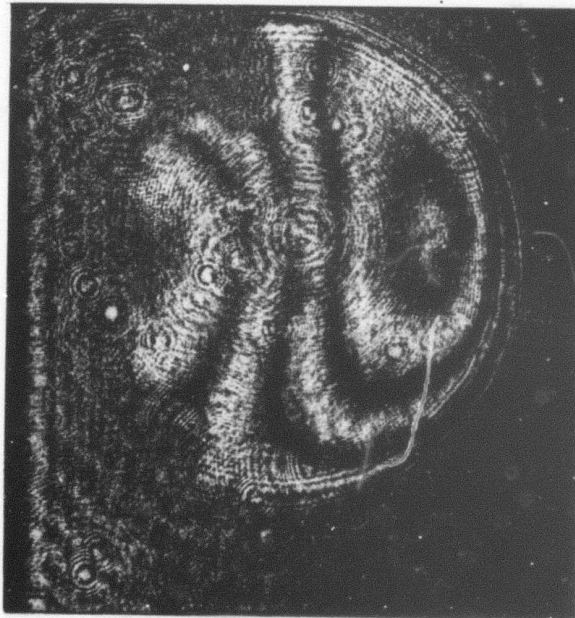


FIGURE 9. INTERFEROGRAM TEST GEOMETRY FOR ASSEMBLED TELESCOPE # 1



(a) 5145 Å



(b) 6328 Å

FIGURE 10. INTERFEROGRAM OF WAVEFRONT ABERRATIONS FOR TELESCOPE #1

A more important gauge of telescope performance is seen in the third test. Figure 11 depicts the test geometry used to determine the angular resolution of the hologram telescope. An Air Force resolution target is back illuminated by a diffuse source of monochromatic light, a high quality imaging lens is used to focus the target at infinity, and a camera is used at the exit pupil to photograph the telescope image. Photographs of the image with illumination wavelengths of 5145^oA and 6328^oA are shown in Figure 12. Detailed inspection of the original films indicates a resolution of 72 lines per millimeter at 5145^oA and 29 lines per millimeter at 6328^oA. These figures are a bit deceiving since the target is imaged at infinity. A better measure is angular resolution, which can be calculated knowing the focal length of the imaging lens; in this case a lens of focal length sixty inches was used, providing an angular resolution of 1.88 arc seconds at 5145^oA and 4.75 arc seconds at 6328^oA.

Similar calculations were performed with the resolution target off axis by $\pm 1^{\circ}$. With a reconstruction wavelength of 5145^oA, a resolution of 8.46 arc seconds was attainable at -1 degree and 11.87 arc seconds at +1 degree. This data agrees well with the predicted wave-

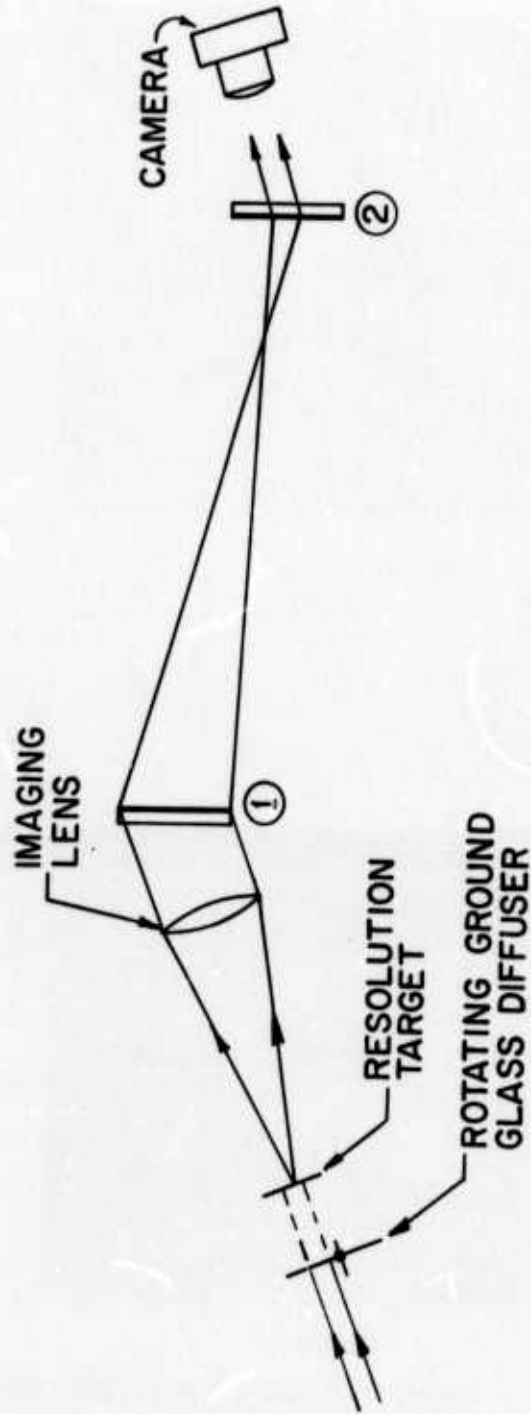
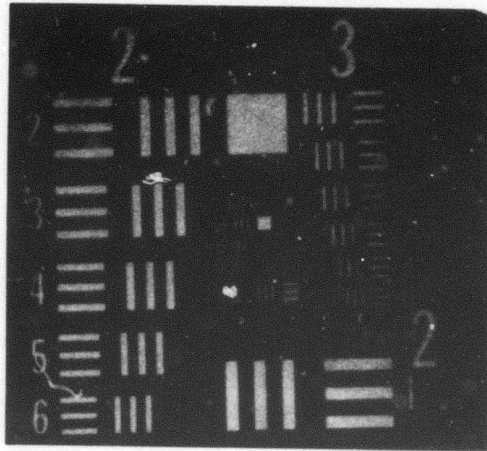
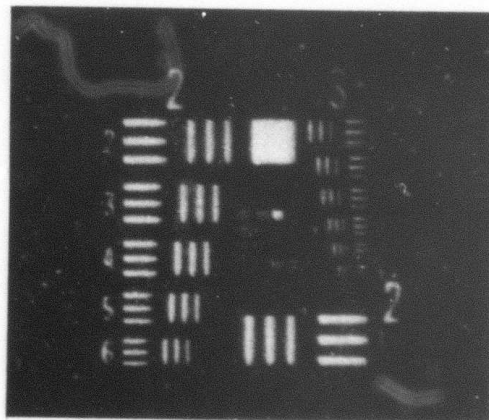


FIGURE 11. RESOLUTION TARGET TEST GEOMETRY FOR ASSEMBLED TELESCOPE



(a) 5145 Å



(b) 6328 Å

FIGURE 12. RESOLUTION TARGET FOR TELESCOPE #1

front aberrations as a function of input angle. In general, the first telescope design worked well and as calculated in the design.

This design was not considered optimum because of the limited field-of-view and the anomalies in the aberrations which were shown in Figure 3. To correct this latter problem a second design was undertaken.

2.2 TELESCOPE #2

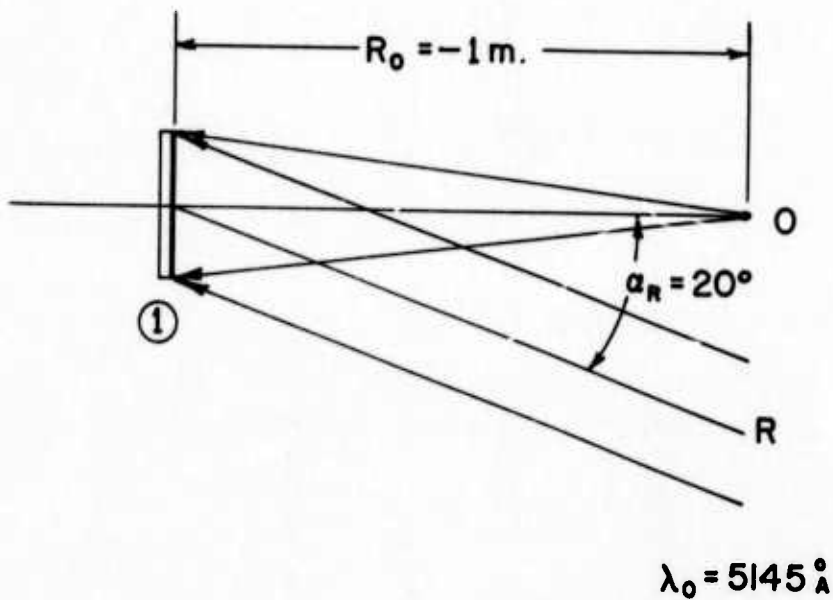
The previous design is best considered as the first approach to the evolutionary design process. One major limitation was image quality which is a direct result of the large and uncontrolled aberrations. The intent of this design is to refine the design and improve the performance substantially.

2.2.1 TELESCOPE # 2 - DESIGN

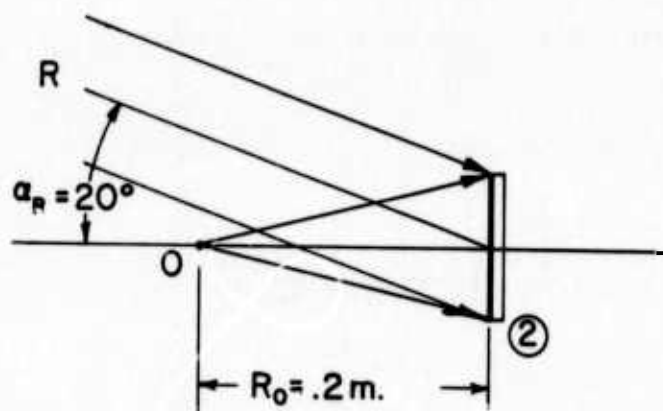
Design of the second telescope proceeded in essentially the same manner as the first telescope. It was possible, however, to take advantage of the results of a concurrent study of single hologram elements with wavelength shift (see Section 7). The results of that study which are applicable to this design are summarized in the following statement: for the case of $Q = 1$ holograms, i.e. holograms made with a plane wave and

a point source, the construction geometry producing the least aberrations upon reconstruction will have the point source on the axis of the hologram and the plane wave off-axis. In addition, if a wavelength shift is employed during reconstruction, the angle of reconstruction should be altered to produce an on-axis image.

Application of these rules to the two element telescope design has produced the construction and reconstruction geometries shown in Figures 13 and 14, respectively. Table 2 contains the specific parameter values as optimized by the hologram ray tracing programs. A graph of total predicted wavefront aberrations as a function of input field angle is shown in Figure 15 for the second telescope design. It is immediately obvious in comparing this graph with the corresponding graph for the first telescope design (Figure 3) that some significant improvements have been made. The second telescope design does not exhibit any aberration anomalies and is very nearly symmetric. In addition, the aberrations on-axis have been reduced to one-tenth of their previous value while the aberrations at +2 degrees off-axis have been reduced to one-half their previous value.



(a) Objective Element



(b) Eyepiece Element

FIGURE 13. CONSTRUCTION GEOMETRIES FOR SECOND TELESCOPE (#2) DESIGN. $\lambda_0 = 5145 \text{ \AA}$.

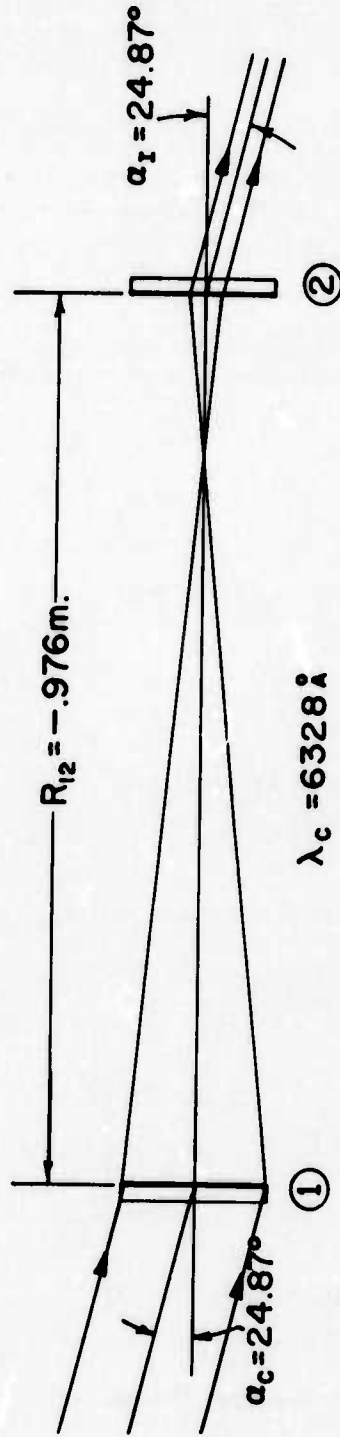


FIGURE 14. RECONSTRUCTION GEOMETRY FOR SECOND TELESCOPE DESIGN. $\lambda_c = 6328 \text{ \AA}$.

TABLE 2. TWO ELEMENT TELESCOPE
#2 DESIGN PARAMETERSHOLOGRAM 1

$$\alpha_O = 0^\circ, R_O = -1 \text{ m}$$

$$\alpha_R = 20^\circ, R_R = \infty$$

HOLOGRAM 2

$$\alpha_O = 0^\circ, R_O = .2 \text{ m}$$

$$\alpha_R = 20^\circ, R_R = \infty$$

$$\alpha_{12} = 0^\circ, R_{12} = -.276 \text{ m}$$

$$\alpha_C = 24.87^\circ, R_C = \infty$$

$$\alpha_I = 24.87^\circ, R_I = \infty$$

$$\lambda_O = 5145\overset{\circ}{\text{A}}, \lambda_C = 6328\overset{\circ}{\text{A}}$$

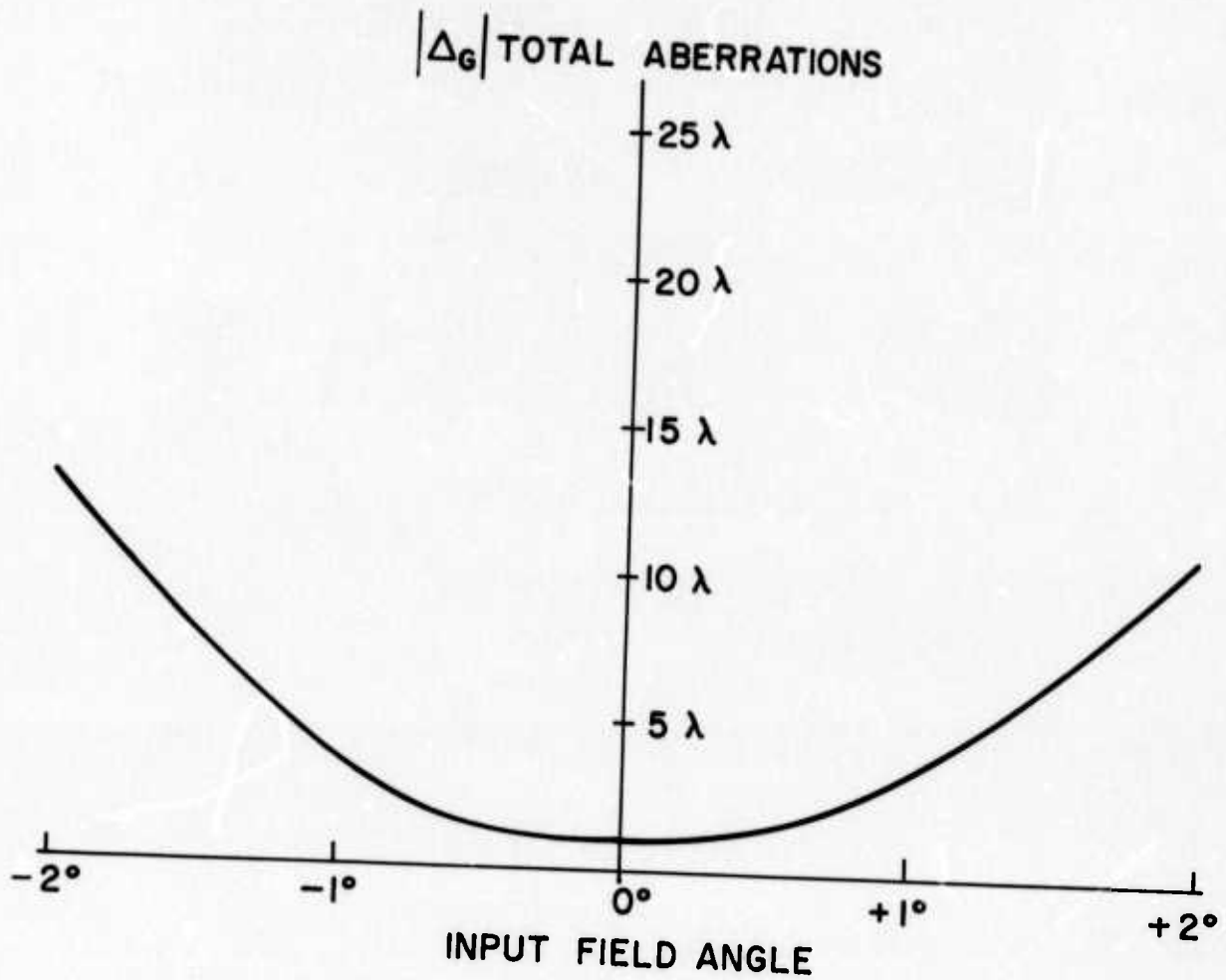


FIGURE 15. EXIT WAVEFRONT TOTAL ABERRATIONS AS A FUNCTION OF INPUT FIELD ANGLE FOR TELESCOPE #2

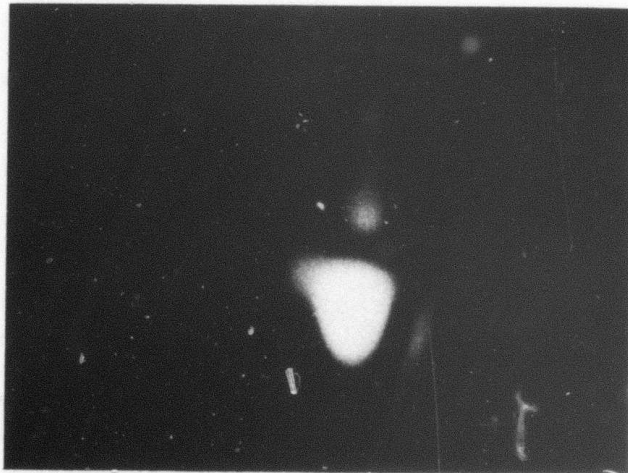
Performing the calculations as previously to determine field-of-view, it is found that the second telescope design has a field-of-view of approximately $\pm 2.6^\circ$. The following section discusses the implementation and testing of the second telescope design.

2.2.2 TELESCOPE #2 - IMPLEMENTATION & TESTING

As before the two hologram elements of the second telescope design were constructed on five-inch square microflat plates, one quarter inch thick. The construction and reconstruction wavelengths were again $5145\overset{\circ}{\text{Å}}$ and $6238\overset{\circ}{\text{Å}}$, respectively. To as great an extent as possible, identical testing procedures were used to test the second telescope design as were used in testing the first telescope design. Using the test geometry as shown in the previous Figure 4, point focus photographs were made of both hologram elements at the two wavelengths. Figure 16 shows the point foci of the first element at $5145\overset{\circ}{\text{Å}}$ and $6328\overset{\circ}{\text{Å}}$ wavelengths while Figure 17 shows the point foci of the second element. As can be seen from these photographs when observing an aberrated point focus, it is difficult to ascertain the degree of aberration present. In an attempt



(a) 5145 Å

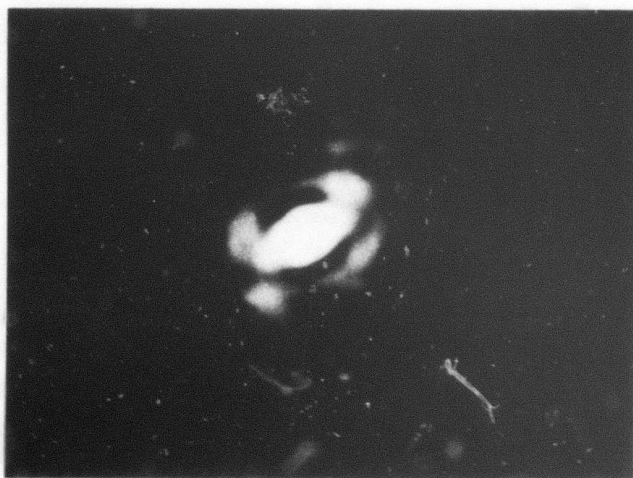


(b) 6328 Å

FIGURE 16. POINT FOCUS OF OBJECTIVE ELEMENT FOR TELESCOPE #2



(a) 5145 Å



(b) 6328 Å

FIGURE 17. POINT FOCUS OF EYEPiece ELEMENT FOR
TELESCOPE #2

to better evaluate the individual hologram elements we decided to perform the point focus test with a reduced aperture and in this way find the largest aperture that would still provide diffraction limited performance.

Figure 18 shows the diffraction limited point foci for the two hologram elements when operated at $6328\overset{\circ}{\text{A}}$. For the first element the aperture was approximately two inches in diameter, while for the second element the aperture was about .8 inch in diameter. These limiting apertures were found to correspond exceedingly well with aperture size predicted by the hologram ray tracing program for one-quarter wavelength aberrations.

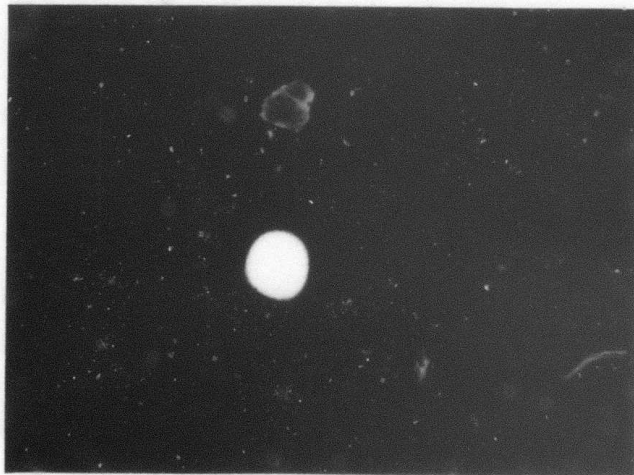
Point focus photographs were also made of the telescope configuration with the test geometry of the previous Figure 7. Figure 19 shows these point foci with input apertures of four inches and 2.8 inches, and a reconstruction wavelength of $6328\overset{\circ}{\text{A}}$. At an aperture of 2.8 inches the telescope is operating at diffraction limit, again agreeing well with the computer analysis.

Finally, resolution target images were photographed using the test geometry depicted earlier in Figure 11. At a full aperture of four inches, the on-axis targets in Figure 20 were recorded. Calculating as before we find that at a



Reproduced from
best available copy.

(a) Objective Element with 2-in. Aperture

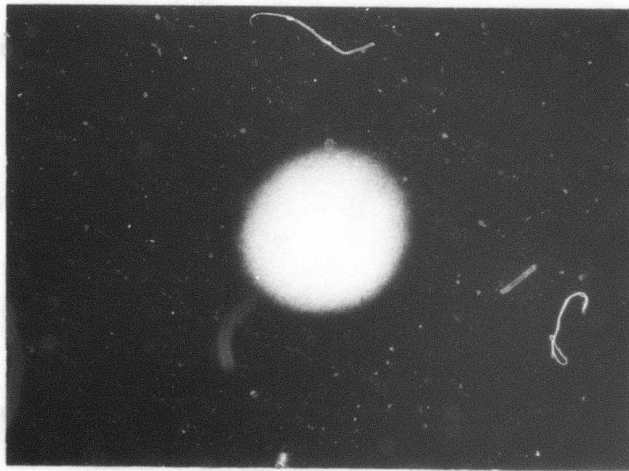


(b) Eyepiece Element with 0.8-in. Aperture

FIGURE 18. DIFFRACTION LIMITED POINT FOCUS AT 6328 Å
FOR TELESCOPE #2

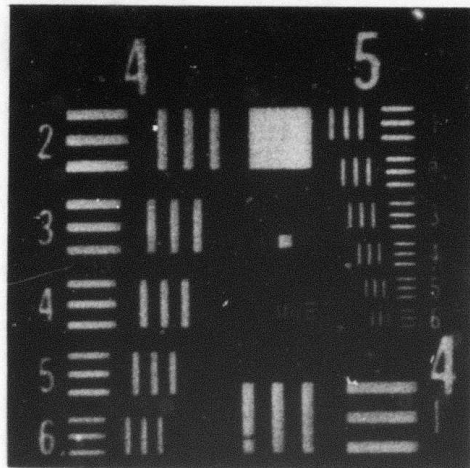


(a) 4-in. Aperture

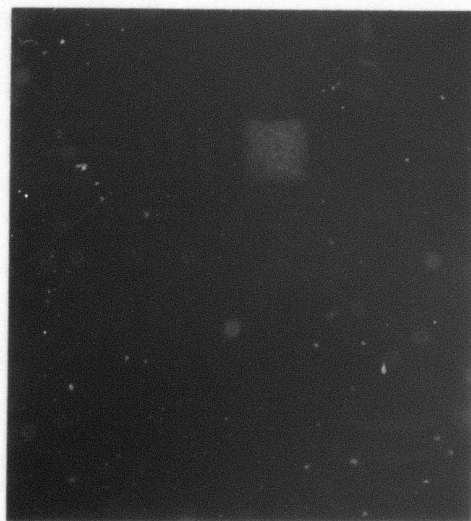


(b) 2.8-in. Aperture

FIGURE 19. POINT FOCUS OF ASSEMBLED TELESCOPE #2
AT 6328 Å



(a) 5145 Å



(b) 6328 Å

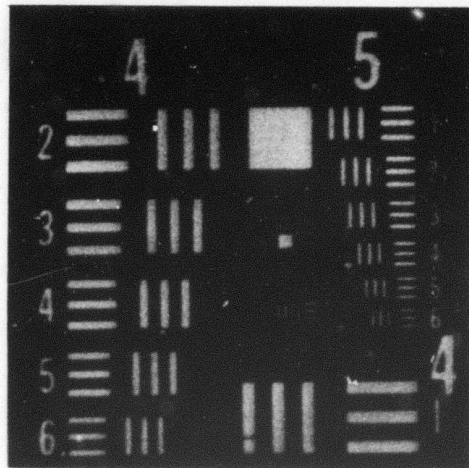
FIGURE 21. RESOLUTION TARGET FOR 2.8-in. APERTURE FOR TELESCOPE #2

wavelength of 5145 $\overset{\circ}{\text{Å}}$ an angular resolution of 1.48 arc seconds is achieved while at 6328 $\overset{\circ}{\text{Å}}$ an angular resolution of 2.11 arc seconds is possible. These results show a small increase in the resolution at 5145 $\overset{\circ}{\text{Å}}$ compared with the first telescope design, but more important, a very significant increase is found in the resolution at 6328 $\overset{\circ}{\text{Å}}$. If the input aperture is subsequently reduced to 2.8 inches, a small additional increase in resolution occurs as may be seen in Figure 21. The final resolutions were 1.32 arc seconds at 5145 $\overset{\circ}{\text{Å}}$ and 1.88 arc seconds at 6328 $\overset{\circ}{\text{Å}}$, comparing extremely well with corresponding theoretical resolutions of 1.49 arc seconds and 1.84 arc seconds.

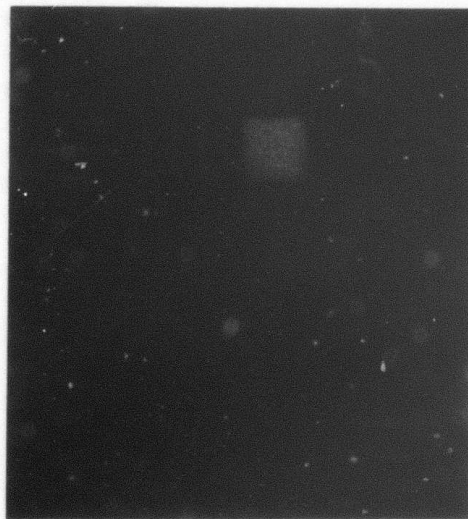
As anticipated, the second telescope design performed better than the first telescope design, particularly when a wavelength shift occurred during reconstruction. This design was consequently used as a starting point for the design of a three element telescope. Before discussing the three element telescope designs, however, it may be interesting to examine a third two element telescope design.

2.3 TELESCOPE #3

The design for telescope #2 represents a reasonable limit to the performance of this basic imaging system.



(a) 5145 Å



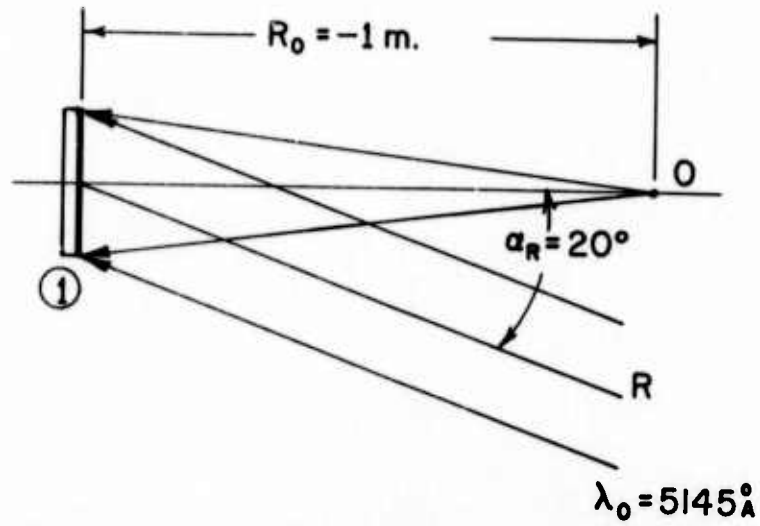
(b) 6328 Å

FIGURE 21. RESOLUTION TARGET FOR 2.8-in. APERTURE FOR TELESCOPE #2

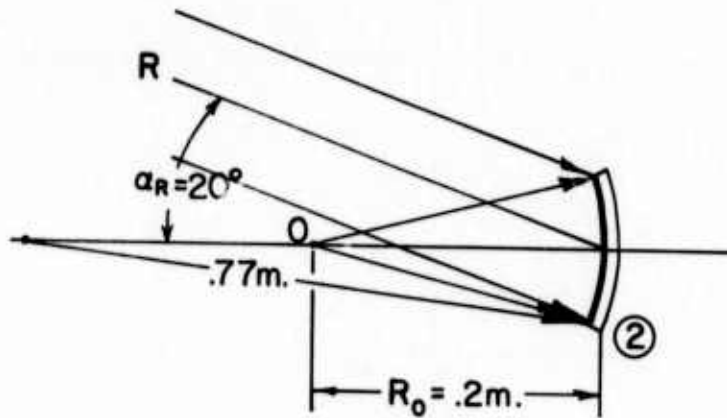
It, however, has several drawbacks as we saw, and these will be addressed in more detail in Section 3. Let us now take a somewhat different tack in that we will vary a parameter that one might not normally modify in a conventional holographic optics design.

2.3.1 TELESCOPE #3 - DESIGN

The hologram ray tracing programs provide a degree of flexibility far greater than that attainable in the laboratory. It is of interest to see what further improvements could be made to the two element telescope design without the limitation that the design be realizable with existing techniques. The third telescope was designed allowing the second element to have a curved substrate. In essence, the second telescope design was optimized allowing the second hologram element to be a spherical surface with its axis collinear with the axis of the first hologram element. The optimized hologram construction geometries are shown in Figure 22 and the telescope geometry in Figure 23. The radius of curvature of the second element providing optimal operation is .77 meters. Figure 24 shows a plot of total aberrations versus input field angle for this third telescope design. Comparing this plot with



(a) Objective Element



(b) Eyepiece Element

FIGURE 22. CONSTRUCTION GEOMETRIES FOR TELESCOPE DESIGN
#3. $\lambda_0 = 5145 \text{ \AA}$.

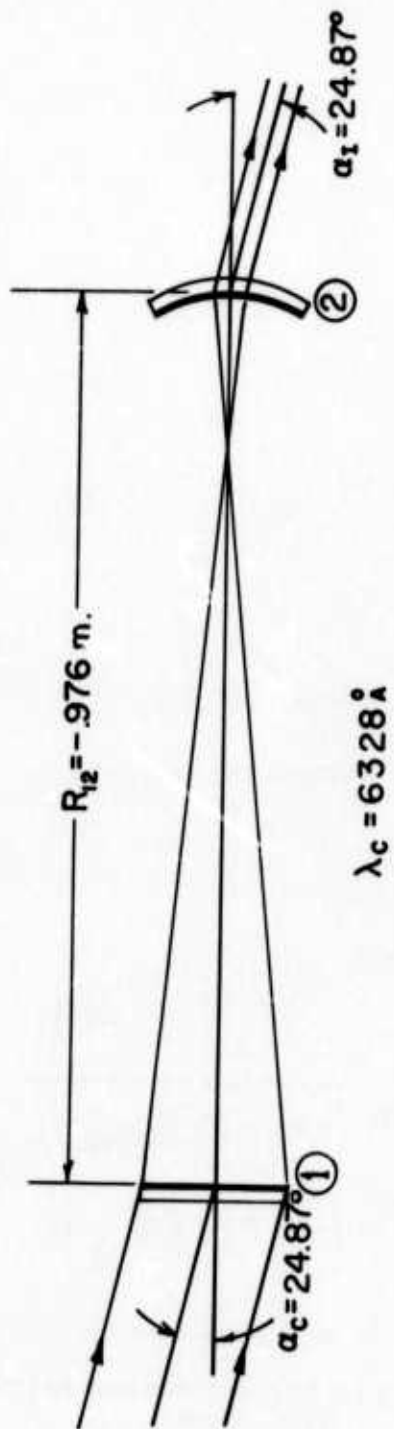


FIGURE 23. RECONSTRUCTION GEOMETRY FOR TELESCOPE DESIGN #3. $\lambda_c = 6328 \text{ \AA}$.

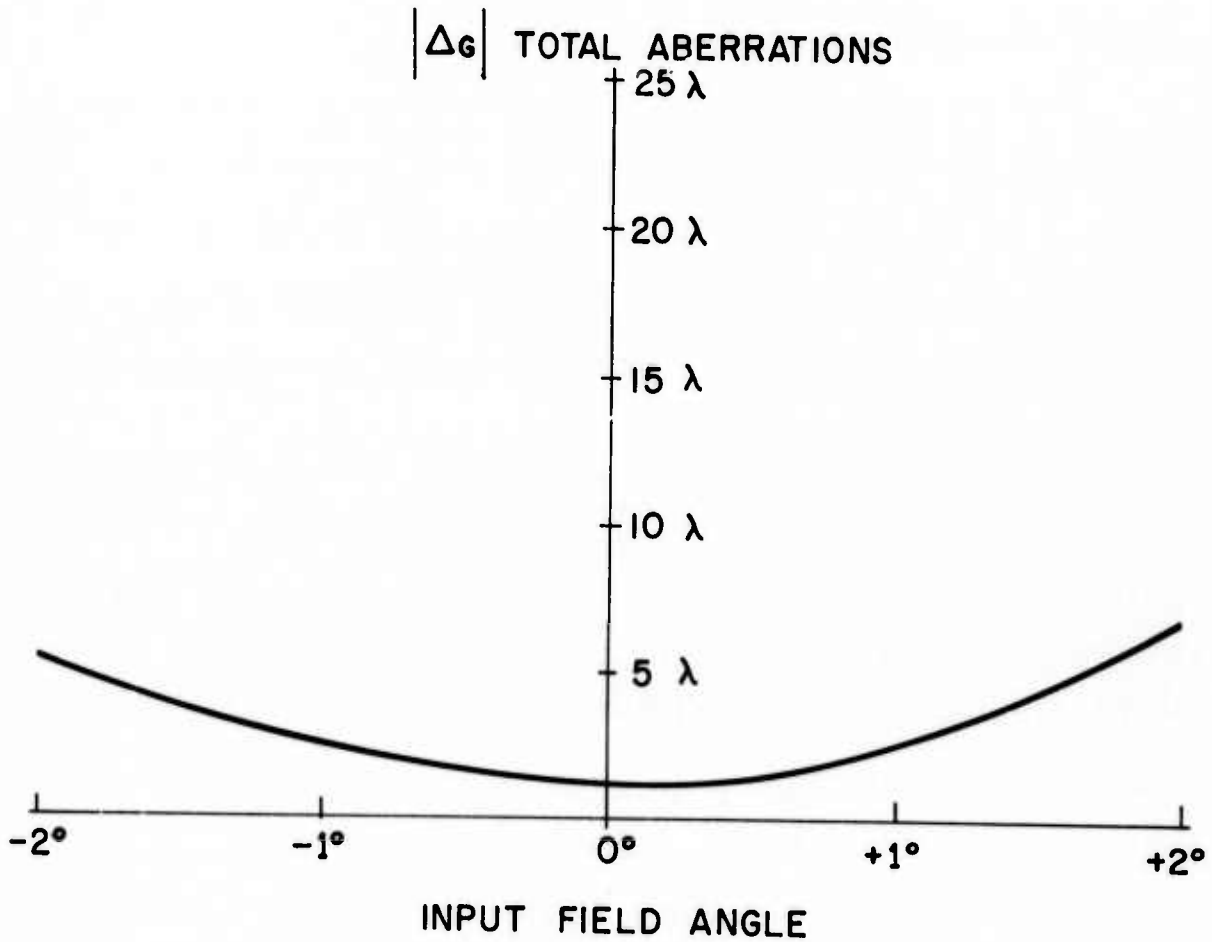


FIGURE 24. EXIT WAVEFRONT TOTAL ABERRATIONS AS A FUNCTION ON INPUT FIELD ANGLE FOR TELESCOPE #3

the corresponding plots for the first and second designs, it is seen that an additional 50% reduction in aberrations at $+2^{\circ}$ has been attained.

Although the construction of this design is difficult from a materials standpoint, it is possible that as substrate and emulsion coating techniques are perfected this design could be employed. Certainly, if the advantages of curved hologram elements are great, the techniques for construction can be developed.

2.4 CONCLUSIONS

This section has illustrated quite well our previous knowledge of the basic two element telescope. That is, there are some severe limitations in that only two elements are present; the major one is that the field-of-view is limited. More importantly the basic design parallels our experience in conventional optics even though a rather significant wavelength shift is present from construction to reconstruction. The work here effectively validates many of the techniques which are used to compensate for the wavelength shift.

3
THREE ELEMENT TELESCOPES

It is often desirable to have a wide field-of-view telescope. With the two element telescopes of the preceding section, we have seen that field-of-view is limited by the aperture of the eyepiece. Inasmuch as the eyepiece inherently has a small focal length to provide high magnification, enlarging the aperture of the eyepiece is limited by the additional aberrations involved with low f-numbers. An alternate method of increasing the field-of-view of a telescope without enlarging the eyepiece aperture is the addition of a third element called a field lens.

In essence, a field lens is placed between the objective and eyepiece at the location of the real image produced by the objective. It has the effect of redirecting the off-axis rays from the objective back onto the eyepiece. In practice, field lenses are displaced slightly from the aforementioned position to allow for the addition of a reticle. In addition, a slight displacement is advisable in preventing blemishes or dust contained on the field lens from being sharply focused by the eyepiece.

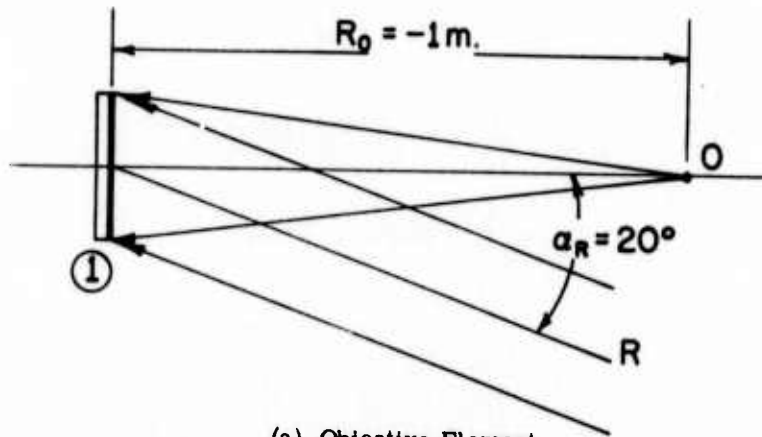
3.1 TELESCOPE #1

In this telescope we would like to take the design developed for the two-element telescope #2 and add a field lens. This then allows us to directly compare the results of the two systems.

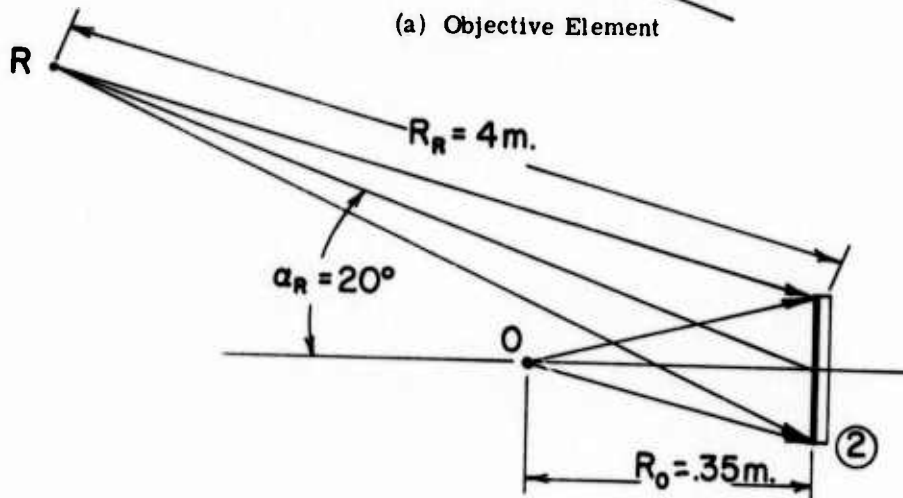
3.1.1 TELESCOPE #1 - DESIGN

A holographic telescope with a field lens for added field-of-view has been designed and tested. Figure 25 shows construction details of the completed design with the second element being the field element. The objective element and eyepiece element of this three element telescope are identical to the elements in the second two element telescope design. In fact, the telescope geometry is very similar with the exception of a rotation and displacement of the eyepiece element as seen in Figure 26. As before, the construction wavelength was $5145\overset{\circ}{\text{A}}$ and the operating wavelength was $6328\overset{\circ}{\text{A}}$. It can be calculated at this point that for a ± 5 degree field-of-view, twice that obtainable with the two element telescope designs, it is only necessary to have a five inch diameter field element. Table 3 illustrates the element sizes necessary for a given field-of-view.

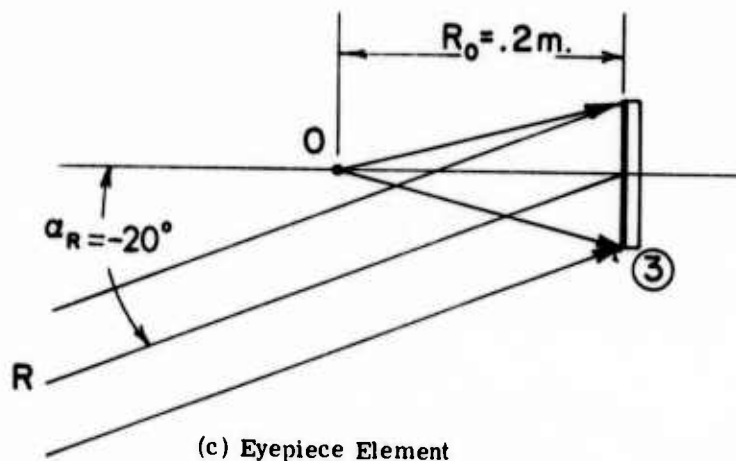
A three element telescope design can provide a reduction in element size but not without a price. Adding



(a) Objective Element



(b) Field Element



(c) Eyepiece Element

FIGURE 25. CONSTRUCTION GEOMETRIES FOR TELESCOPE DESIGN #1

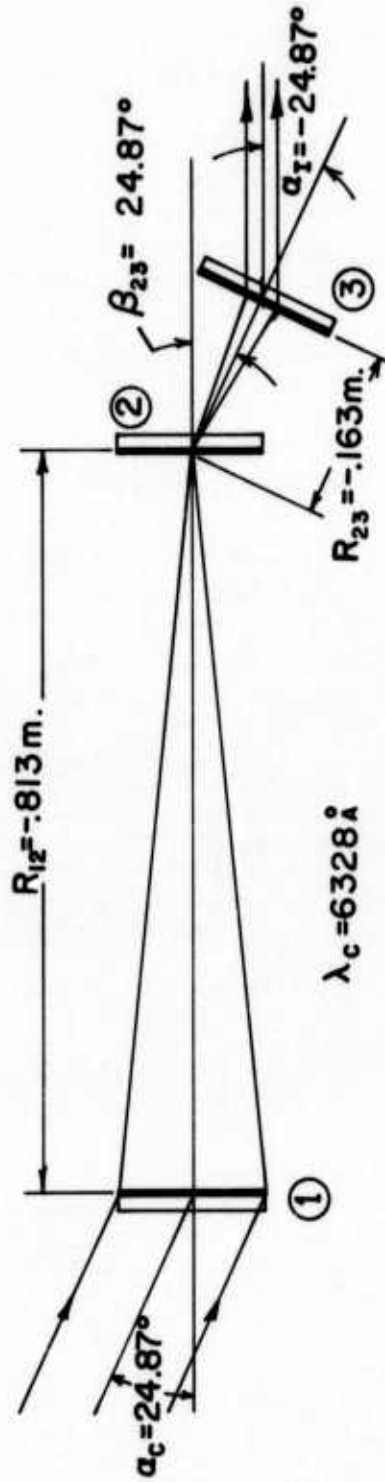


FIGURE 26. RECONSTRUCTION GEOMETRY FOR TELESCOPE DESIGN #1

TABLE 3
 TWO AND THREE ELEMENT DIAMETERS FOR TWO ELEMENT
 DESIGN #2 AND THREE ELEMENT DESIGN #1 AS A
 FUNCTION OF THE FIELD-OF-VIEW

	Two Element Design #2		Three Element Design #1		
	Element 1	Element 2	Element 1	Element 2	Element 3
Minimum Element Diameter - $+2.5^\circ$ Field-of-View	.1016 m	.0992 m	.1016 m	.0647 m	.0582 m
Minimum Element Diameter - $+5^\circ$ Field-of-View	.1016 m	.1805 m	.1016 m	.1318 m	.0973 m

an additional hologram element reduces the overall telescope efficiency. The added element may also introduce unwanted aberrations into the system, and since the eyepiece operates at larger input angles, it may also introduce efficiency fall-offs due to mismatch with the Bragg angle. Despite these drawbacks, the first three element telescope design performs well, considering its wide field-of-view, as may be seen from the graph of Figure 27. The total aberrations remain under 15λ for negative input field angles to minus five degrees. Positive input field angles, however, show a sharp increase in total aberrations approaching 60λ at plus five degrees. Such asymmetry has been found in the past to be indicative of a system which is not optimized completely. In the second three element telescope design, this problem will be studied.

3.1.2 TELESCOPE #1 - IMPLEMENTATION & TESTING

Construction of the first three element telescope design simply entailed making the field element, the objective and eyepiece elements having already been constructed for the second two element design. A test geometry similar to that described previously in Figure 11 was used to determine the angular resolution of the telescope. Figure

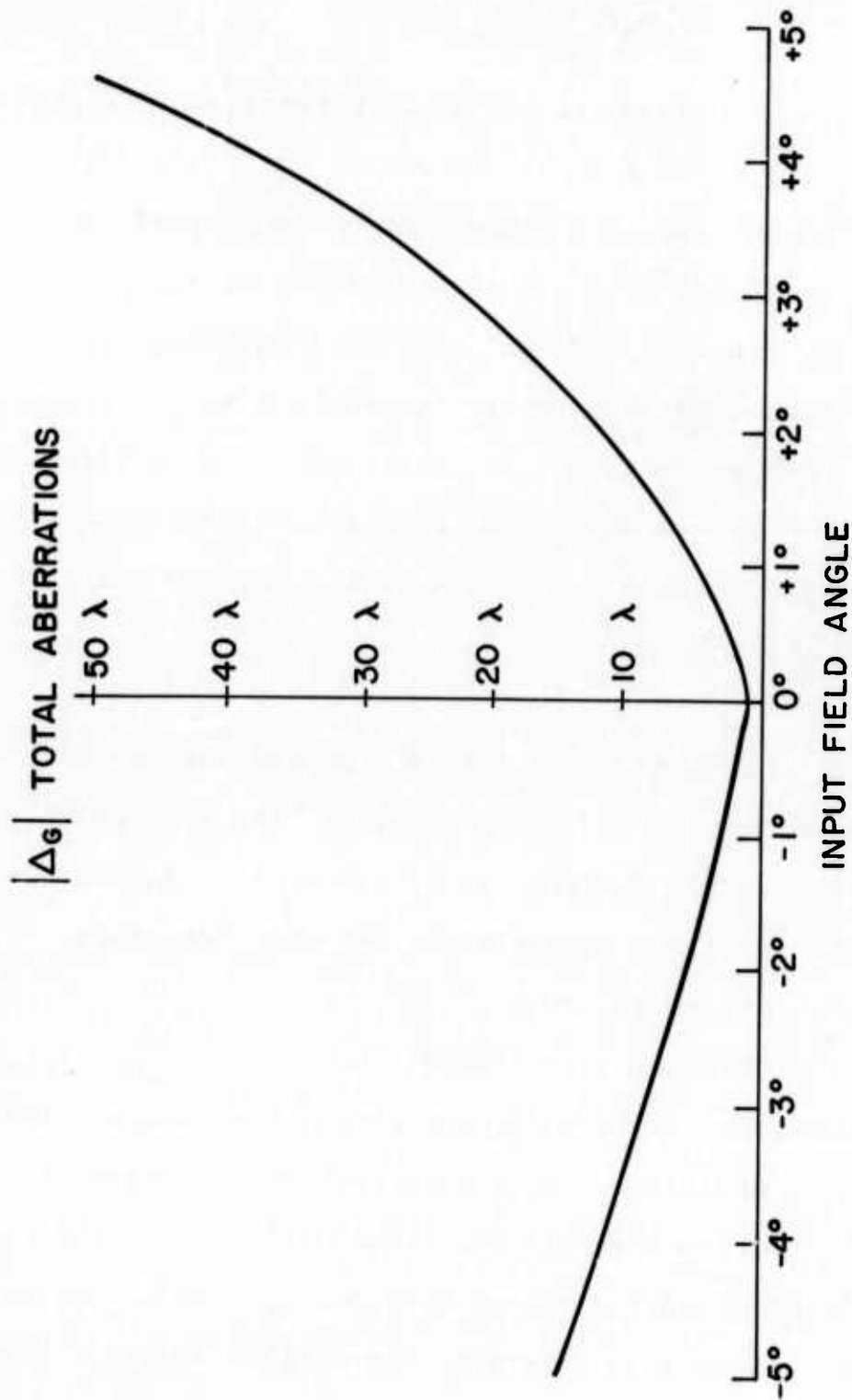


FIGURE 27. EXIT WAVEFRONT TOTAL ABERRATIONS AS A FUNCTION OF INPUT FIELD ANGLE FOR TELESCOPE #1

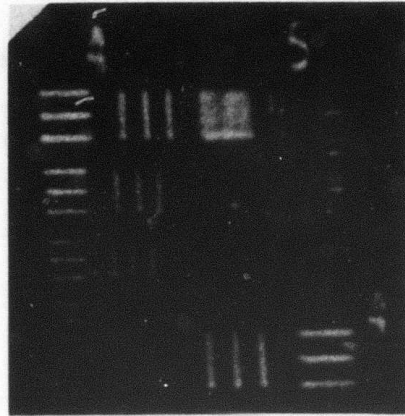
28 contains photographs of the on-axis resolution target with the field element in two different positions. In the first photograph, the field element is located precisely at the focal point of the objective element, while for the second photograph the field element was displaced approximately one centimeter from its previous location. As may be seen, the second position is somewhat better than the first. Calculation of the angular resolution for each case yields 4.75 arc seconds and 3.33 arc seconds, respectively.

3.2 TELESCOPE #2

Let us now consider another design, similar to that discussed in Section 2.3, where we would like to significantly extend the design. We will resort to techniques that may be difficult to implement but with the intent of improving the performance.

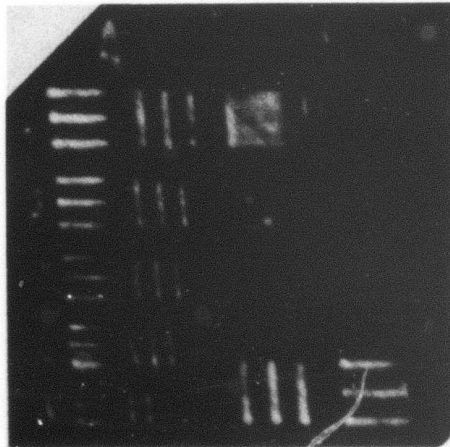
3.2.1 TELESCOPE #2 - DESIGN

As mentioned previously, the first three element telescope design exhibited a nonsymmetrical distribution of aberrations across the exit pupil, indicative of a non-optimal design. In the second three element telescope design an attempt was made to determine the optimal design. Figure



Reproduced from
best available copy.

(a) Field Element at Focal Point
of Objective Element



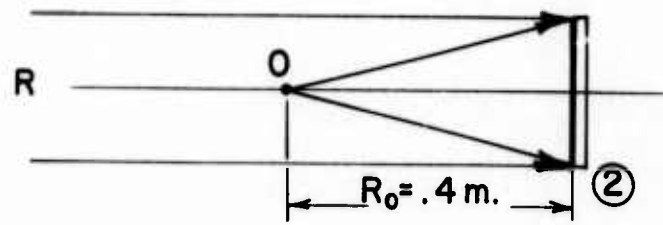
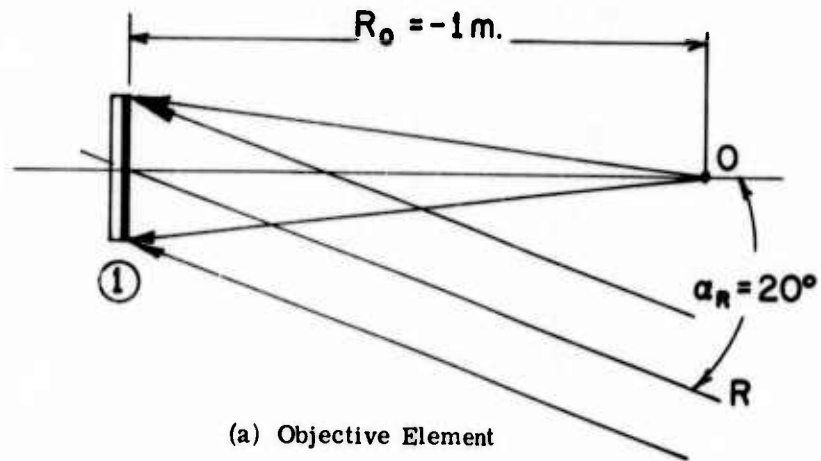
(b) Field Element Displayed 1 cm
from Focal Point of Objective Ele-
ment

FIGURE 28. RESOLUTION TARGET
AT 6328Å FOR TELESCOPE DESIGN #1

29 and Figure 30 show the construction and reconstruction geometries of the totally optimized three element design. As can be seen, it was necessary to make the field element an in-line hologram. Although such a construction is possible, it is impractical due to interference from the conjugate image and from the undiffracted term. In addition, such a construction geometry results in a thin hologram, characterized by a less than optimum efficiency. Figure 31, however, demonstrates the superior theoretical performance of such a system should the above mentioned drawbacks be eliminated.

3.3 CONCLUSIONS

The results quite clearly indicate that the addition of a third element to the design has significantly improved the system performance. In general, a penalty has been paid by light loss because the added element will not have 100% transmission efficiency. The second design is interesting in that it illustrates the limit to which these systems may perform with only a slight change in the design parameters.



$\lambda_0 = 5145 \text{ \AA}$

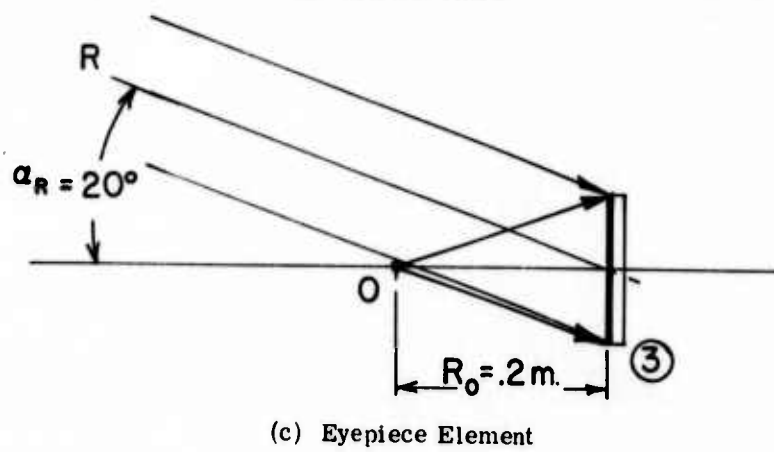
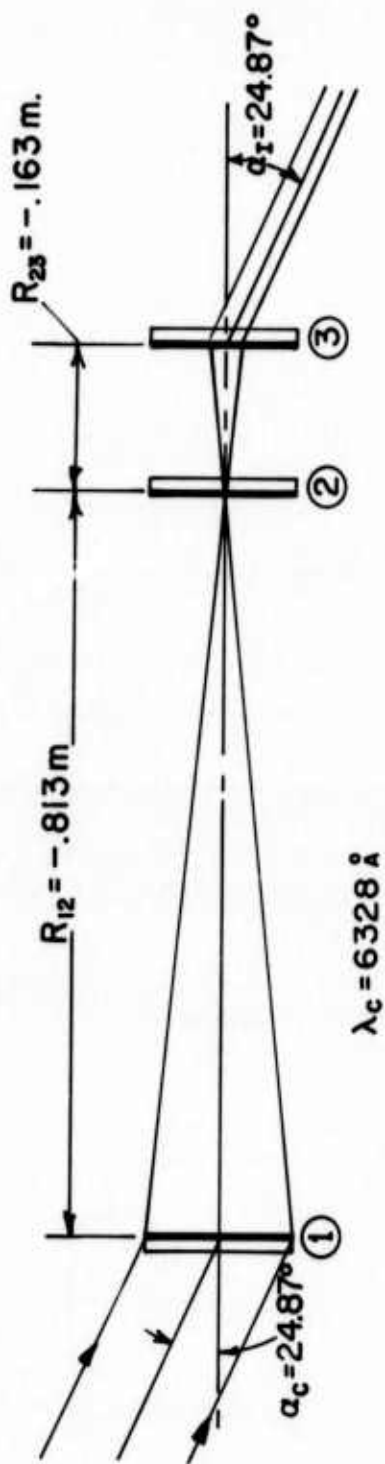


FIGURE 29. CONSTRUCTION GEOMETRIES FOR TELESCOPE DESIGN
#2. $\lambda_0 = 5145 \text{ \AA}$.


 FIGURE 30. RECONSTRUCTION GEOMETRY FOR TELESCOPE DESIGN #2. $\lambda_c = 6328 \text{ \AA}$.

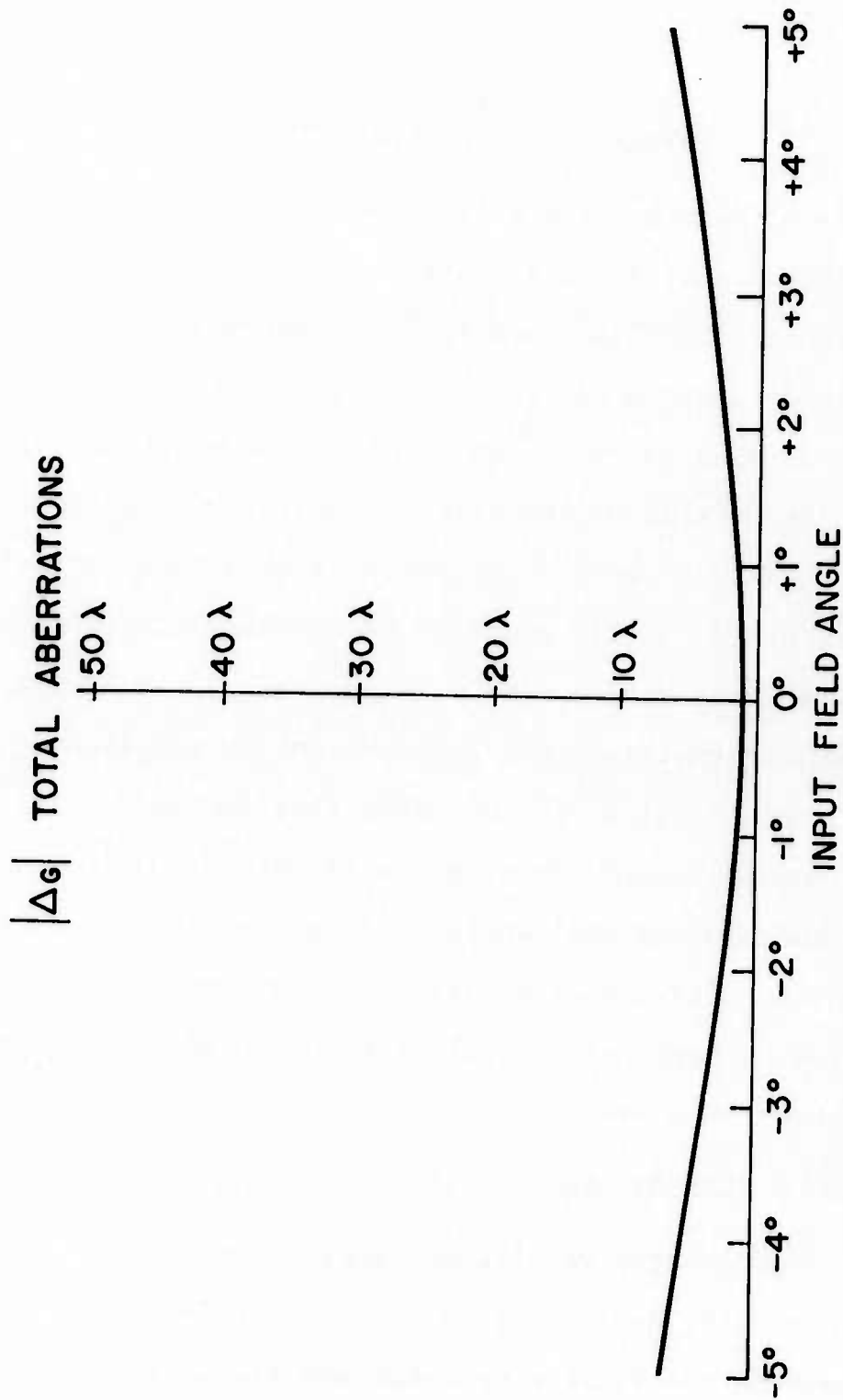


FIGURE 31. EXIT WAVEFRONT TOTAL ABERRATIONS AS A FUNCTION OF INPUT FIELD ANGLE FOR TELESCOPE DESIGN #2

4
INFRARED OPTICAL ELEMENTS

One of the most interesting and most promising areas for application of hologram optical elements is the infrared spectrum. The less than optimal performance of conventional refractive optics in the near infrared and their inherent complexity of design makes hologram optical elements a very viable alternative. A drawback in the past, however, has been the lack of suitable emulsions sensitive in the infrared, not to mention the availability of good coherent sources at infrared wavelengths. These drawbacks have been circumvented to a large extent by the technique of wavelength shift developed under this contract. In essence, conventional coherent sources at visible wavelengths and conventional emulsions are used to produce a holographic optical element usable at infrared wavelengths. The following sections describe the design and evaluation of just such an element.

4.1 SINGLE ELEMENT LENS - 1.15 μ

As a first step we will consider a very simple large wavelength shift design. This is a simple lens that is to be made in the visible spectrum and reconstructed at

1.15 μ . The lens will then be tested to determine its agreement with the design parameters.

4.1.1 INFRARED LENS - DESIGN

The techniques developed through the single element analysis at large wavelength shifts were applied to design an infrared lens. The construction wavelength was chosen to be 5145⁰A and the reconstruction wavelength was chosen to be 1.15 μ . The element size was specified at four inches diameter. Figure 32 shows the construction and reconstruction geometry of the optimized element. The on-axis total aberration as predicted by the ray tracing programs is $.90\lambda$ across the four inch aperture.

4.1.2 INFRARED LENS - IMPLEMENTATION & TESTING

The infrared holographic element was constructed as shown in Figure 32. Reconstruction was performed with a helium-neon laser modified to operate at 1.15 μ . Inasmuch as 1.15 μ radiation is invisible to the human eye and also most photographic film, evaluation of the performance of the lens was difficult. A test geometry as shown in Figure 33 was finally employed to obtain a photograph of the point focus. Essentially the test setup consists of a four inch off-axis collimating mirror to provide a plane wave reconstruction beam. The resulting infrared

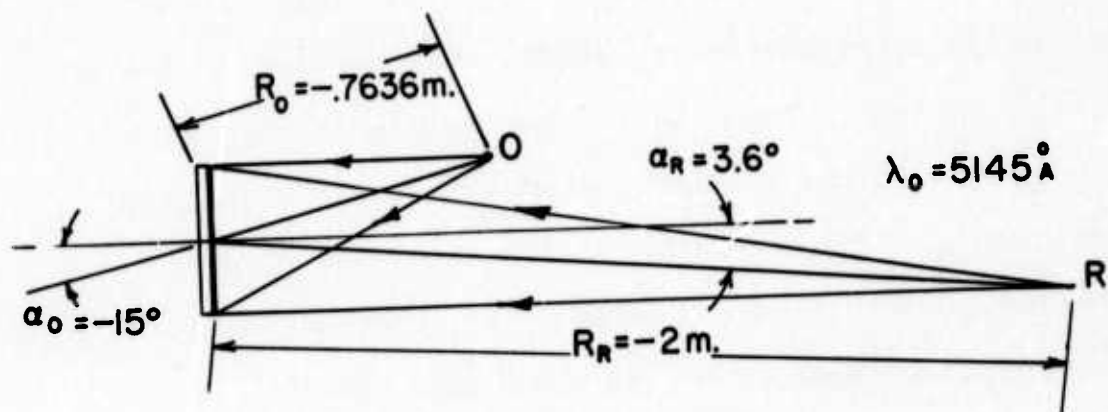
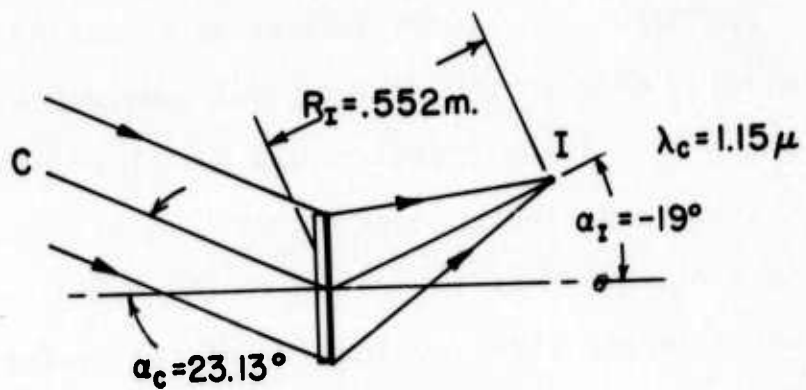

 (a) Construction, $\lambda_o = 5145 \text{ \AA}$

 (b) Reconstruction, $\lambda_c = 1.15 \mu$

FIGURE 32. CONSTRUCTION AND RECONSTRUCTION GEOMETRIES OF INFRARED HOLOGRAPHIC LENS

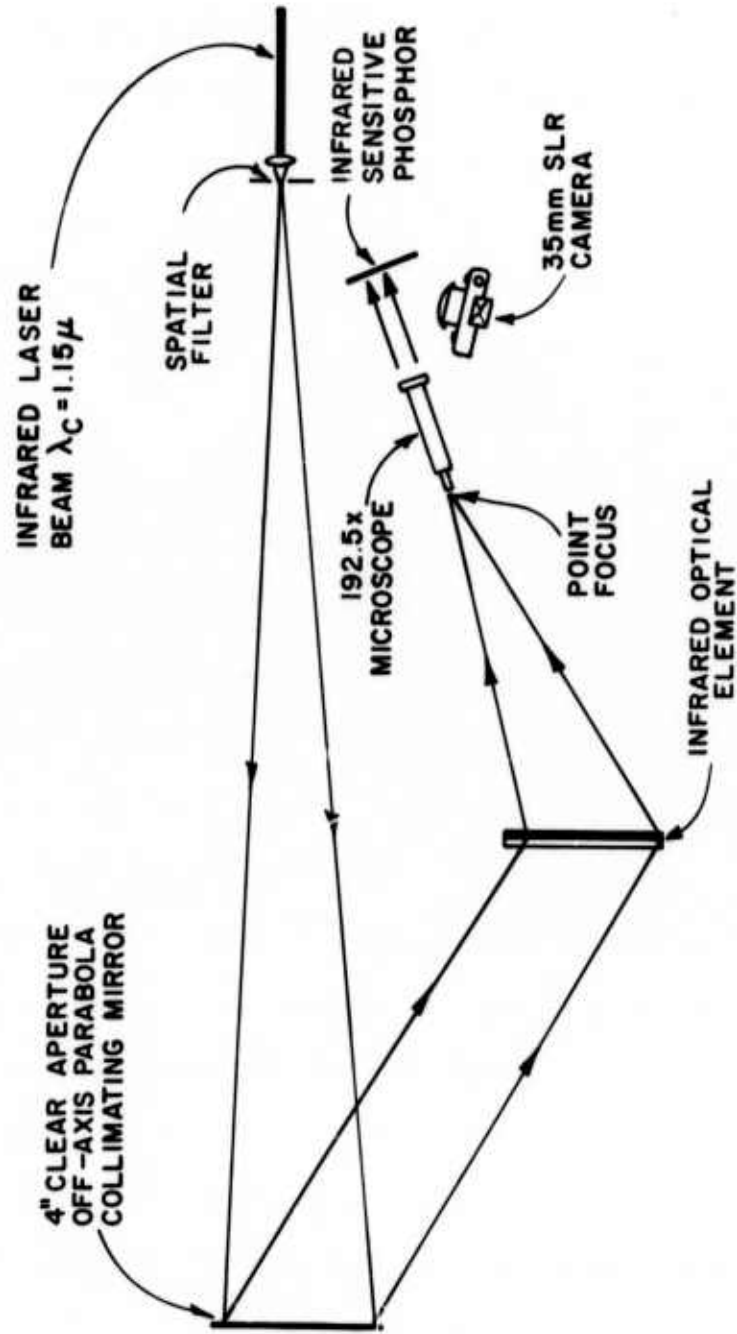
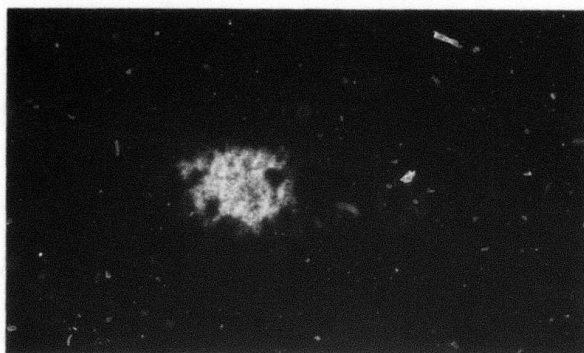


FIGURE 33. POINT FOCUS TEST GEOMETRY FOR INFRARED HOLOGRAPHIC ELEMENT AT $\lambda_c = 1.15 \mu$

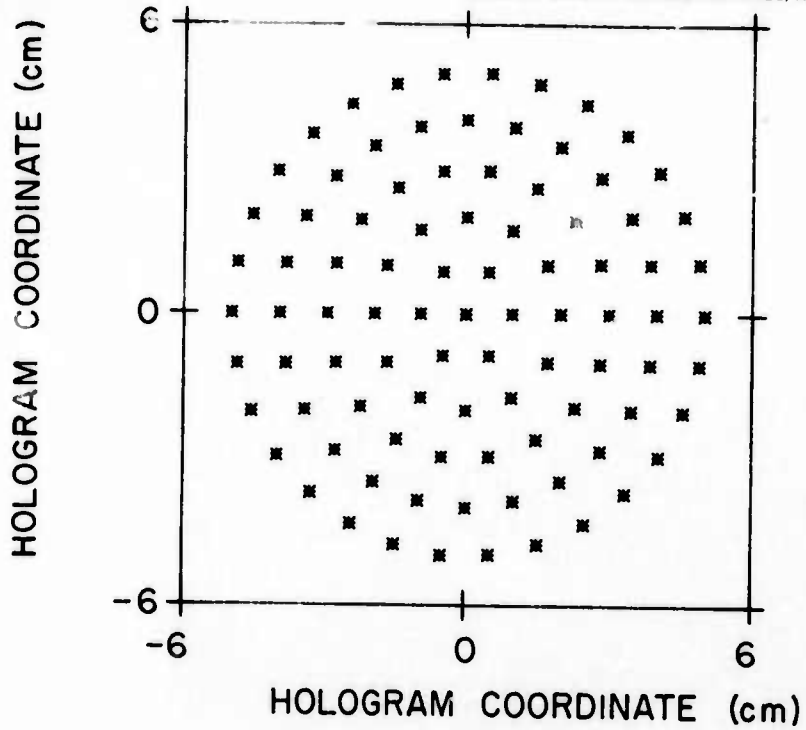
point focus was then magnified by a microscope assembly and projected onto an infrared sensitive phosphor. The phosphor emits in the green region of the visible spectrum when illuminated at 1.15μ . The resulting phosphor image was then photographed and is shown in Figure 34. The dark spots seen in the photograph are characteristic of the grain inherent in the phosphor.

The spot size of the infrared point focus was determined to be on the order of 20μ diameter compared with a diffraction limited spot size of 7.6μ diameter. In order to see how well the spot size compared with that predicted by the hologram ray tracing program, a series of intercept plots were generated. The first point plot shown in Figure 35 shows the distribution of rays used as input to the infrared lens. The resulting point focus is shown in the second plot. As may be seen, the entire point focus occupies a region of approximately 50μ diameter with the major portion of the point focus lying within 20μ . This corresponds well with the observed spot size taking into account the limited resolution and response provided by the imaging phosphor.

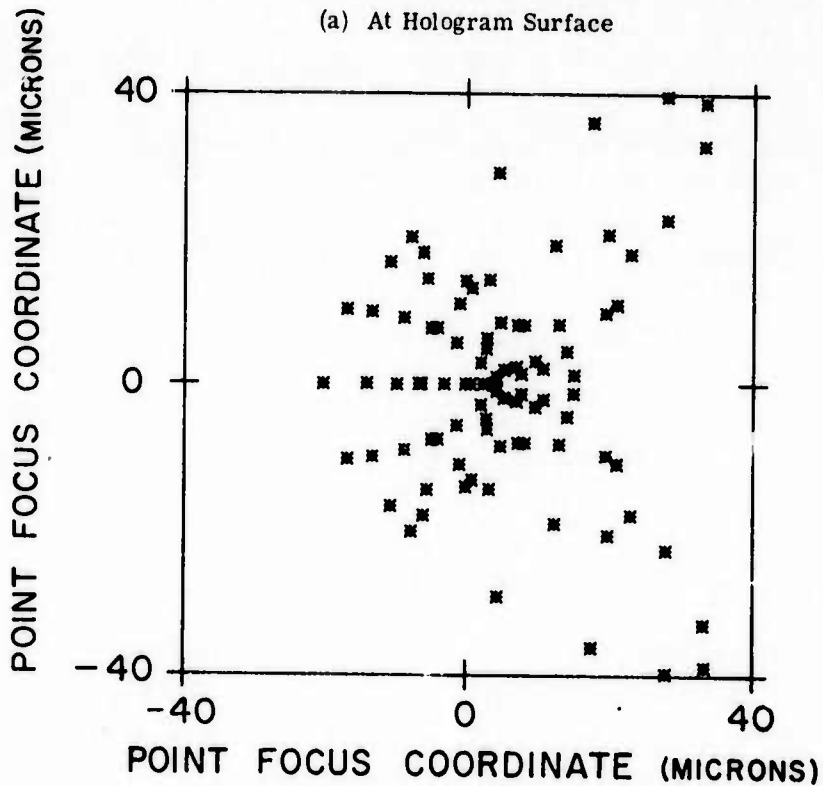


→ | 10 μ | ←

FIGURE 34. POINT FOCUS OF INFRARED HOLOGRAPHIC ELEMENT AT 1.15 μ . Diffraction limited spot size = 7.63 μ .



(a) At Hologram Surface



(b) At Plane of Best Focus

FIGURE 35. COMPUTER GENERATED POINT PLOT

4.2 TWO ELEMENT TELESCOPE - 10.6 μ

At infrared wavelengths beyond 1.15 μ the performance of conventional refractive optics begins to deteriorate rapidly: at 10.6 μ , for example, conventional glass becomes highly absorptive. Yet 10.6 μ is a wavelength of considerable interest for several reasons. The highly powerful CO₂ laser has its primary line at 10.6 μ , and in addition, there exists an atmospheric window around the 10.6 μ wavelength region. It is reasonable to consider the use of 10.6 μ for high data rate space and satellite communications.

4.2.1 DESIGN

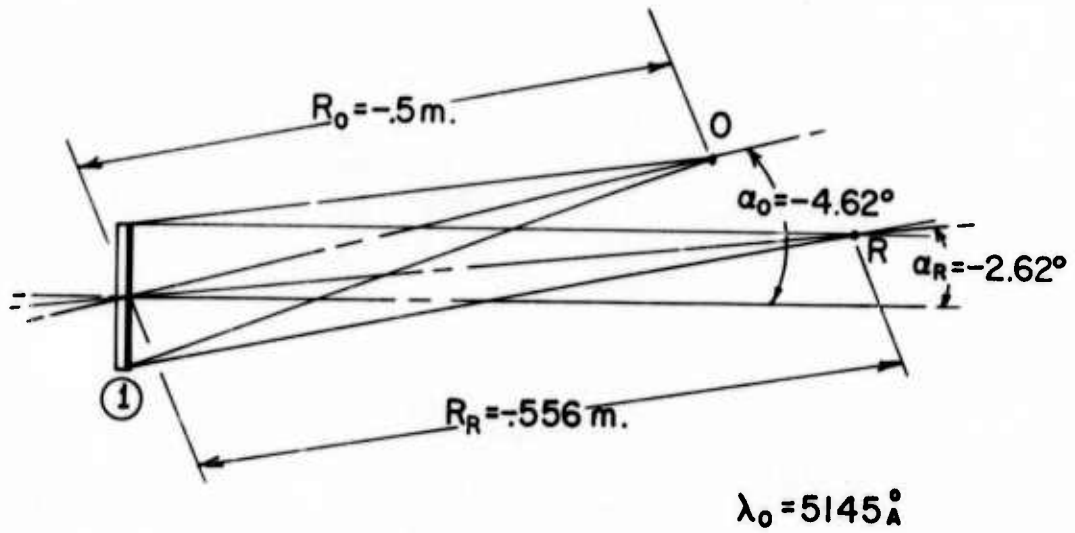
It was decided to try to apply the techniques developed in the single element analysis (presented in Section 7 of this report) to the problem of imaging at 10.6 μ . In light of the absorption of 10.6 μ radiation by glass substrates, not to mention photographic emulsions, reflection type diffractive optics are a necessity. Such a reflective grating relies on surface relief for its diffractive imaging. In practice, a hologram element is made with a photoresist emulsion which is subsequently overcoated with a highly reflective material to assure maximum

efficiency. A more detailed discussion concerning this process may be found in Appendix A.

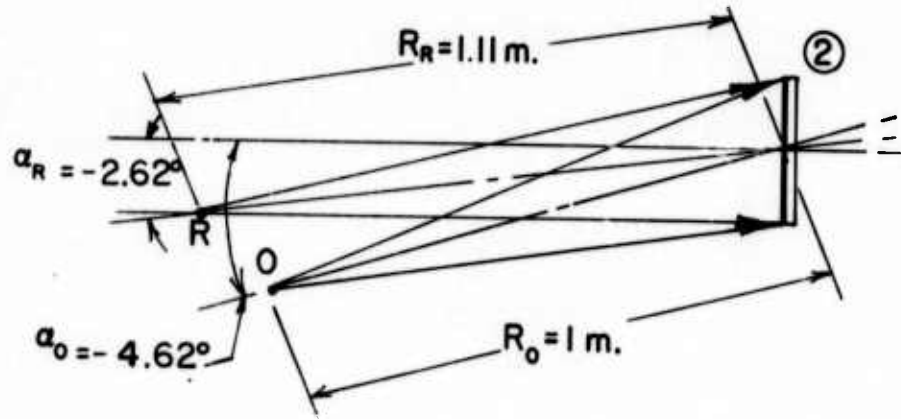
Figure 36 contains construction details for a two element telescope operating at 10.6μ with a magnification power of 2X. The construction wavelength specified was $5145\overset{\circ}{\text{A}}$, however, any visible wavelength could be used with appropriate alterations of the construction geometry. The telescope geometry is shown in Figure 37. It should be noted that the telescope operates as a reflective system. The element sizes are designated to be of four inch diameter, however, larger aperture systems are certainly feasible. A graph of total aberrations across the exit pupil versus the input field-of-view as shown in Figure 38 depicts a system of fairly reasonable aberrations across a ten degree field-of-view. Two anomalies near the on-axis condition give rise to higher aberrations, but these may be eliminated with further design refinements.

4.3 CONCLUSIONS

These results for both the single lens at 1.15μ and the two lens design at 10.6μ graphically illustrate the flexibility with which holographic optics may be used.



(a) Eyepiece Element



(b) Objective Element

 FIGURE 36. CONSTRUCTION GEOMETRIES FOR INFRARED TELESCOPE. $\lambda_0 = 5145\text{ \AA}$.
 $\lambda_C = 10.6\text{ }\mu$

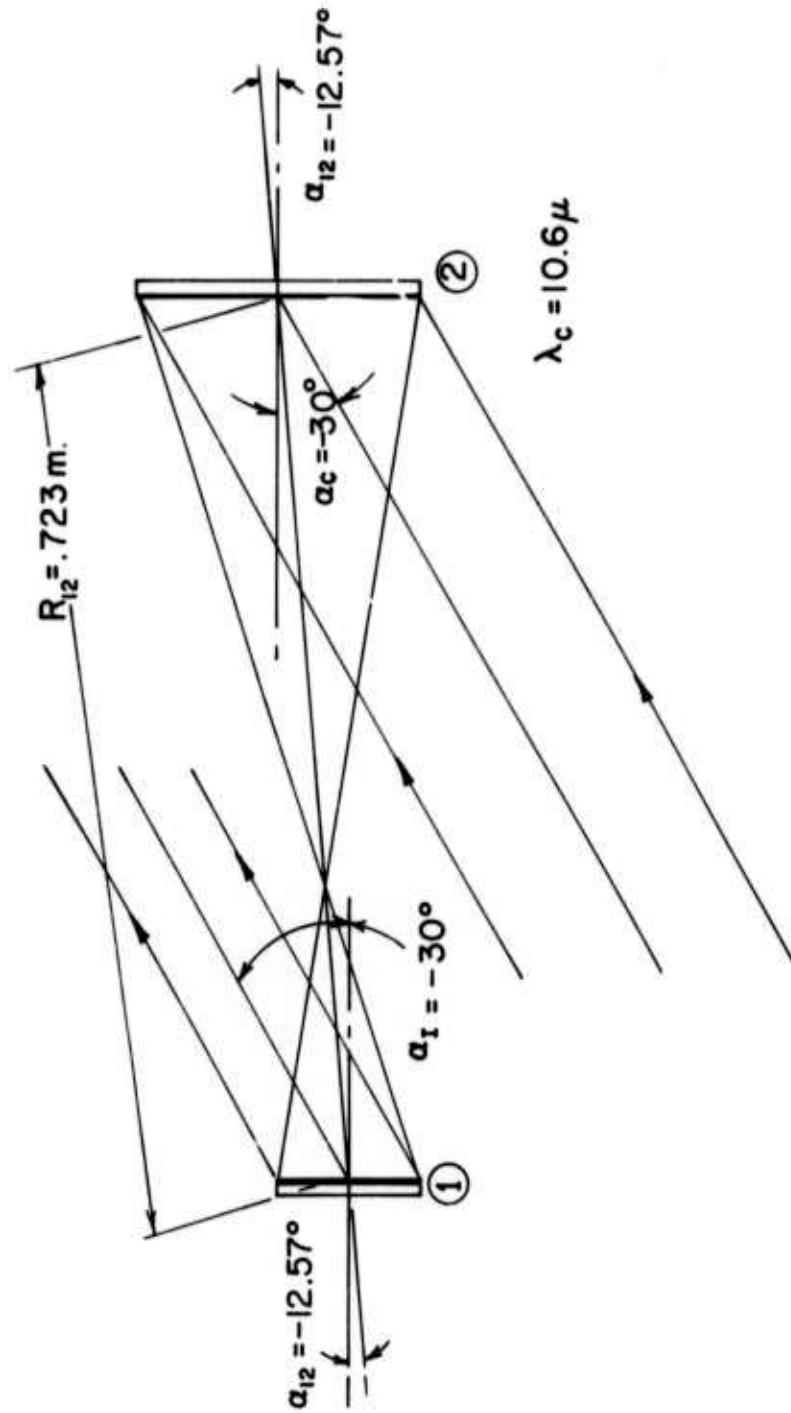


FIGURE 37. RECONSTRUCTION GEOMETRY OF INFRARED TELESCOPE AT $\lambda_c = 10.6 \mu$

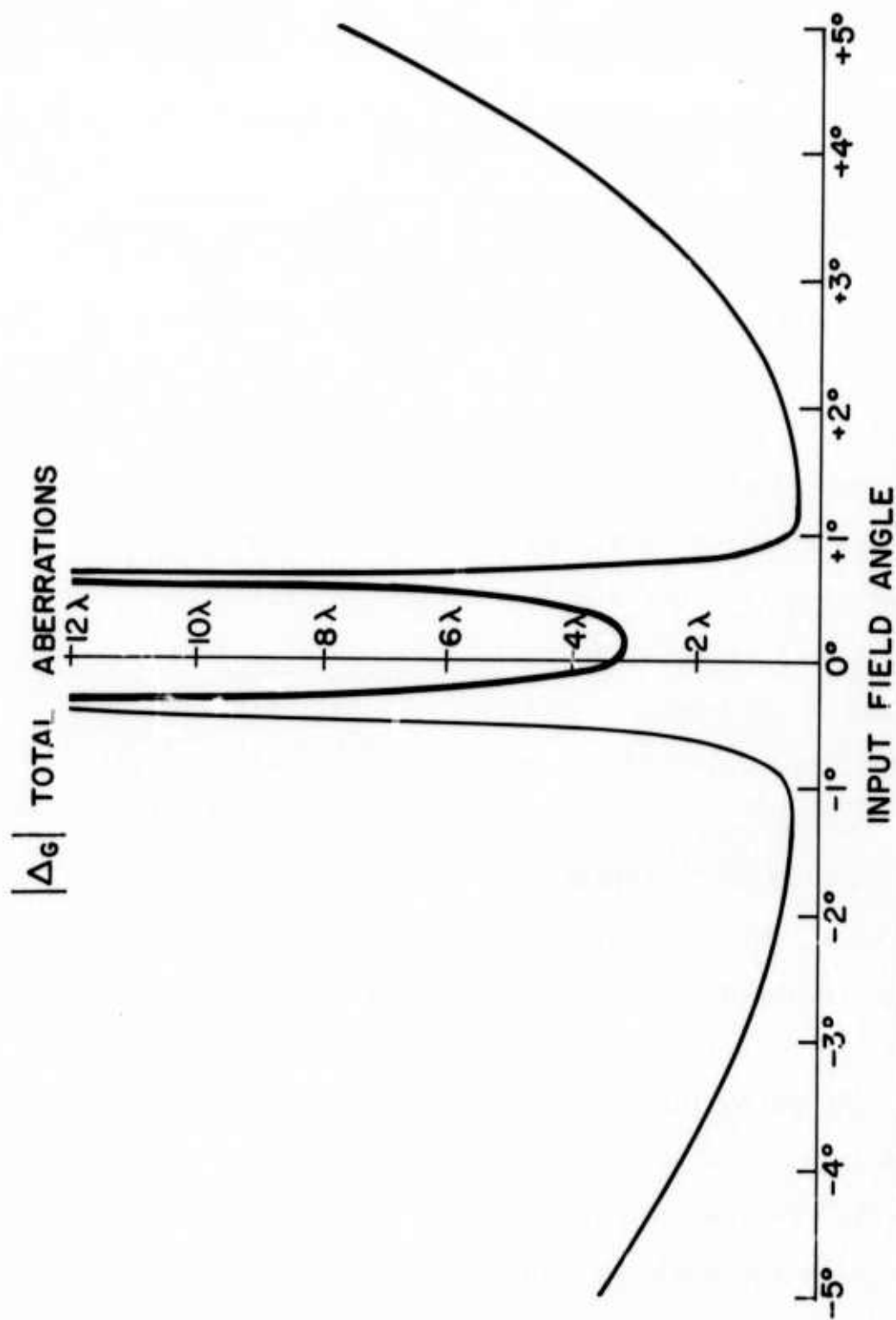


FIGURE 38. EXIT WAVEFRONT TOTAL ABERRATIONS AS A FUNCTION OF INPUT FIELD ANGLE AT $\lambda_C = 10.6 \mu$

5
WIDE ANGLE IMAGING LENS DESIGN

In the previous sections the emphasis has been placed on a single basic design objective: telescope. This particular optical configuration is characterized by relatively limited fields of view. Even with the addition of a field lens the angle in the object field is rather limited. In an opposite sense we also explored the possibilities of a wide angle lens design. The design objective was a system that used reflective elements, was focused at infinity, and operated at $f/20$. Further, we attempted to design for a half-field of 30° , however, the practical maximum which was realized was 15° .

5.1 DESIGN AND PERFORMANCE

As a result of several design iterations the following design parameters were established as shown in Figure 39 and Table 4 for the lens objectives given above. The light ray paths for angles of $\alpha_c = 0^\circ$, 10° and -15° are shown in Figures 40a, 40b, and 40c. The limitation at $\alpha_c = +10^\circ$ is due to excessive field curvature and image aberration for angles greater than this. Imaging the orthogonal object angle, i.e., β_c , can easily be done from -15° to $+15^\circ$.

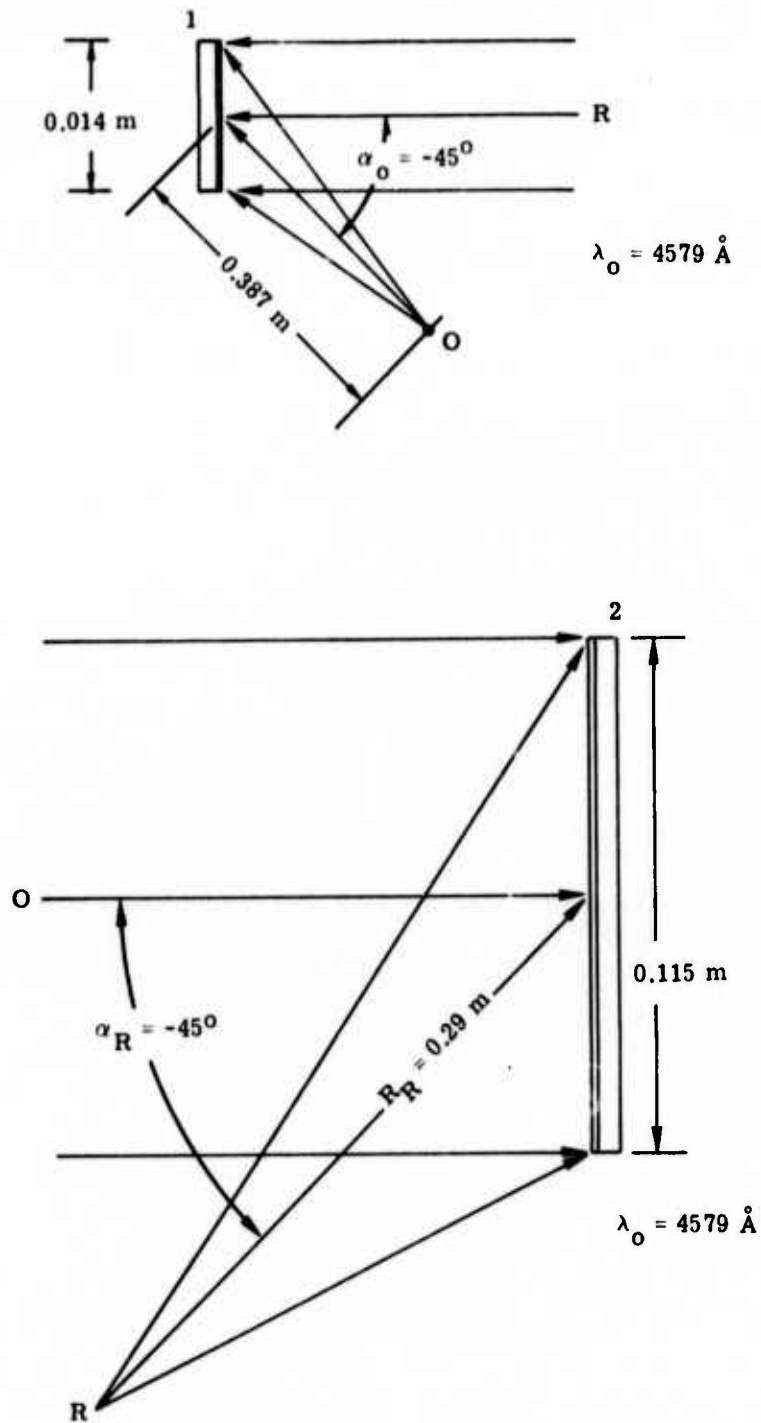


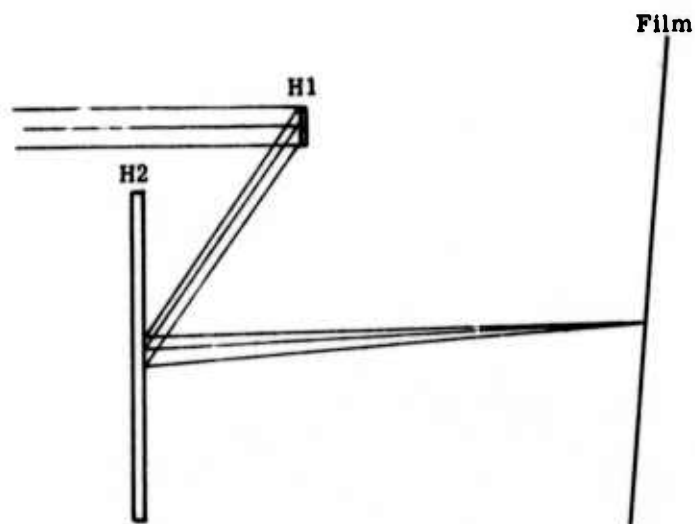
FIGURE 39. CONSTRUCTION GEOMETRIES FOR THE TWO ELEMENT WIDE ANGLE IMAGING LENS. $\lambda_o = 4579 \text{ \AA}$

TABLE 4
WIDE ANGLE IMAGING LENS CONSTRUCTION
AND RECONSTRUCTION GEOMETRY PARAMETERS

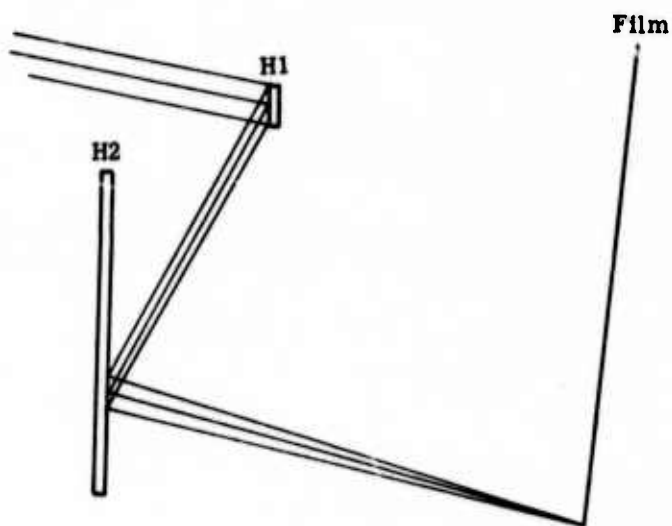
HOL 1: $\alpha_O = -45^\circ$, $R_O = 0.387$ m
 $\alpha_R = 0$, $R_R = +\infty$
 $D = .014$ m

HOL 2: $\alpha_O = 0$, $R_O = 0.181$ m
 $\alpha_R = -45^\circ$, $R_R = 0.290$ m
 $D = .115$ m
ORDER = -1
 $\lambda_O = .4579$ μm

SYSTEM: $\alpha_{12} = -55^\circ$, $R_{12} = .097$ m
 $\lambda_C = .4579$ m
 $R_C = +\infty$

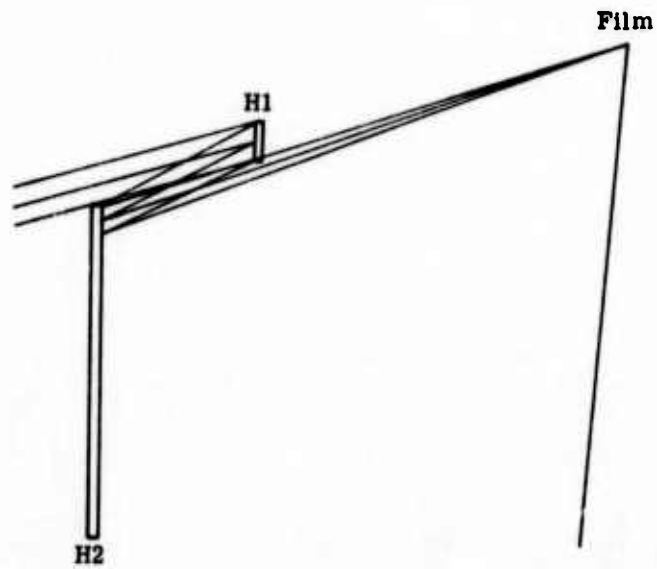


(a) $\alpha_C = 0^\circ$



(b) $\alpha_C = 10^\circ$

FIGURE 40. RECONSTRUCTION LIGHT RAY PATHS FOR THE TWO ELEMENT HOLOGRAPHIC WIDE ANGLE LENS

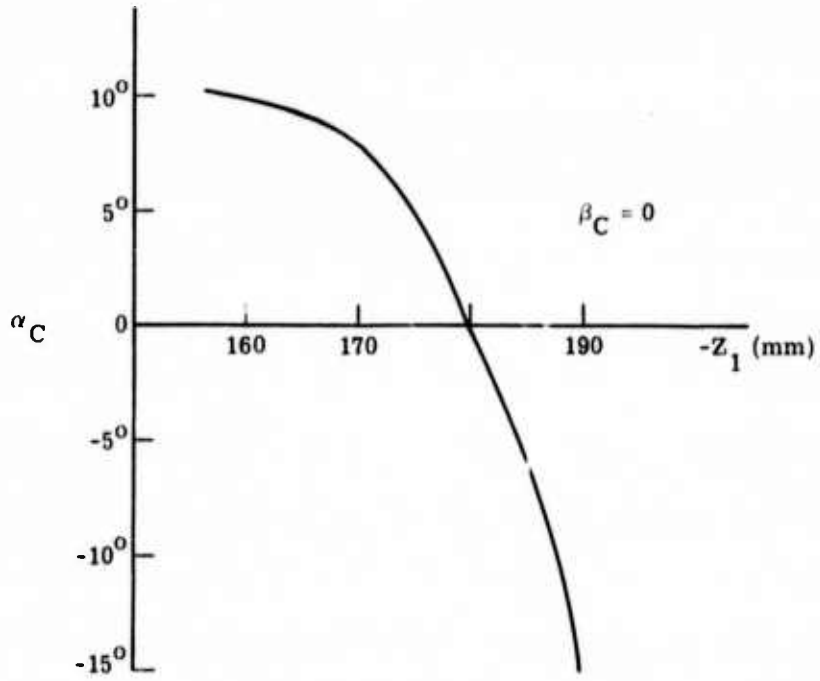


(c) $\alpha_C = -15^\circ$

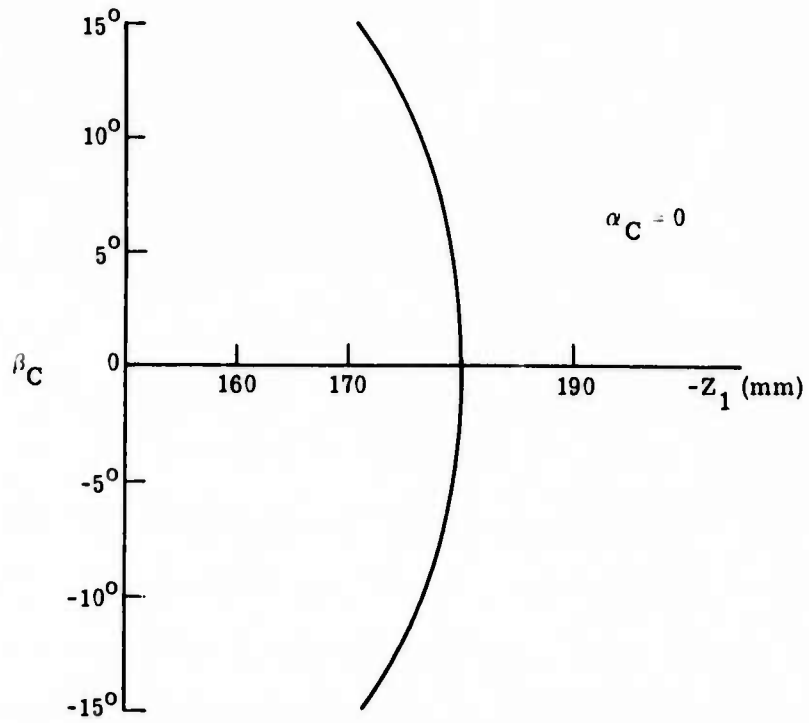
FIGURE 40. RECONSTRUCTION LIGHT RAY PATHS FOR THE TWO ELEMENT HOLOGRAPHIC WIDE ANGLE LENS (Concluded)

Figures 41a and 41b show the image location Z_I as a function of field angles α_C and β_C , respectively. In the β direction, there is a considerable amount of field curvature symmetrically arranged about $\beta_C = 0$. For sharp focus across the entire field with a flat film, the depth of focus would have to be ± 5 mm, about an order of magnitude greater than can be expected for an $f/20$ system. In the α direction, there is less field curvature for $\alpha_C < 7.5^\circ$, but the image plane is tilted by about 5° . This is due to the change in system focal length caused by changes in the distance rays travel between holograms for different field angles α_C . Although this problem exists for conventional optical systems, it is aggravated by the dispersive nature of the holographic optical elements. In addition to field curvature, this lens design also suffers from barrel distortion.

Still more distortion is introduced by the nonlinear variation in creep on Hologram 2 with changes in α_C . This has the effect of causing the image plane to be larger in the x-dimension than in the y-dimension for the same range of α_C and β_C . In this design, such distortion is considerable, causing the image plane to be elongated in a 3:2 ratio.



(a) As a Function of α_C



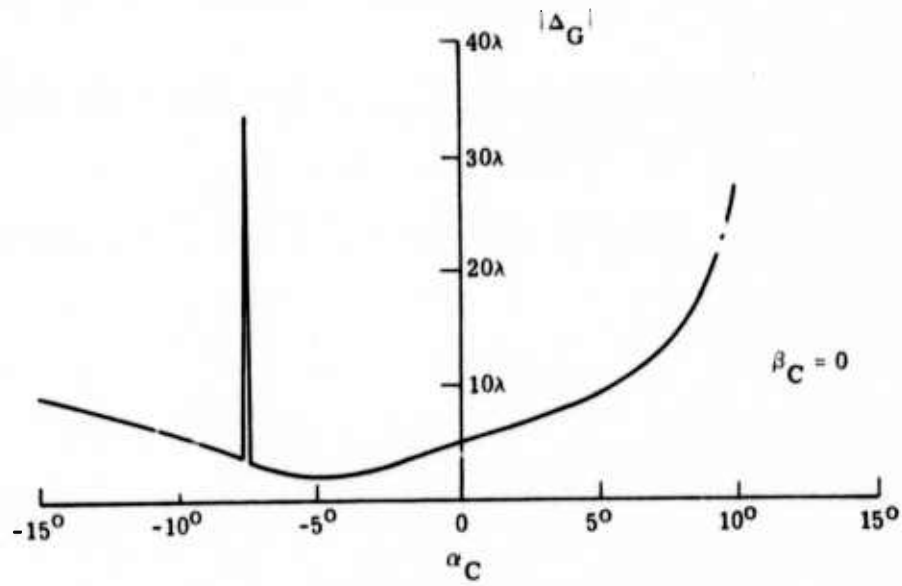
(b) As a Function of β_C

FIGURE 41. IMAGE LOCATION Z_1 FOR THE TWO ELEMENT LENS

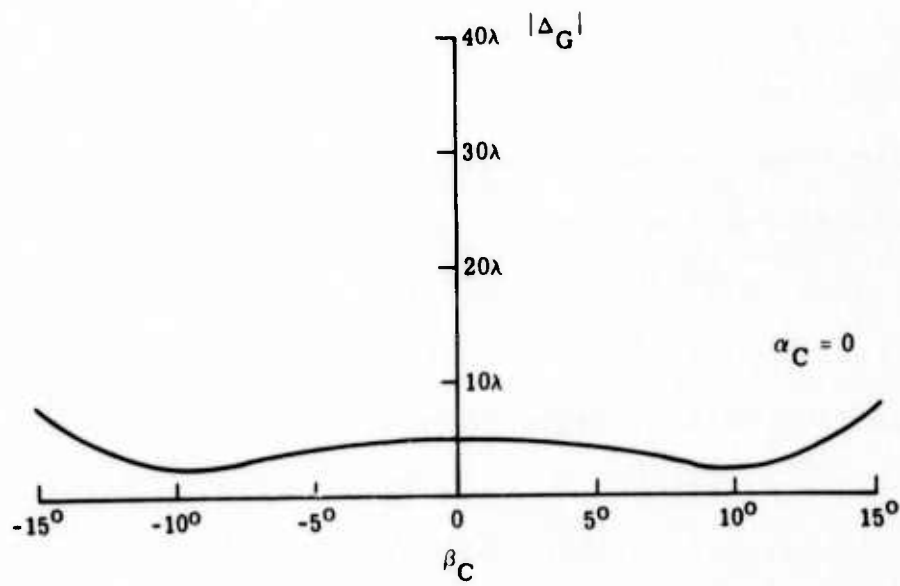
Figures 42a and 42b show the total wavefront aberrations as a function of α_C and β_C , respectively. With the exception of an anomaly at $\alpha_C = -7.5^\circ$, the aberrations are less than 15λ for $\alpha_C \leq 8^\circ$, and are less than 8λ for the entire range of β_C . Astigmatism and coma are the dominant terms.

A multielement holographic lens system intended to work over a relatively large field-of-view must be carefully designed so that unwanted diffracted or undiffracted orders do not reach the image plane. High offset angles, volume holograms, and suitably located stops can be used to minimize the problem, but may reduce the lens performance in other respects. Although an offset angle of 45° was chosen for the elements of the lens described here, it can be seen in Figure 40c that the reflected zero order from Hologram 2 will strike the film.

Other geometric configurations considered were limited by aberrations of several hundred wavelengths. These configurations included rotation of Hologram 2 by 45° or 90° with respect to Hologram 1, and specification of equal but opposite bending factors for the holograms. Only the parallel configuration with dimensions close to those



(a) As a Function of α_C



(b) As a Function of β_C

FIGURE 42. WAVEFRONT ABERRATIONS, $|\Delta_G|$, FOR THE TWO ELEMENT WIDE ANGLE IMAGING LENS

of the final system had low aberrations. In fact, an evaluation of Champagne's equations² for this system showed astigmatism coefficients that were very nearly equal but opposite for the two holograms, indicating that the relatively low aberrations are due to compensation by the two holograms in the parallel configuration.

The dimensions were chosen so that the image would fit approximately onto 4 inch film. The actual image size in the β direction for a 30° field-of-view is 0.171 m, or 6.93 inches. The dimensions can all be reduced by a scale factor to cover smaller film sizes.

This analysis can only be considered as a preliminary approach to the problem of designing a wide angle lens using holographic lens elements. Although the aberrations are probably tolerable for many applications, the field curvature and distortion are probably too great for most applications. It may be possible to reduce the aberrations still further by slight modification of the geometric parameters to provide even better aberration compensation by the two elements. Image distortion may be reduced by locating a stop between the lens elements, and by altering the relative positions of the two elements. It

² Champagne, E. B., A Qualitative and Quantitative Study of Holographic Imaging, Ph.D. Thesis, Ohio State University, Columbus, Ohio, July 1967 (Univ. Microfilms No. 67-10876).

may be possible to reduce the field curvature by increasing the symmetry of the bending factors of the elements, although this may greatly increase the lens aberrations.

The 30° field-of-view is not very large for a wide angle lens. It nevertheless seems unlikely that the field-of-view can be increased significantly in the α direction for a system employing two thin hologram elements operating in the reflective mode. A true wide angle design employing a multielement holographic lens system may not be possible even in transmission, however, because of the problem of preventing unwanted orders from reaching the image plane for all field angles.

6
LARGE APERTURE HOLOGRAM OPTICAL ELEMENT

One part of this effort was to investigate the fabrication of large aperture hologram optical elements. This was done in two ways. The first was to implement a general means by which large aperture elements can be made with few geometric constraints and can also be used in optical systems. The second was the letting of a subcontract to Radiation, Inc. for the fabrication of a specific element. The emphasis was placed here on the material aspects and producibility of these elements. This latter work is given in Appendix A.

6.1 DESIGN

The design of this element was quite straightforward. The parameters are shown in Figure 43.

6.2 FABRICATION

The optical element was made on an 11" x 11" x 1/4" Kodak 649F microflat plate. The plate was exposed to two point sources of light as shown in Figure 43. In the vertical direction the points were centered on the plate. After an exposure of 1500 ergs/cm^2 by $5145\overset{\circ}{\text{A}}$ argon laser

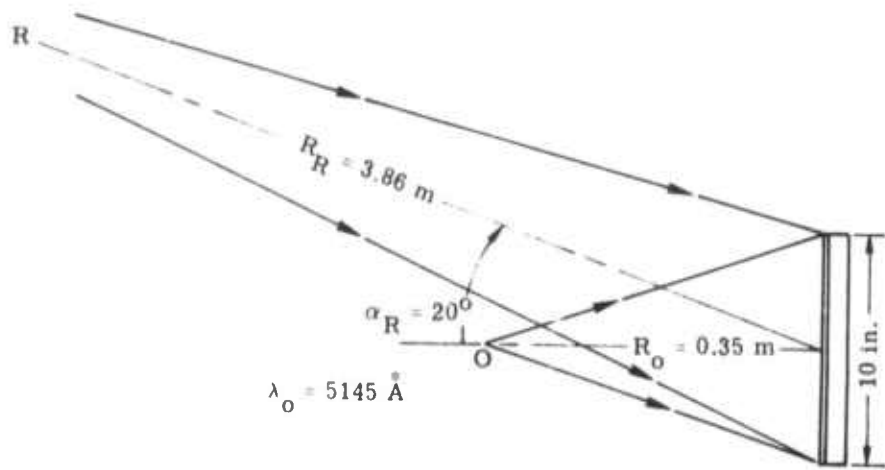


FIGURE 43. CONSTRUCTION GEOMETRY FOR LARGE APERTURE HOLOGRAPHIC ELEMENT

light, the plate was developed for 6 minutes in Kodak D-19 developer, fixed and marked. It was then bleached until clear in a solution of 6.3 gm of $K_3Fe(CN)_6$ (potassium ferricyanide) per liter of water. The plate was then washed for 10 minutes in flowing water and dried.

The element had the same efficiency as the smaller elements, about 35%. When replaced in the original position and illuminated as in the recording process, the resulting interference pattern showed about two wavelengths of wavefront deformation. Figure 44 shows the hologram mounted in a plateholder for reconstruction.

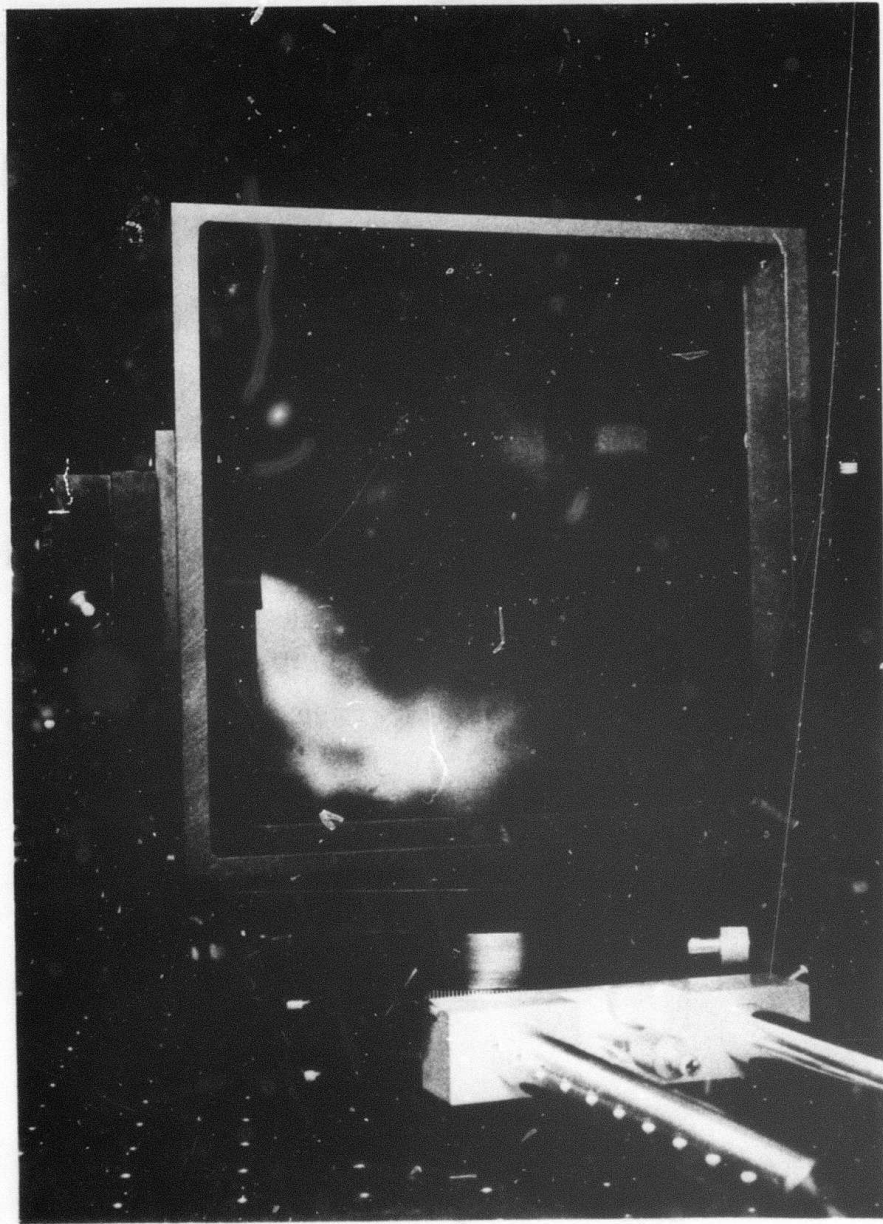


FIGURE 44. PHOTOGRAPH OF LARGE APERTURE ELEMENT

7
SINGLE HOLOGRAM ELEMENT PROPERTIES

In an effort to better understand the effects of various hologram design parameters on the imaging properties of multiple element hologram optical systems, a study of single hologram elements was begun. A few key design parameters were chosen from previous experience for a study of their mutual effect on the imaging of a single hologram element. The results of this study are indeed significant and have made possible the design of the large wavelength-shift hologram optics discussed elsewhere in this report.

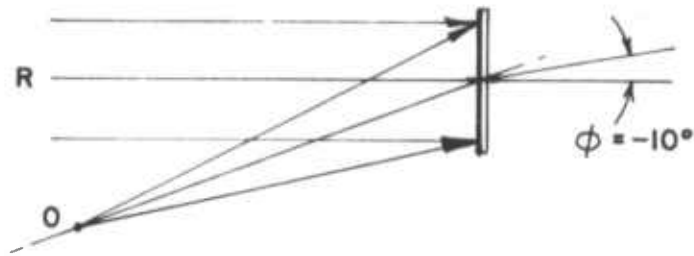
7.1 SELECTION OF STUDY PARAMETERS

A first step in the design of any optical system, or for that matter any other type of system, is the separation of parameters which the designer can readily control. In the case of hologram optics, although a large number of variables have been included in the design model such as emulsion thickness, emulsion index, and media index, in practice only a few parameters such as construction beam geometries, construction wavelengths and reconstruction

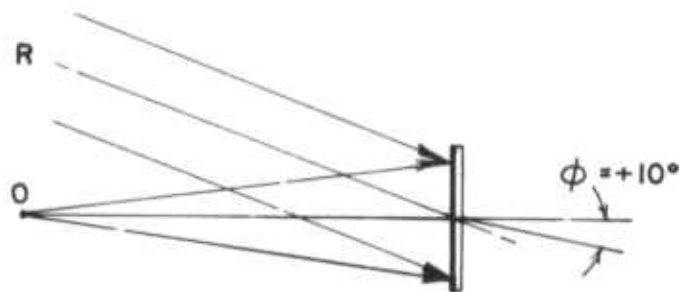
wavelengths are easily manipulated. Even the very promising areas of curved surface and conformal hologram optics are severely hampered by the current state-of-the-art of emulsion coating and fabrication.

With this in mind, a selection of relevant parameters for a single hologram optical element was made. Three construction parameters were ultimately chosen for study; bisector angle, Q factor, and μ factor. The first parameter, bisector angle, involves some slightly new notation. Basically the bisector angle is defined as the angle formed by the normal to the photographic emulsion and the bisector of the object and reference beam axes during construction. The sign of the bisector angle is defined in the same manner as that of the construction and reconstruction beams. Figure 45 shows three geometries illustrating different bisector angles. The Q factor and μ factor have been defined in previous reports but are reiterated here for clarity.³ The Q factor, or "bending factor," relates the wavefront curvature of the object and reference beam as follows:

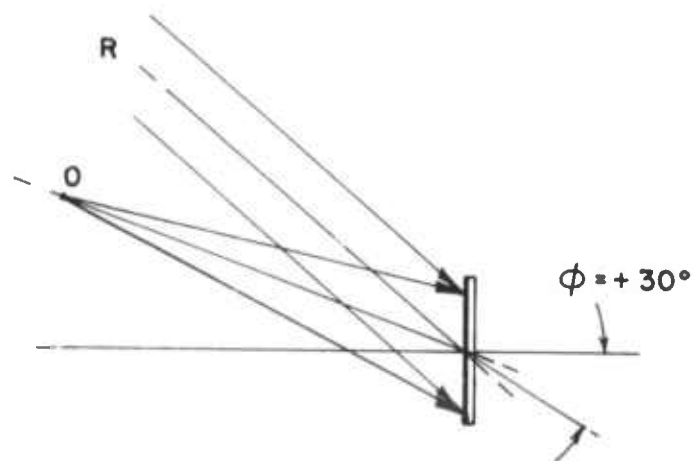
³Latta, J. N., Computer-Based Analysis of Holography, Ph.D. Thesis, The University of Kansas, Lawrence, Kansas, December 1970.



(a) $\phi = -10^\circ$



(b) $\phi = +10^\circ$



(c) $\phi = +30^\circ$

FIGURE 45. REPRESENTATIVE CONSTRUCTION GEOMETRIES FOR $Q = 1$

$$Q = \frac{R_R + R_O}{R_R - R_O}$$

where R_R and R_O are the radial point source distances for the reference and object beams, respectively. It will be noted that for the case of a plane wave reference beam, i.e., $R_R = \infty$, the Q factor is just 1. In general, since the roles of object and reference beams are interchangeable, the reference beam radius will always be assumed longer than the object beam radius resulting in Q factors which are always greater than 1. The μ factor relates construction and reconstruction wavelengths as follows:

$$\mu = \frac{\lambda_C}{\lambda_O}$$

where λ_C is the reconstruction wavelength and λ_O is the construction wavelength. All that remains to be defined is a criterion of merit. Inasmuch as we are interested in having good imaging characteristics as a holographic lens we have chosen on-axis aberrations as our criterion.

Having defined the parameters of interest and a performance criterion, the single element study results will be outlined. The basic approach was to allow the bisector angle to vary between plus and minus thirty degrees for a given Q factor and μ factor. It should be noted that the

angle between object and reference beams has been fixed at twenty degrees and that the Greek letter ϕ has been used to denote bisector angle. Basically four cases have been examined as shown in Table 5.

7.2 CASE 1: $Q = 1$; $\mu = 1$

This case covers the most familiar geometry where the hologram is made with a point source and a plane wave, i.e., $Q = 1$, and the reconstruction wavelength is the same as the construction wavelength, i.e., $\mu = 1$. This case is actually somewhat degenerate in the sense that the on-axis aberrations are always zero regardless of bisector angle ϕ . In an effort to gain some information from this case the performance criterion has been extended to include the aberrations inherent at the edge of an arbitrarily chosen $\pm 5^\circ$ field-of-view. Figure 46 shows a plot of this aberration as a function of bisector angle ϕ . As may be readily seen, the full field maximum aberrations are reduced significantly for $\phi = +10^\circ$. Referring back to Figure 45b it is seen that this corresponds to having the object beam axis coincide with the normal to the emulsion.

TABLE 5
LIST OF THE IMPORTANT CASES TO BE ANALYZED
IN THE SINGLE HOLOGRAM ELEMENT PROPERTIES STUDY

Case 1: $-30^{\circ} \leq \phi \leq 30^{\circ}$, $Q = 1$, $\mu = 1$

Case 2: $-30^{\circ} \leq \phi \leq 30^{\circ}$, $Q = 2$, $\mu = 1$

Case 3: $-30^{\circ} \leq \phi \leq 30^{\circ}$, $Q = 1$, $\mu = 1.23$

Case 4: $-30^{\circ} \leq \phi \leq 30^{\circ}$, $Q = 2$, $\mu = 1.23$

where $\mu = 1.23$ corresponds to a $\lambda_C = 6328\text{\AA}$ and
 $\lambda_0 = 5145\text{\AA}$

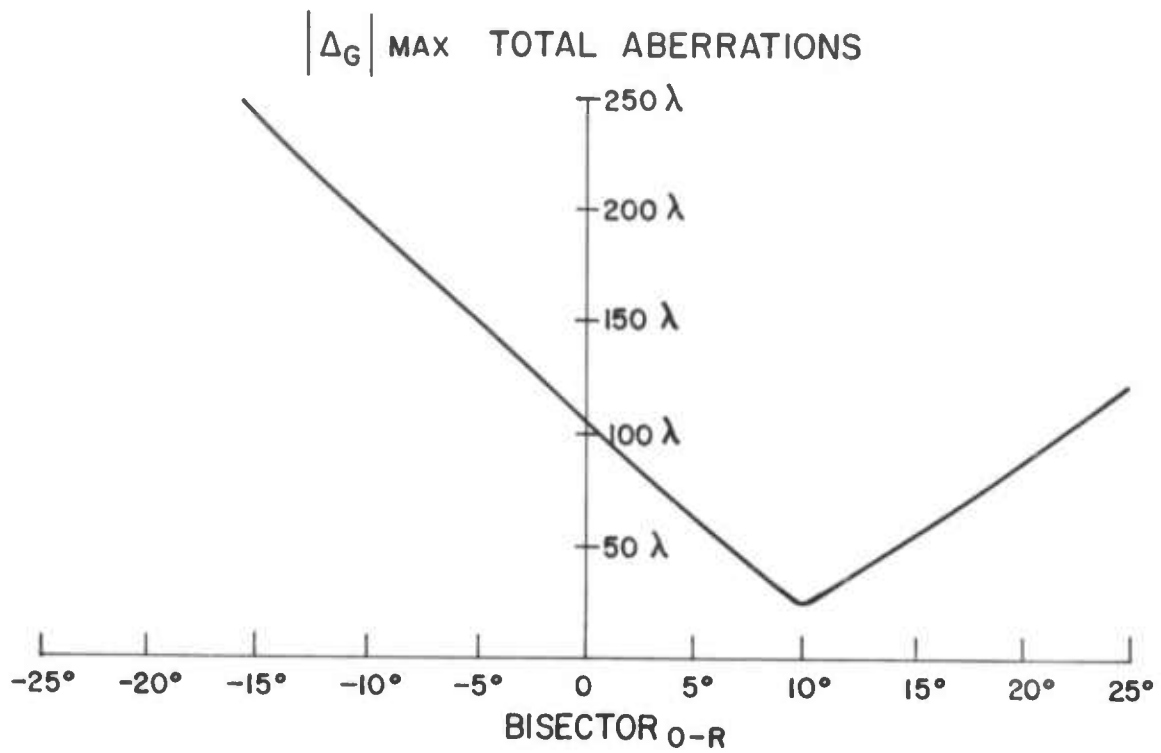
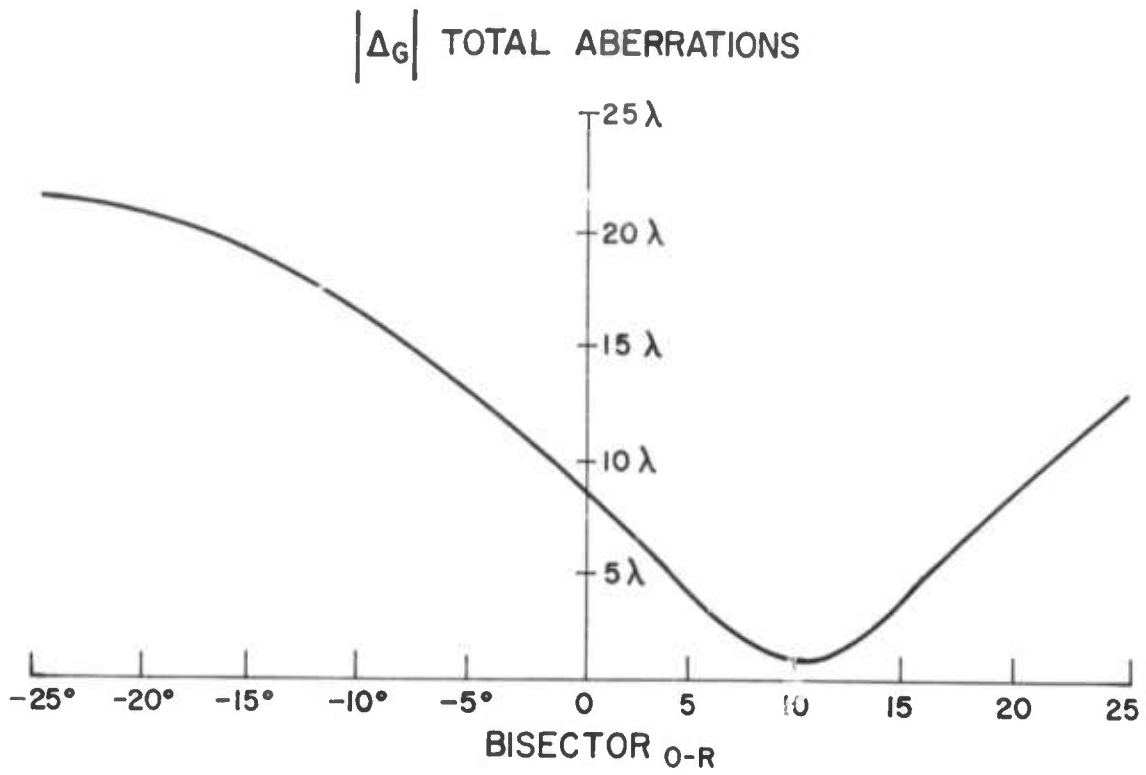
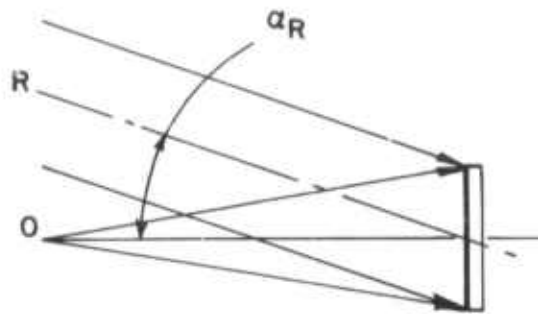


FIGURE 46. MAXIMUM TOTAL ABERRATIONS ACROSS A $\pm 5^\circ$ FIELD FOR $Q = 1$, AND $\mu = 1$

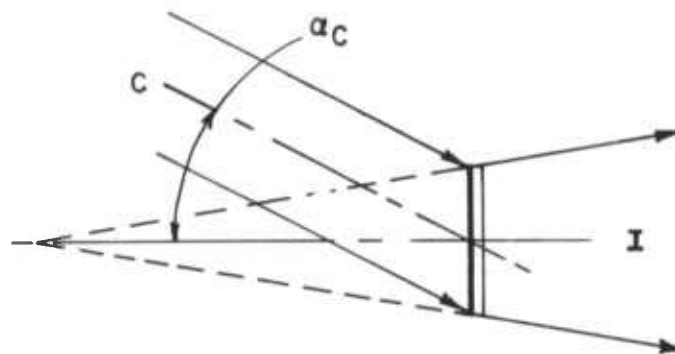
7.3 CASE 2: $Q = 1, \mu = 1.23$

This case is similar to Case 1 except that now the reconstruction wavelength is different from the construction wavelength. The wavelengths chosen for this study were a construction wavelength λ_0 of 5145Å, and a reconstruction wavelength $\lambda_C = 6328\text{Å}$. These particular wavelengths were chosen to facilitate experimental verification of the study results. As may be seen from Figure 47, the total on-axis aberrations are less than one wavelength when the bisector angle is $+10^\circ$. As in Case 1, this corresponds to having an on-axis object beam. It should be noted that in this and the following cases, it is necessary to optimize the reconstruction beam angle for each point on the curve. In other words, once ϕ , Q , and μ are specified, the reconstruction angle is optimized for lowest aberrations. In most cases this optimum reconstruction beam angle will not coincide with the construction reference beam. It was noted during the evaluation of this case that at the optimum bisector angle, namely $\phi = +10^\circ$, the optimum reconstruction angle was such to produce an image beam coinciding with the construction object beam. This result is perhaps better explained by Figure 48 which shows the optimum construction and reconstruction geometries. To better understand the

FIGURE 47. TOTAL ABERRATIONS FOR CASE 2, $Q = 1$ AND $\mu = 1.23$



(a) Construction



(b) Reconstruction

FIGURE 48. OPTIMUM CASE 2 GEOMETRIES SHOWING INCREASED RECONSTRUCTION/ANGLE α_C

types of aberrations present in the total aberrations of Figure 47, a breakdown into the primary aberration components has been given in Figure 49. Clearly both coma and astigmatism aberrations are minimized at $\phi = +10^\circ$.

7.4 CASE 3: $Q = 2, \mu = 1$

A Q-factor of two was chosen for this case, i.e. reference and object beams both point sources such that

$$Q = \frac{R_R + R_O}{R_R - R_O} = 2$$

In addition $\mu = 1$, meaning that the reconstruction wavelength is the same as the construction wavelength. Examination of the total aberrations plotted in Figure 50 for this case reveals a substantially greater amount of aberration at optimum ϕ . A further examination of the primary aberrations plotted in Figure 51 reveals the reason for the higher inherent total aberrations of this configuration. Although both the astigmatism and coma aberrations attain low levels for some given bisector angle, the separation of these minima results in an overall higher total aberration. It is interesting to note that the optimum configuration for $Q = 2$ and $\mu = 1$ constraints is a bisector angle of approximately 0° or in

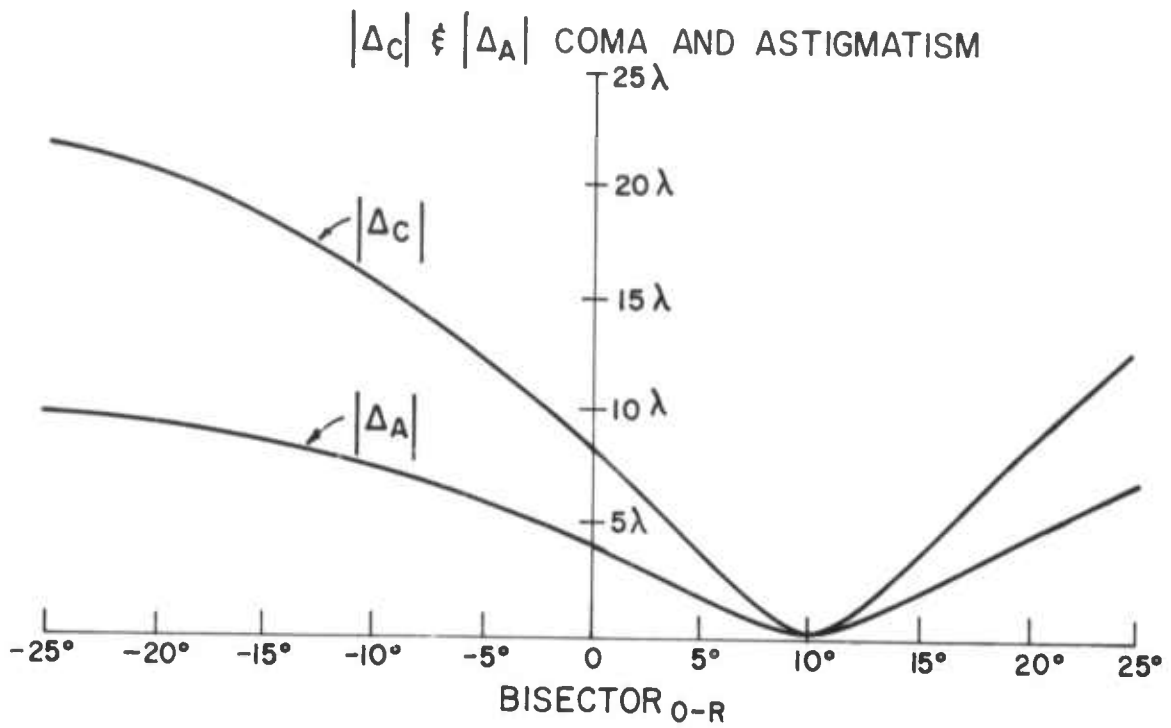


FIGURE 49. COMPONENT ABERRATIONS FOR CASE 2

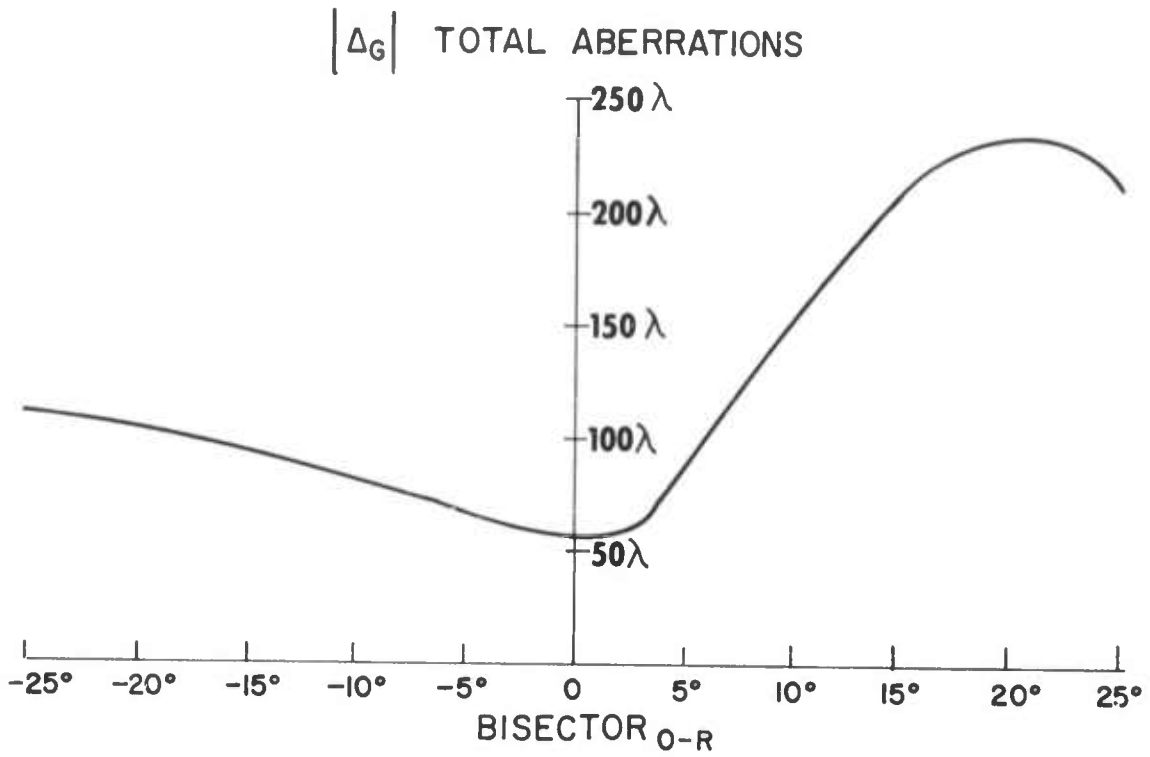


FIGURE 50. TOTAL ABERRATIONS FOR CASE 3, $Q = 2$ AND $\mu = 1$

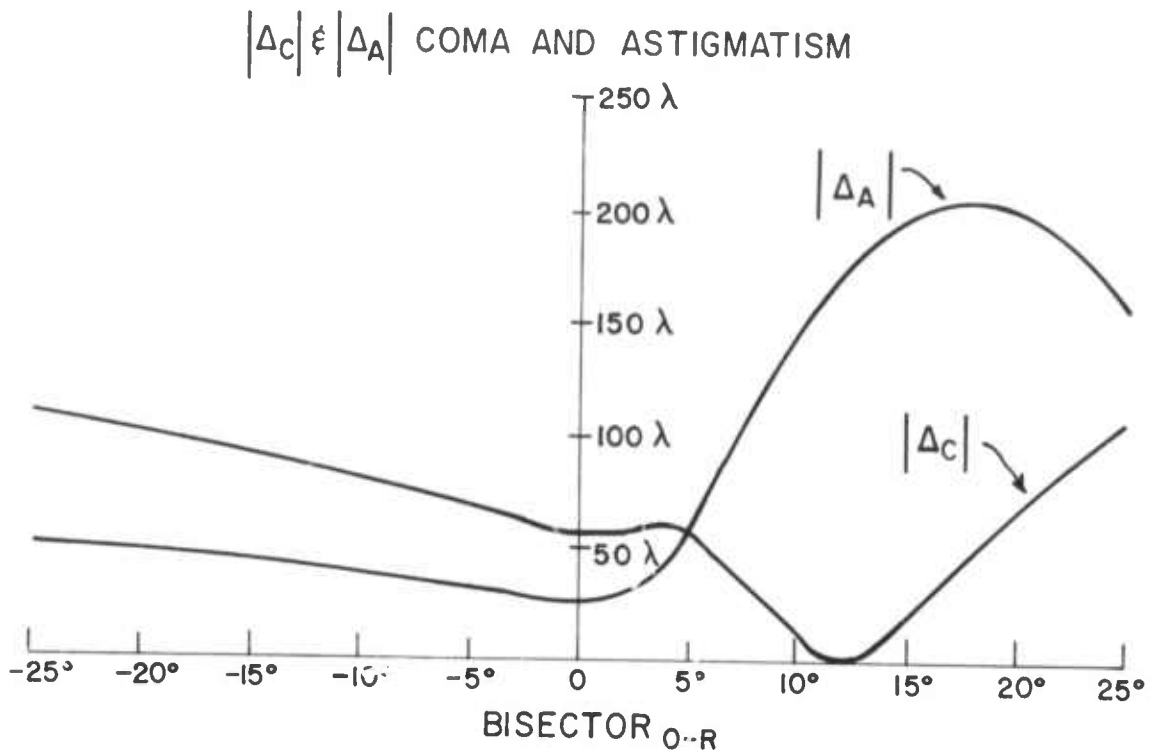


FIGURE 51. COMPONENT ABERRATIONS FOR CASE 3

other words, object and reference beams forming equal but opposite angles with the normal to the emulsion.

7.5 CASE 4: $Q = 2$, $\mu = 1.23$

This case is similar to Case 3 with the exception that the reconstruction wavelength is greater than the construction wavelength. Comparison of the total aberrations for this case, shown in Figure 52, with the results obtained in the previous Case 3, reveals that the aberration curves are very similar. There is one significant difference however, the minimum aberration for Case 4 is less than the minimum for Case 3. In other words, for the $Q = 2$ condition a better performance has been attained with a wavelength shift. Looking at the component aberrations in Figure 53 reveals that both astigmatism and coma aberrations are reduced slightly for Case 4, particularly for negative values of bisector angle.

7.6 LARGE WAVELENGTH SHIFTS

At this point a little contemplation will suggest that perhaps the aberration reduction realized in Case 4 could be extended by using a larger wavelength shift. To this end an additional case was evaluated with $Q = 2$

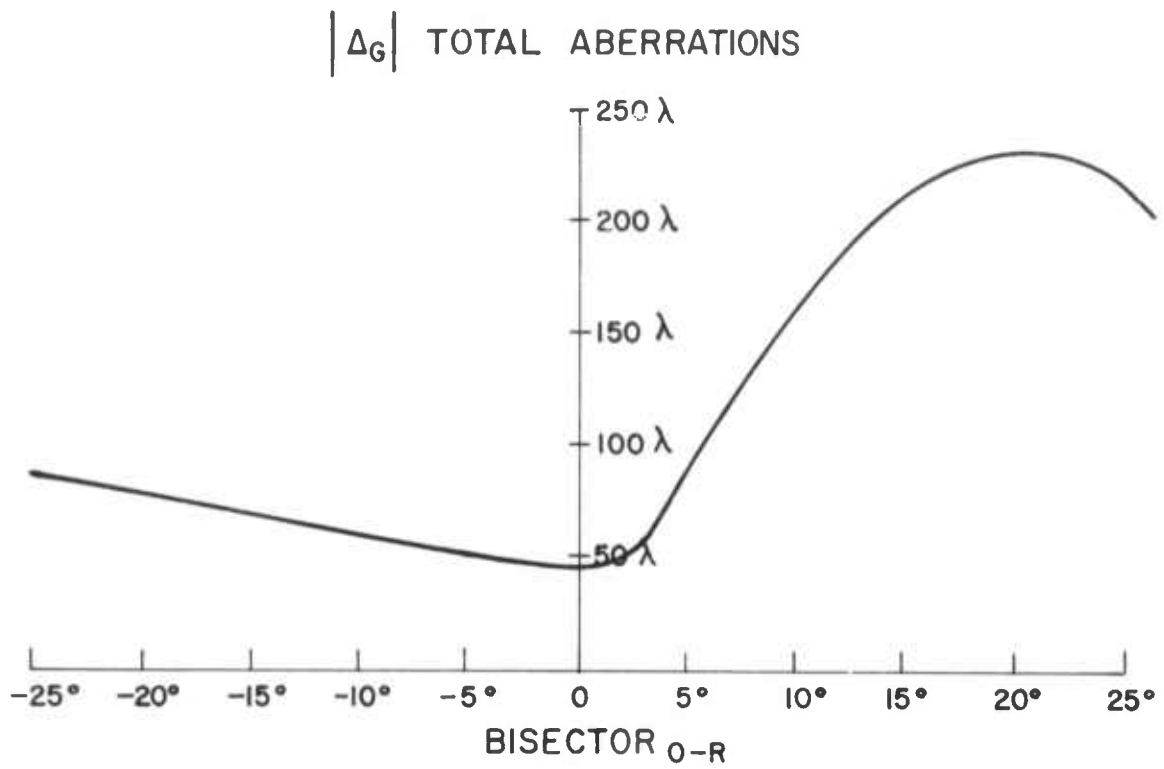


FIGURE 52. TOTAL ABERRATIONS FOR CASE 4, $Q = 2$ AND $\mu = 1.23$

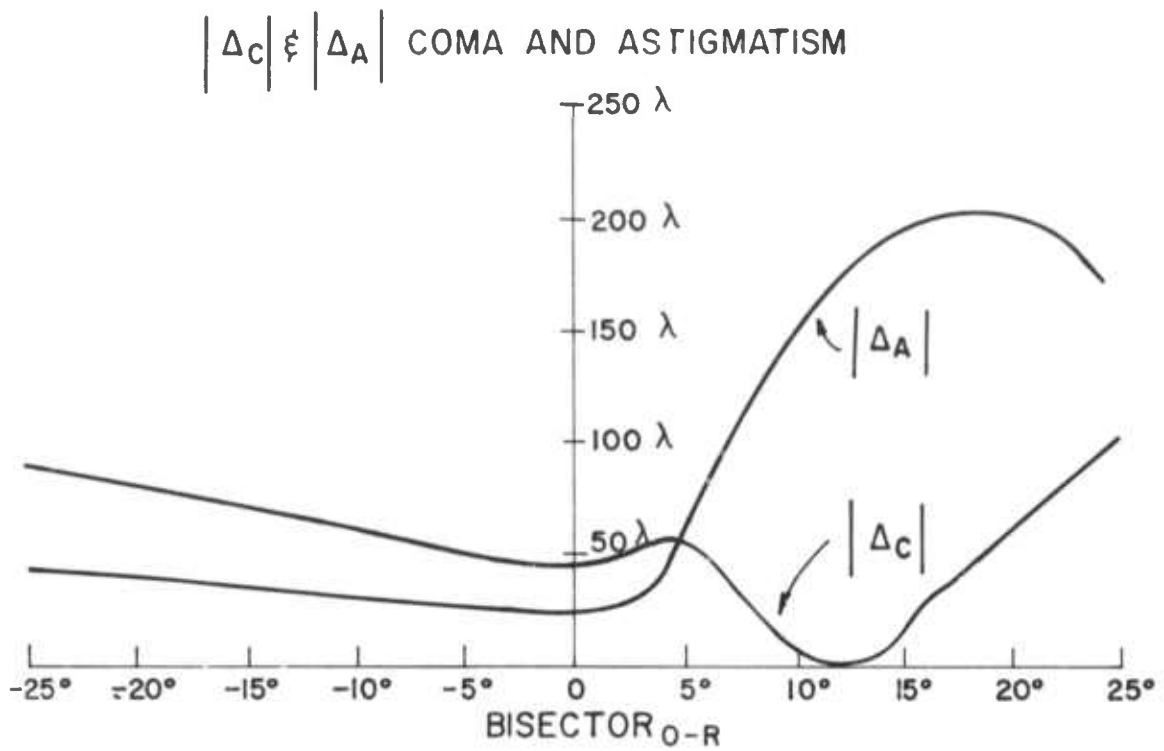


FIGURE 53. COMPONENT ABERRATIONS FOR CASE 4

and $\mu = 2.06$. The $\mu = 2.06$ factor was obtained with a construction wavelength of $5145\overset{\circ}{\text{A}}$ and a reconstruction wavelength of $10,600\overset{\circ}{\text{A}}$ or 1.06 microns, a common infrared laser wavelength. Figures 54 and 55 present the aberrations of such a case. As will immediately be seen, the total aberrations have been significantly reduced for bisector angles less than zero.

These results have opened up a whole new area for implementation of holographic optical systems which may be constructed at visible wavelengths with ordinary emulsions for use in the infrared spectrum. Further investigation has shown that by proper adjustment of the Q-factor, very large wavelength shifts may be obtained as demonstrated in the infrared telescope operating at 10.6 microns described previously.

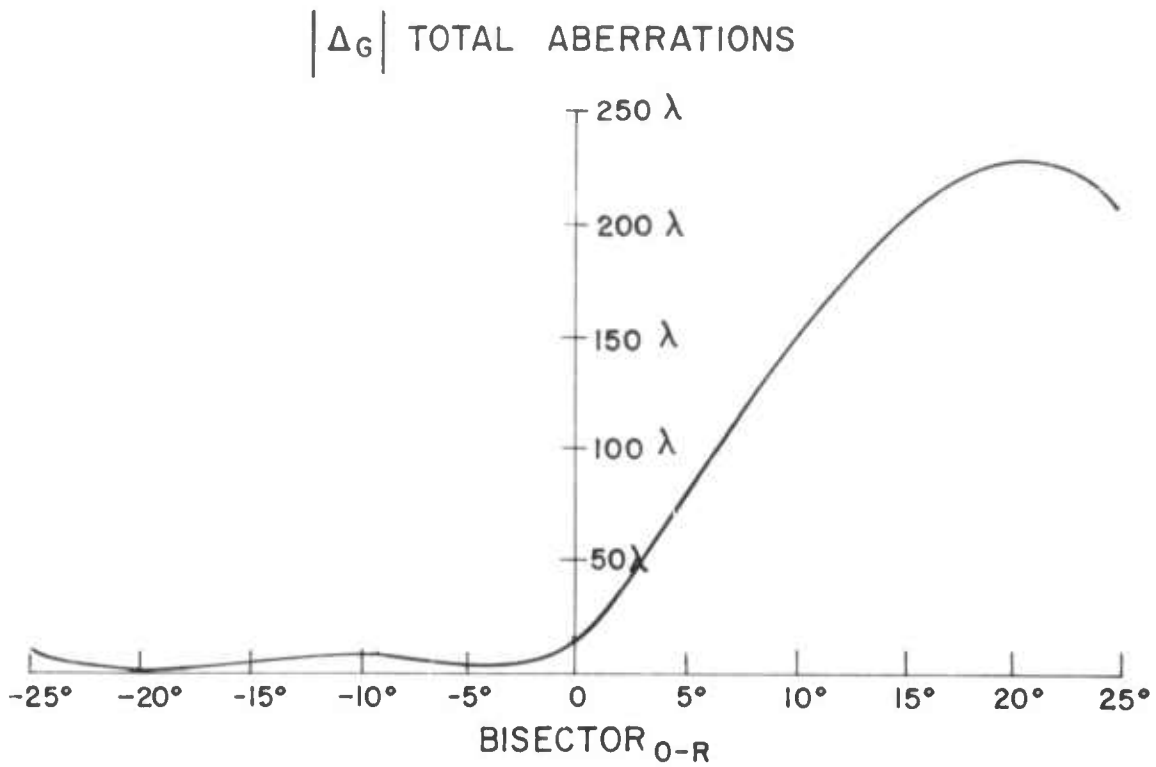


FIGURE 54. TOTAL ABERRATIONS FOR LARGE WAVELENGTH SHIFT

$|\Delta_C|$ $|\Delta_A|$ COMA AND ASTIGMATISM

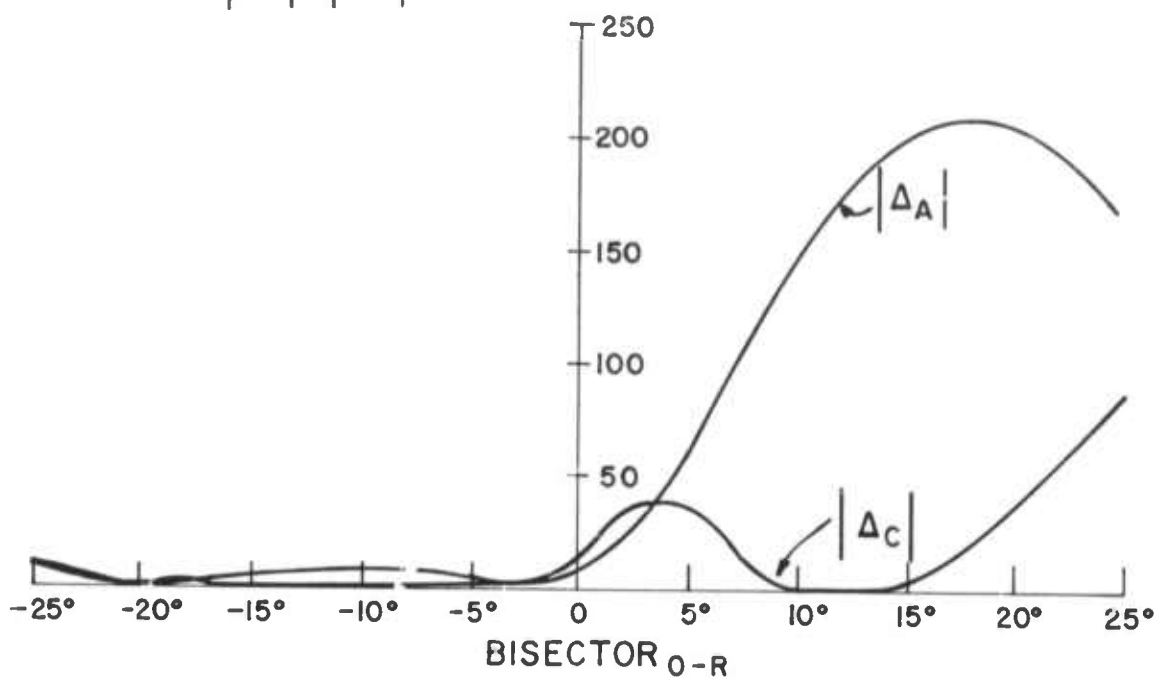


FIGURE 55. COMPONENT ABERRATIONS FOR LARGE WAVELENGTH SHIFT

8
DESCRIPTION OF FACILITIES

A basic rule of thumb with holographic optics is that if one is to obtain optical image quality on the order of the dimensions of the wavelength used to obtain the image, the construction and reconstruction tolerances will be to the same order. The same basic rule applies to conventional optics; however, both the science and art of conventional optics fabrication and assembly are well developed. In holographic optics this presents a new problem in that one must develop new methods related to the accurate recording and fabrication of holographic elements and systems. In particular the problem grows more acute as the aperture increases. These are essentially the areas which we addressed in attempting to upgrade the facilities at ERIM for use in high quality optical systems using holographic elements.

Holography is quite different from conventional optics in that a stable surface is required to fabricate the basic components of the system. This poses some problems in that a simple 10" f/10 lens requires a stable table approximately 10 feet in length for a $Q = 1$

hologram. Further the offset angle between the construction beams determines the width of the table. To meet the objectives of this effort a large stable table was purchased. It is shown in Figure 56. This table was placed in a special isolated building that has separate dark room and air conditioning facilities. The table dimensions are 8' x 16', however, with the space occupied by the lasers at the end of the table the useful space was limited to approximately 8' x 14'. In order to isolate the air currents from the room and table top a table cover was especially fabricated. During an exposure the air currents can effectively be isolated when the cover is closed. The table has six air suspension legs and is very effective in isolating any ground vibrations.

To permit the construction of large and medium aperture elements two sets of high quality off-axis collimators were purchased. These are shown in Figures 57 and 58. The large aperture collimators operate at $f/8$ and have a 10" clear aperture. A special mount was made for the large aperture mirrors to provide for accurate independent axis adjustment of the mirror.

The accurate fabrication of elements and their assembly into a system has been a continuing problem

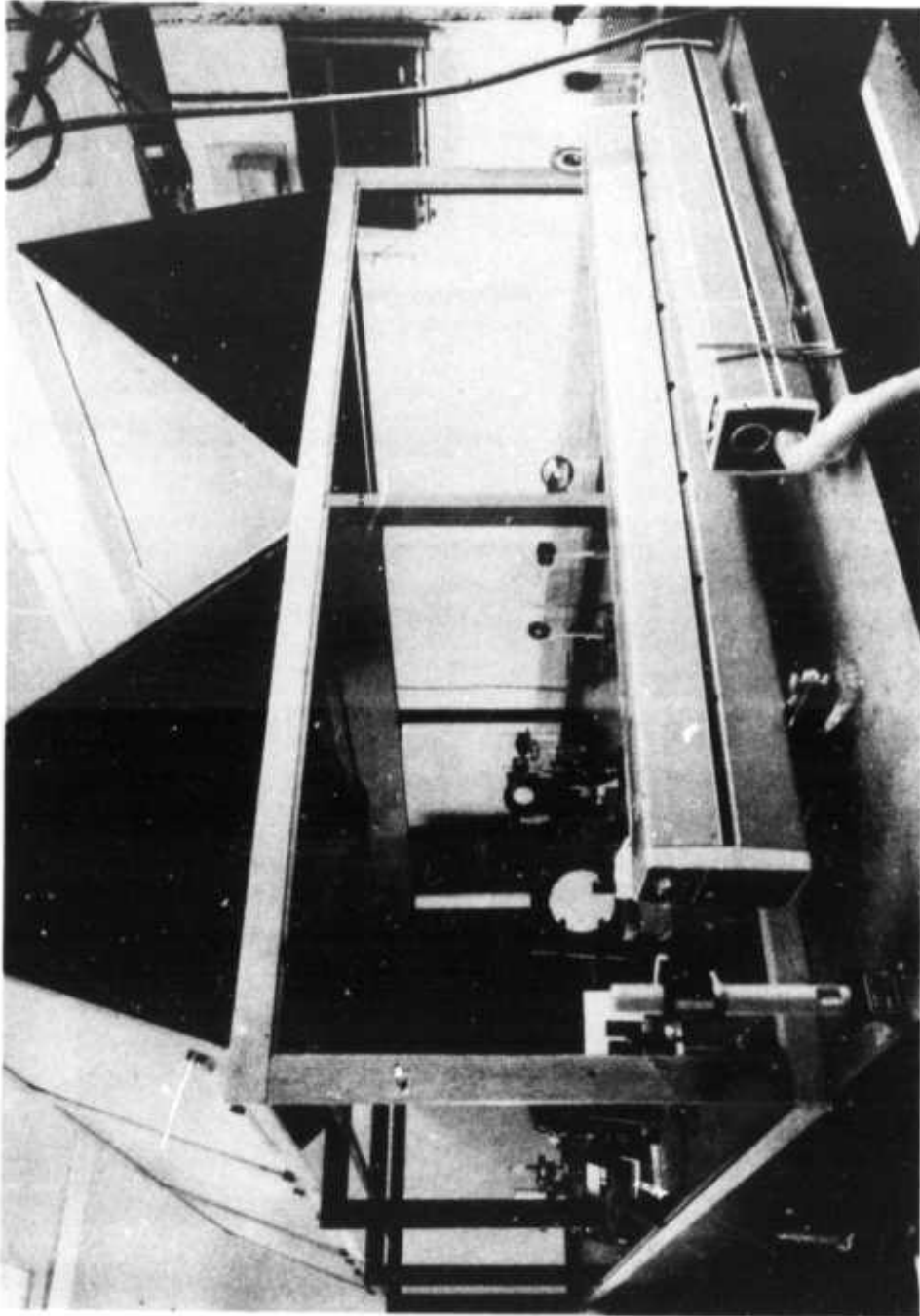


FIGURE 56. PHOTOGRAPH OF 8' x 16' STABLE TABLE WITH TWO LASERS AND ASSOCIATED OPTICAL COMPONENTS ON THE TABLE. All parts of the table cover have been raised.

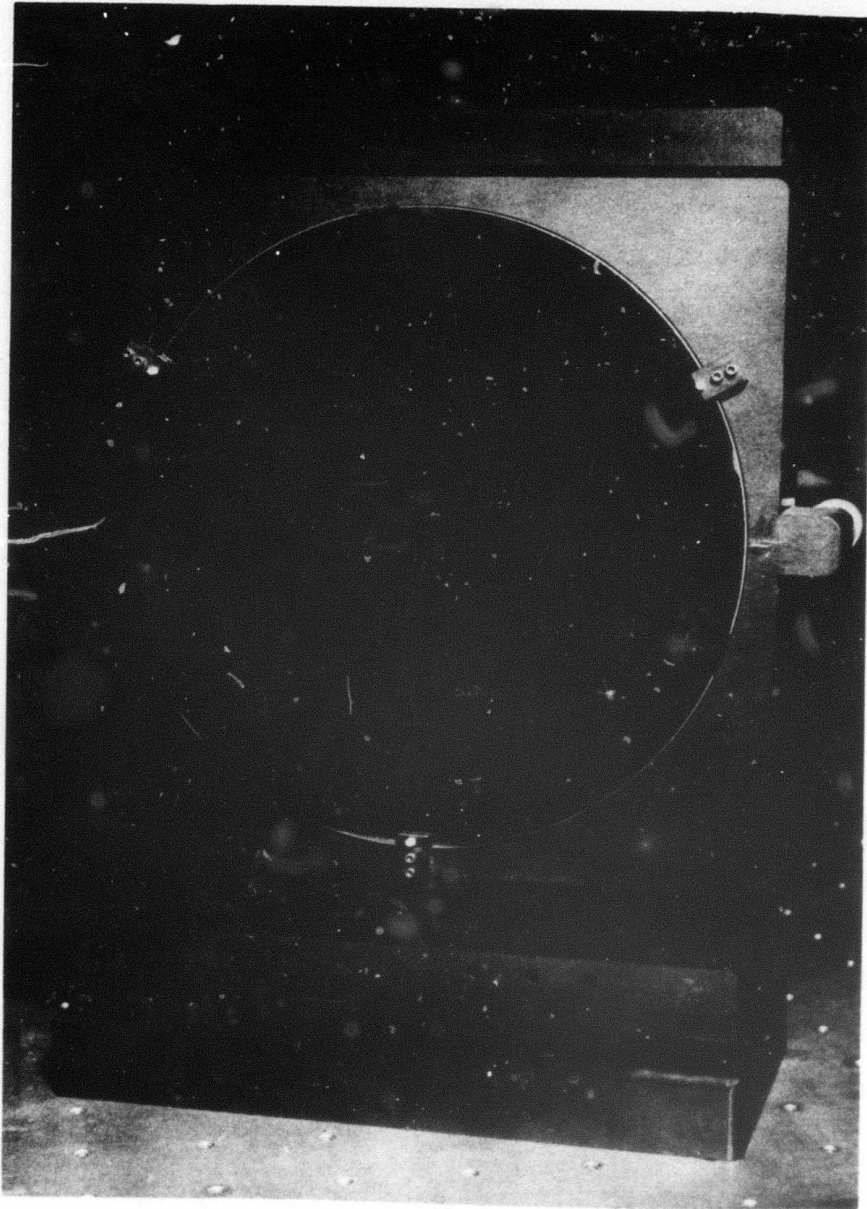


FIGURE 57. PHOTOGRAPH OF A LARGE APERTURE OFF-AXIS COLLIMATOR INCLUDING MOUNT

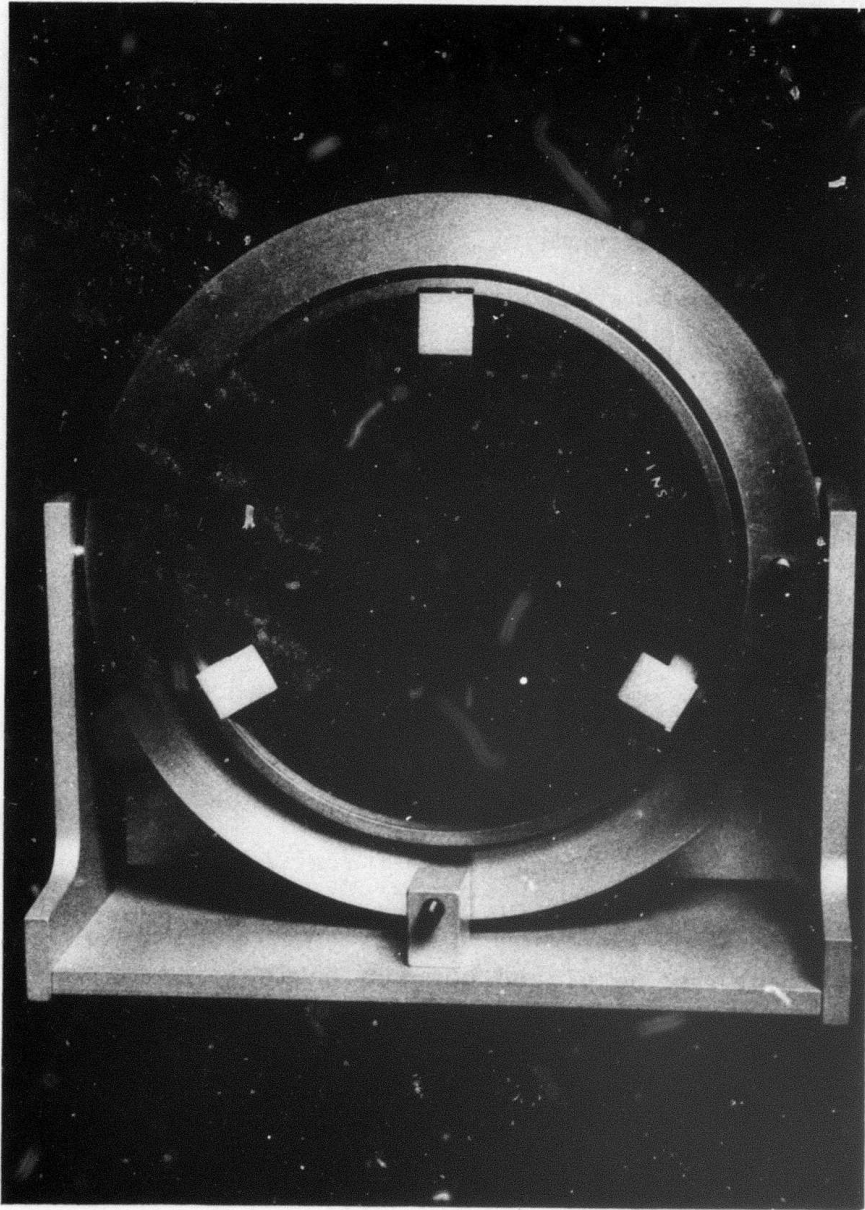


FIGURE 58. PHOTOGRAPH OF A MEDIUM APERTURE OFF-AXIS COLLIMATOR

because most holographic systems are not made to the precision which are required in some of the designs outlined here. Another major point is that accurate alignment equipment is also required to test the elements. In conjunction with Data Optics we undertook the design of a system specifically suited for holographic systems. An example of a typical setup is shown in Figure 59. The equipment is designed to be modular with the basic element as the table shown in Figure 60. Each table is connected with two stainless steel indexing rods. By using the micrometer positioning assembly shown in Figure 61 it is possible to accurately space one table with respect to another. Further the angles between two tables may be accurately set using the engraved scales on the bottom of the table. Auxiliary components are provided so that equipment may be placed between tables; examples include microscope objectives or apertures. Another degree of flexibility is also provided with respect to the hologram in that it may be tilted with respect to the table surface. This is especially convenient for system tolerance studies.

The facilities which were assembled under both ARPA and ERIM support have proven very valuable in studying

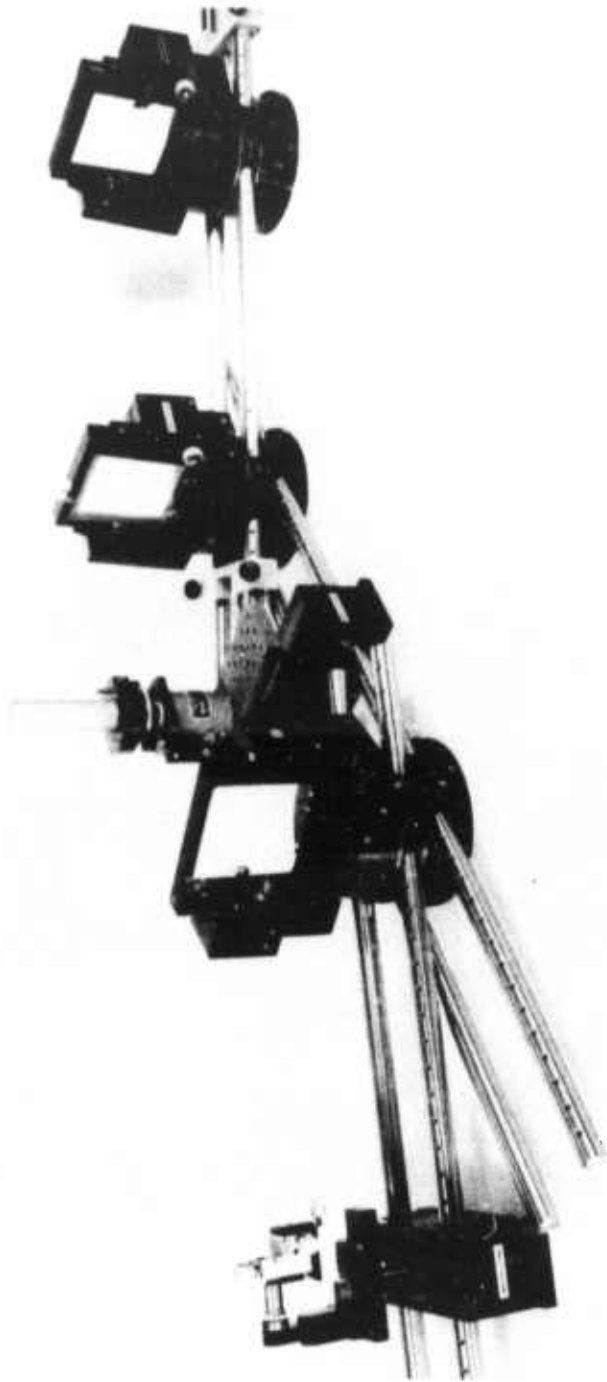


FIGURE 59. HOLOGRAPHIC OPTICS ALIGNMENT AND POSITIONING EQUIPMENT WITH THREE HOLDERS

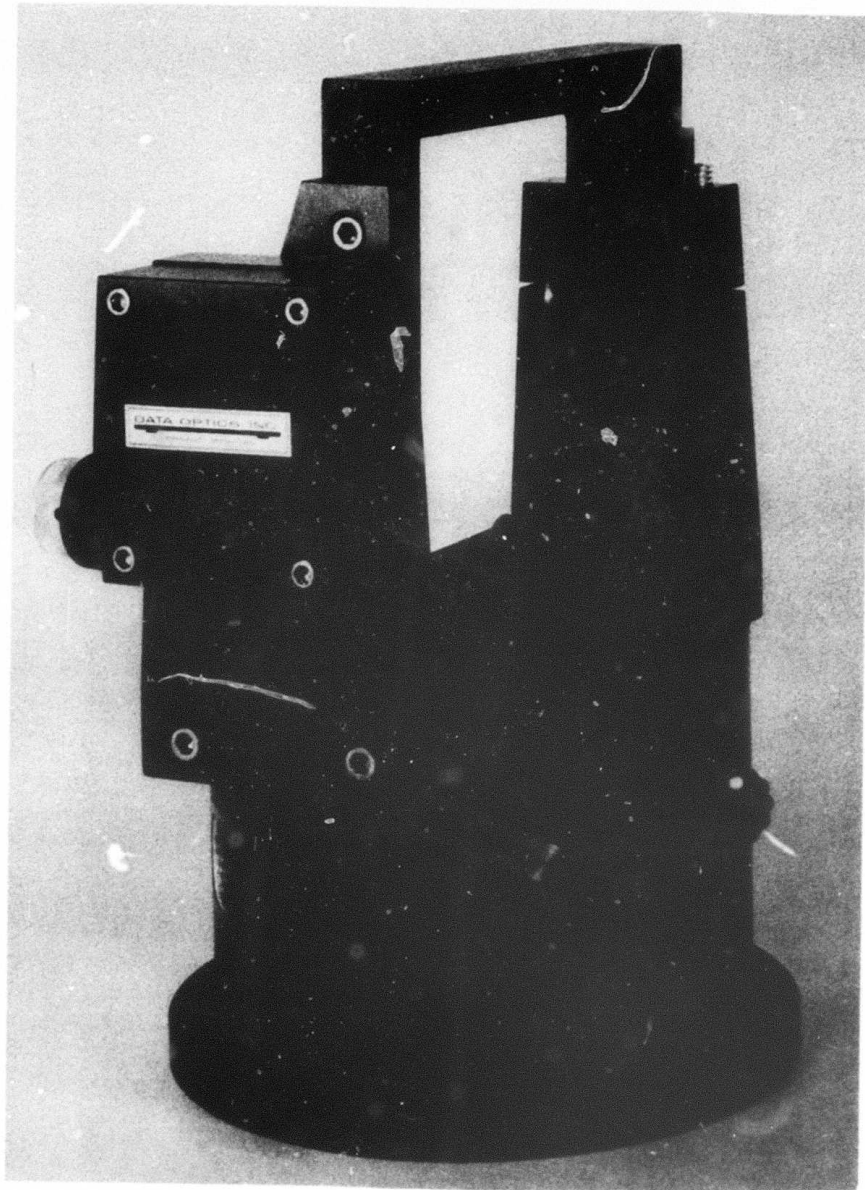


FIGURE 60. A SINGLE HOLOGRAPHIC ELEMENT-HOLDER TABLE

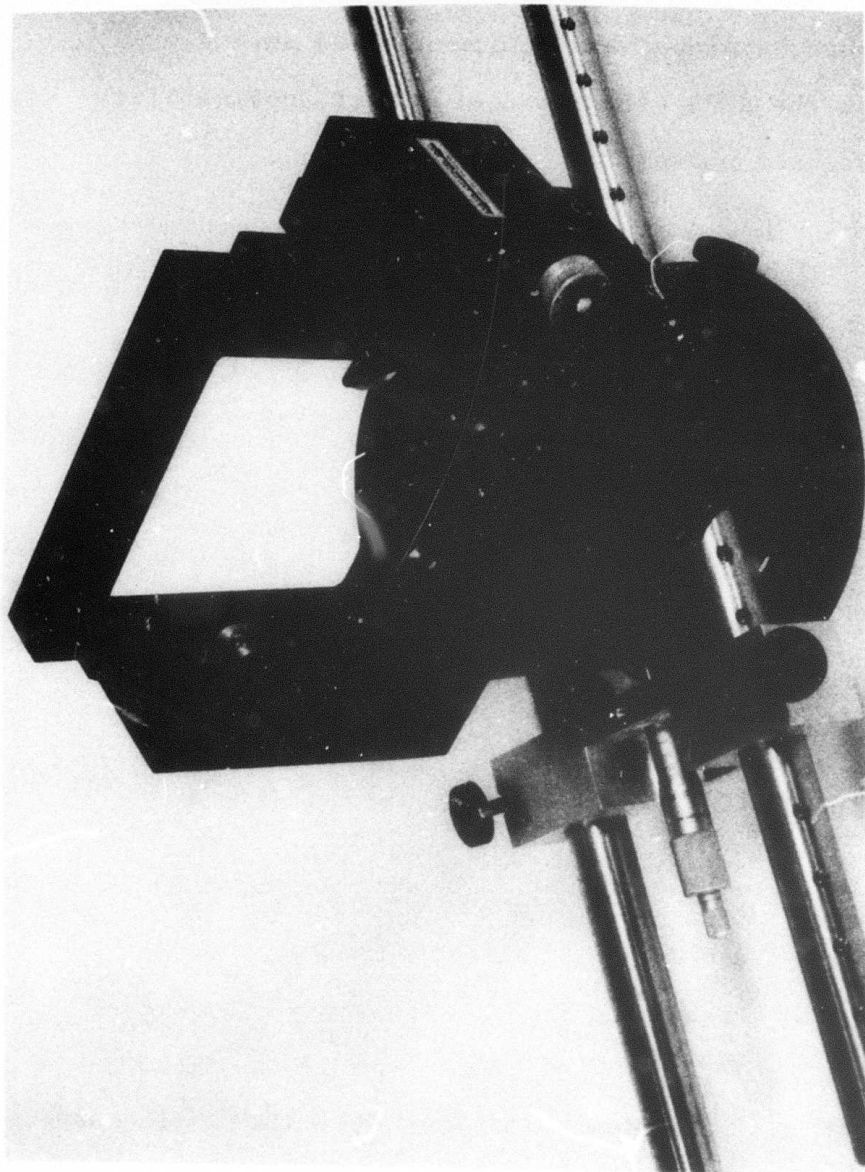


FIGURE 61. A SINGLE HOLOGRAPHIC ELEMENT HOLDER TABLE WITH POSITIONING RODS AND MICRO POSITIONER

the properties of these elements and systems. In fact, the techniques developed and equipment used during phase two of the ARPA effort was of direct applicability to the subsequent phase.

9
SUMMARY AND CONCLUSIONS

This report has described a broad study into several areas of holographic optics. These areas include the following:

1. Infrared optical elements and systems for 1.15 μ and 10.6 μ
2. Multi-element telescopes
3. Wavelength shift techniques to permit a construction wavelength different than at reconstruction
4. Large aperture holographic optics elements in both transmission and reflection
5. Wide angle reflection type holographic optics
6. Facilities for precision recording and assembly of holographic optics
7. Considerations for producing holographic optics.

Each of these areas has provided us with a greater insight into many of the practical problems and considerations associated with holographic optics. For example, some of the results of the areas discussed above have led us directly into the third phase of ARPA support and a direct application of the concepts developed to date.

As a result of this study the following conclusions are applicable:

1. One of the most promising areas for application of holographic optics is in the infrared.
2. Reasonable high quality single wavelength telescopic systems can be designed and built using holographic optics.
3. The design process plays a critical role in any holographic optics system. This was seen especially in the study of the wavelength shift properties of single elements.
4. Large aperture holographic elements (approximately 10" in diameter) can be produced in both transmission and reflection with reasonably high quality. We expect that such elements can also be mass produced.
5. Wide angle reflective holographic optics are difficult to design and suffer from difficult mechanical constraints.
6. Significant advances have been made in the facilities for the recording and testing of holographic optics.

As a result of this study we continue to feel that holographic optics holds considerable promise. It has many unique attributes that may have either negative or positive effects, depending on the particular application under consideration. We feel that what is essential is a thorough understanding of all those parts of holography and optics that give the optical element its properties. These include but are not limited to: imaging, recording materials, construction and reconstruction geometries and illumination source properties, and the substrates. It has also been our experience that the design of these optical systems plays a critical role in the end system performance.

Appendix A

"LARGE APERTURE HOLOGRAPHIC OPTICAL ELEMENTS"

This appendix is a reproduction of ARPA Report 6317-F, prepared under subcontract for the Environmental Research Institute of Michigan by Radiation, a division of Harris-Intertype Corporation.

6317-F
ARPA HOE

FINAL REPORT

**LARGE APERTURE
HOLOGRAPHIC OPTICAL ELEMENTS**

**PREPARED BY:
ELECTRO-OPTICS OPERATION**

24 SEPTEMBER 1973

**PREPARED FOR:
RADAR AND OPTICS LABORATORY
ENVIRONMENTAL RESEARCH INSTITUTE OF MICHIGAN
P.O. BOX 618
ANN ARBOR, MICHIGAN 48107**



FOREWORD

This report was prepared for Dr. John Latta, Director of Digital Analysis, Radar and Optics Laboratory, Environmental Research Institute of Michigan, under subcontract from an ARPA sponsored research project. The principal investigators were R. G. Zech and Lynda M. Ralston. Program management was the responsibility of R. G. Zech. This report was prepared under the direction of R. M. Montgomery, Director of Engineering and Advanced Development.



TABLE OF CONTENTS

<u>Section</u>		<u>Page</u>
1.0	INTRODUCTION	1
2.0	RECORDING MATERIALS	2
3.0	FABRICATION STUDY	4
	3.1 Substrate Fabrication	4
	3.2 Surface Adhesion	4
	3.3 Coating Techniques	6
	3.4 Hologram Recording	11
4.0	COMPLETION OF FABRICATION	13
5.0	CONCLUSIONS	14
6.0	RECOMMENDATIONS	14



1.0 INTRODUCTION

This is a final report briefly summarizing an investigation of problems related to the fabrication of large aperture holographic optical elements. Although the properties of a hologram are invariant with size, this is not true with regard to construction. That is, large holograms intended for imaging applications are significantly more difficult to construct than small holograms. High quality light-sensitive materials and optical quality substrates of large area are minimum requirements. The substrate must be coated with the light-sensitive recording material in the most uniform way possible to avoid aberrations and other imaging defects. Over small areas this is not difficult; however, it is not a trivial task for holographic elements 25 cm in diameter or larger.

It was decided in the initial stages of the project to concentrate on a reflective element. The specifications were a 25 cm diameter, a focal length of 1.2 meters, and a bending factor of 2.2. Two approaches were possible: a reflection hologram of the Lippmann-Bragg type or a planar reflection hologram. We decided that the latter was potentially more useful, especially when metal or dielectric reflective coatings are considered. Obvious applications come to mind for optical systems operating in the UV or IR spectrum. The best recording medium in terms of resolving power and efficiency is a high resolution photoresist. Several are available, they will be described subsequently.

We divided our investigation into a number of areas. The most important were recording materials, substrate fabrication, coating techniques, and hologram formation. A summary and discussion of the main results of our study follow.



2.0 RECORDING MATERIALS

The fabrication of high quality holographic optical elements (HOE) requires exceptionally well-qualified recording materials. Not only must the recording media be capable of good holographic performance, but must also possess favorable physical and chemical stability. The latter is of particular importance for large diameter HOE. From previous experimental work related to the present effort, it was clear that only a few recording materials would be suitable. Although we eventually chose a photoresist for constructing the HOE because a reflective element was specified, we surveyed a number of potentially useful recording materials. Table 1 summarizes the main properties and characteristics of the better candidate light-sensitive materials for HOE applications.

The best photoresists available for holographic recording are Shipley AZ 1350 and Horizons Research LHS7. Shipley AZ 1350 is widely used in the microelectronics industry. It is UV-blue sensitive with a resolving power of about 1500 cycles/mm (70% response). Maximum reported efficiency for plane wave gratings is 30%. Processing involves a liquid development and postbaking. The Horizons Research LHS7 photoresist is new. It is characterized by a relatively high orthochromatic exposure sensitivity, a resolving power of 800 cycles/mm (70% response), and a maximum diffraction efficiency of 31%. Cosmetic quality is very good. A unique aspect of this photoresist is that it is completely developed and fixed with heated air (at 160°C for 90 seconds).



B11 472

Recording Material	Type ^a	Speed ^b (mj/cm ²) at 488 nm	R.P. ^c (cycles/ mm)	Spectral Response	D.E. ^d (%)	SNR ^e (dB)	Processing Reqt's.
Dichromated Gelatin	VP	100	> 3000	blue - green	> 90	> 25	Chem.
Acrylate Photopolymer - (DuPont)	VP	10	> 2000	UV blue - green	> 50	> 25	None
Bleached Photo. Emulsion (Kodak 649F)	PP VP	.01	> 3000	UV visible	> 30	> 20	Chem.
Photoresist	PP						
a) Shipley AZ1350		10 ⁴	> 1500	UV blue	> 25	> 15	Chem.
b) Horizons LH57		5	> 1000	UV blue- green	> 25	> 20	Heat
Photodegradable Thermoplastics	VP	10 ³	> 3000	blue - green	> 60	> 30	None
Photoplastics	PP	.01	> 1000	UV visible IR	> 20	> 15	Heat

CANDIDATE HOE RECORDING MEDIA

^a VP = volume phase
PP = planar phase

^b Speed = exposure for maximum diffraction efficiency

^c R.P. = resolving power

^d D.E. = diffraction efficiency (ratio
of diffracted light to incident
light for a plane wave grating.)

^e SNR = signal/noise ratio. All data for a
fixed packing density and beam
ratio.



3.0 FABRICATION STUDY

3.1 Substrate Fabrication

There was a limited choice of substrate materials. We considered glass and plastic. Plastic was rejected because of surface adhesion problems, and because it is fairly difficult to obtain a large plastic sheet with a good optical surface. Due to time limitations, we selected a readily available plate glass substrate with dimensions of 27.5 x 27.5 cm² and 2.54 cm thick. It was ground and polished to $\lambda/4$ on the front surface and lapped and felt polished on the back surface. Edges were beveled, ground, and polished. The work was done by Jan Vanden Broeck at the McDonald Douglas Electronics Corporation (St. Charles, Mo.) optical fabrication shop for a total price of \$550.

We should point out that selection of a substrate is determined mainly by optical figure requirements. In general the substrate thickness needed increases with surface quality. However, some glasses are better (and more expensive) than others in terms of figuring. A good grade of quartz, e.g., T14 Optosil 3 (Amersil Co.), is recommended because of superior dimensional stability that allows a 30% decrease in thickness (and also weight).

3.2 Surface Adhesion

The adhesion to glass of most photoresist materials is generally poor. The large area of the HOE compounded the problem. We concluded at the start of the program that a substratum layer was required. Unfortunately, a subbing compound was not available from the manufacturers of the photoresists. We performed a literature search, but discovered that the most effective (and nonscattering) subbing



chemicals were proprietary to the large photographic film manufacturers. The most attractive alternative remaining was to develop a suitable technique for cleaning the glass substrate. As is well known, the adhesive properties of a surface are enhanced by thorough cleaning.

The procedures we evolved are elementary but effective. Two cases were of interest: (1) previously uncoated substrates and (2) previously coated substrates from which the photoresist layer was stripped. To clean new substrates we recommend the following steps:

- 1) airknife off dust and large surface artifacts.
- 2) rinse in a solvent consisting of equal parts of methyl alcohol, chloroform, and benzene.
- 3) wash in a multicomponent detergent, e. g. , Micro-clean^(R).
- 4) triple rinse in distilled water and free air dry.

Cleaning previously coated substrates was complicated by the residue of the stripped photoresist layer. As a consequence, a more vigorous cleaning technique was required. We found by trial and error that the following procedure was effective for the Horizons Research photoresist:

- 1) Bathe in Horizons Research photoresist developer.
- 2) Rinse in warm methylene chloride for 30 minutes.
- 3) Scrub in fresh methylene chloride with a teflon^(R) pad.
- 4) Scrub in a multicomponent detergent with a teflon^(R) pad.
- 5) Triple rinse in distilled water and free air dry.

Just prior to coating the photoresist layer, we discovered that two other steps were necessary. First, we baked the substrate at



150° C for 1 hour to remove surface moisture. A high wattage air gun (rated to 500° C) is also effective for this task. After cooling to room temperature and transporting to the clean room, the substrate was bathed in filtered dry nitrogen. These steps are of particular importance under conditions of high relative humidity.

When the procedures just outlined are used, good adhesion between the photoresist layer and the glass substrate are consistently obtained. We note, however, that this assumes that the photoresist layer is continuous, and that the edges of the substrate are sealed. When these conditions are not realized, the coating can be damaged, as will be discussed later.

3.3 Coating Techniques

Coating a 27.5 cm square glass substrate with various photoresist solutions required the investigation of numerous coating techniques. Because of the uniformity and cosmetic quality requirements, only three techniques appeared feasible. They were spin-coating, dip-coating, and gravity-flow coating. Each has advantages and disadvantages. For example, spin-coating was feasible with modification to the spinning apparatus. However, the large mass of the glass substrate prevents sufficient acceleration to spinning speed. As a result, nonuniform coatings are obtained.

High quality coatings were obtained on small substrates by dip-coating. The extension of this technique to 27.5 cm square substrates was not possible for three reasons. First, the thickness of the photoresist layer was found to vary in a nonlinear way (a linear wedge is acceptable). The height profile of the photoresist layer was linearly wedged (approximately) over the first 75 percent of the substrate withdrawn, and increased more rapidly for the remainder for substrates on the order of 7.5 cm square. We concluded that the same characteristics



would apply to the larger substrates. Second, a large volume of photoresist was required to be maintained free of dust and moisture. A significantly larger than average cleanbox was needed for this purpose in order to also allow for withdrawing the entire length of the substrate from the coating solution. Finally, the coated layer must dry in a solvent atmosphere to insure a smooth, uniform photoresist layer. The solvents used in both the Shipley and Horizons Research photoresists have insufficient room temperature vapor pressure for this purpose.

Our preliminary investigation established that gravity-flow coating was the only feasible technique. Although there are a number of ways to implement this method, we describe ours to illustrate some of the problem areas. The details of our approach are outlined in the following paragraphs.

The gravity-flow setup consisted of a 30 cm granite table flat to $0.5 \mu\text{m}$, a 2.5 cm thick tripod surface plate for leveling the granite slab, an aluminum casting frame, and an airtight cover to provide a solvent atmosphere for slow drying. The granite slab and leveling plate were located in a vibration free area to minimize surface perturbations. The casting frame, shown in Figure 1a was made from four 27.5 cm strips of 0.32 cm aluminum. The corners are cut to 45° and the strips were bent along the center to approximately 45° . When taped to the substrate the frame draws up the solution by capillary action forming an edge of zero thickness just inside the frame, as shown in Figure 1b.

A 10 cm x 12.5 cm substrate coated by this method was supplied by C. Leonard of the Environmental Research Institute of Michigan. It was tested with a Leitz reflecting interference microscope for surface uniformity. Ignoring edge effects, we found a maximum thickness

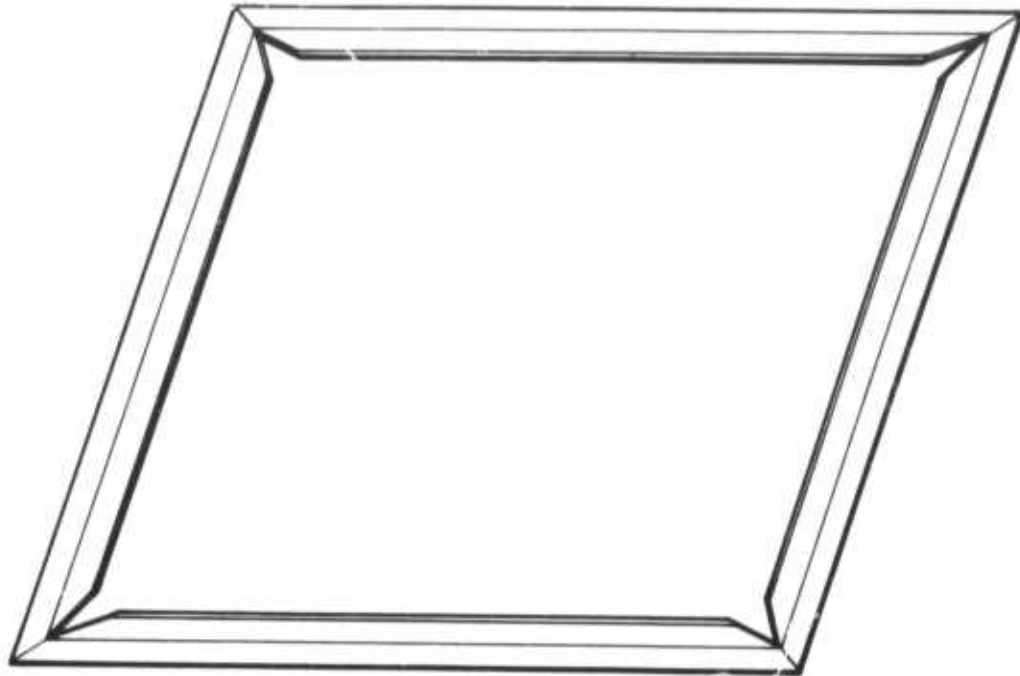


FIGURE 1a



87554-2

FIGURE 1b

FIGURE 1. CASTING FRAME AND PHOTORESIST PROFILE (GREATLY EXAGGERATED) FOR GRAVITY FLOW CASTING.



variation of less than $0.225 \mu\text{m}$. This test showed that gravity flow casting can be used to coat substrates with sufficient uniformity. That is, the recording material will cause a random wavefront aberration of less than $\lambda/2$ over the 25 cm aperture of the HOE.

The airtight cover had a dual purpose; to keep out light and dirt, and to provide a solvent atmosphere. If the coated substrates were allowed to free-air dry, the top layer of the photoresist which is in direct contact with the atmosphere dries first. Then as the lower layers dry, the solvent must evaporate through the top surface layer; this causes a rippled surface (orange peel). Substrates allowed to dry entirely in a solvent atmosphere in general have good surfaces, but can take up to eight hours to completely dry. The airtight cover was used to provide a compromise between these extremes. That is, the photoresist solution was flowed on the substrate and the cover was tightly closed for one hour to allow the solution to spread uniformly. The cover was then opened briefly to vent the solvent atmosphere, and then closed. The rate of drying was controlled by the frequency with which the solvent atmosphere was vented. If the photoresist was allowed to dry too fast, orange peel formed; too slowly and the plate was covered with dust and other artifacts.

The first coatings were cast in a photographic dark room using Shipley AZ 1350 photoresist. In order for the resist to uniformly spread over the entire substrate, it was diluted to a concentration one part AZ 1350 to eight parts methyl ethyl ketone (MEK). On the order of 15 cc of the photoresist solution was flowed in the center of the substrate and dried completely in a solvent atmosphere. The resultant coatings were uniform but cosmetically poor due to a large amount of dust particles. We used internal filtered air (fan-driven) to reduce the dust particle concentration; this proved to be helpful, but insufficient. The entire casting apparatus



was then moved to a clean room environment, and setup under a laminar flow hood. Plates fabricated in the clean room dried with a lower dust particle concentration than those cast in the dark room. However, cosmetic quality remained below acceptable standards. We reached the conclusion that Shipley AZ1350 has a natural affinity for airborne particulate matter.

The evaluation of the Horizons Research photoresist was initiated in the clean room environment. We found that diluting one part of HR photoresist with five parts solvent provided a uniform coating of approximately one micron thick. The coatings were significantly cleaner than coatings made with Shipley AZ1350. In addition, we found that coatings made with the Horizons Research photoresist were more consistent. However, the Horizons Research photoresist required a much longer drying time than the Shipley photoresist drying time (drying time is a critical factor in providing good surface). Nevertheless, we decided that an increased drying time was a favorable tradeoff in order to gain acceptable cosmetic quality and consistency. Therefore, we selected Horizons Research photoresist for fabrication of the HOE.

In addition to the problems caused by dust and other airborne artifacts, we encountered two more subtle problems. The first was glass warpage. When a large glass substrate is fabricated to a specified optical quality (in this case $\lambda/4$ surface flatness) there can be differences between neighboring areas that require a precision optical flat of comparable area to defect (in the present case this implies a flat that is $\lambda/20$ and $25\sqrt{2}$ cm in diameter). The second was stability. We found that the level of the substrate could be significantly changed for example, by foot traffic in the region of the clean area. Both of these problems resulted in low quality photoresist layers. Our solution to the first problem consisted of weighting the casting frame to compensate for the warpage. This was done with aluminum blocks. We avoided stability problems by casting during



evening and weekend hours when activity in the clean room area was at a minimum. A better solution would be a small floating table, e. g., mercury supported.

Finally, we again stress the problems caused by particulate matter. The photoresist solution can be purged by microfiltering prior to use. Airborne contaminants must be avoided by the use of a laminar airflow in a clean room environment. Our study indicated that temperature, relative humidity, drying time, and photoresist solvent (including diluent) are also important factors.

3.4 Hologram Recording

The hologram recording setup is shown in Figure two. It consists of two point sources located at 2 m and 0.75 m distance from the center of the hologram recording plane. The angular separation, measured with a goniometer, was 15°. The plateholder was oriented to produce on the average fringes normal to the surface of the recording material.

In order to insure spherical waves of uniform intensity over the entire aperture of the HOE, we expanded each beam to an area twice the diagonal of the glass substrate. This significantly reduced the laser power density available for exposure. Total irradiance of the hologram plane was only $10 \mu\text{W}/\text{cm}^2$. A 2W argon laser operating at 488 nm in a single transverse and longitudinal mode (output was 300 nW) provided the laser power. Exposure time was 12 minutes; this indicates the value of high exposure sensitivity. If Simplex AZ1350 had been used, more than 8 hours of exposure would be needed.

Prior to hologram recording, an optical black laquer was applied to the back of the coated substrate. After exposure, the holograms were stripped of the antihalation backing, and then processed with a hotplate (100°C) and an argon gun (160°C). The hotplate was used to heat the

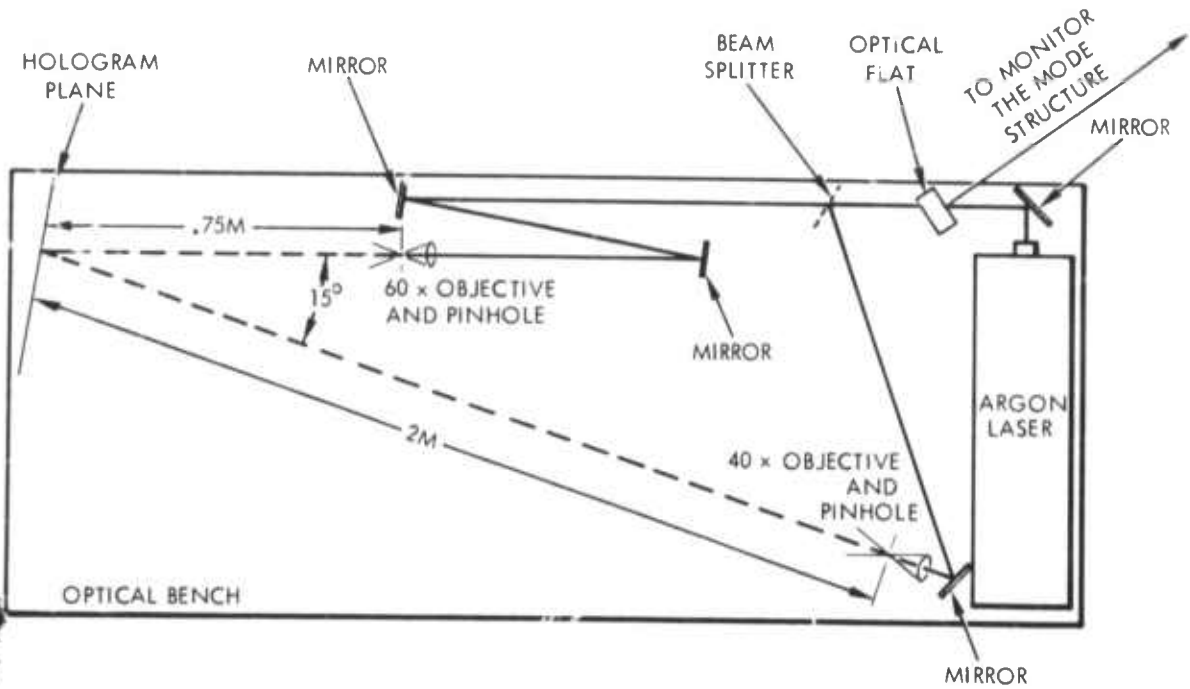


FIGURE 2. SCHEMATIC OF THE HOLOGRAM CONSTRUCTION SETUP.

87554-1



substrate and thus, to avoid thermal shock when the airgun was applied to the photoresist layer for development.

4.0 COMPLETION OF FABRICATION

After processing, the best holograms were aluminized and silicon monoxide overcoated to produce reflective elements. This work was done at the optical facilities of the McDonnell Douglas Electronics Corporation (St. Charles, Mo.) The price was \$51 per hologram.

As part of the preparation for aluminizing, the photoresist layer was cleaned with dry air to remove dust particles and then washed with a detergent and water. All holograms except the deliverable HOE survived this treatment. It was later discovered that one corner of the substrate did not seal. This caused a section of the photoresist to lift off the substrate. A small scratch permitted the same phenomenon to occur near the center of the HOE. This was unfortunate because the damaged HOE was of high quality otherwise, and also of high efficiency.

Following the transfer of the Electro-Optics Center to the Radiation facilities, Melbourne, Florida, we repeated much of our previous fabrication work. A new set of holograms was recorded and aluminized. The results were satisfactory this time in terms of cosmetic quality; there was no damage to photoresist coating. However, the efficiency of the deliverable HOE was found to be much reduced. We eventually discovered that the fresh order of photoresist purchased for our second effort was inadvertently modified to be more suitable for PC and IC applications. The end result was that by using a previously established empirical dilution constant, we obtained a much thinner coating and a lower diffraction efficiency.



Before delivery, each HOE was painted on the back surface with an optical black lacquer. The front surface of the HOE was covered with a black aperture 25 cm in diameter. The aperture is not necessary, but serves to define the usable area of the HOE (the edges are of poor quality) in an obvious way. A photograph of the completed HOE is shown in Figure three.

5.0 CONCLUSIONS

The fabrication of large aperture HOE is feasible. In the limited context of our investigation we sought to isolate problem areas. A great number were discovered. However, none were found to be insoluble. But it is clear that very exacting procedures are required if optimum results are to be obtained. In particular, we emphasize the need for high quality substrates, a superior clean room facility, and a fairly sophisticated coating apparatus.

We find no reason to believe that large aperture HOE could not be produced in large numbers. In fact, many of the problems we encountered were those of scale, and would normally be absent in a production facility. Once procedures were optimized, large aperture HOE could be fabricated on a mass production basis.

6.0 RECOMMENDATIONS

Further study of fabrication techniques is warranted. The major areas are substrates (materials, subbing, optical figure, etc.), coating techniques (optimization of the gravity flow method), and overcoating (metal versus dielectric, and also surface preparation). Each area represents a phase of construction that merits optimization if high quality HOE are to be produced that are competitive with conventional optics.



FIGURE 3. COMPLETED 25 cm HOLOGRAPHIC OPTICAL ELEMENT

Appendix B

"NEW DEVELOPMENTS IN THE DESIGN OF HOLOGRAPHIC OPTICS"

This appendix is a reprint of a paper presented at SPIE Seminar-in-Depth on "Applications of Geometrical Optics," August 27-28, 1973, San Diego, California.

NEW DEVELOPMENTS IN THE DESIGN
OF HOLOGRAPHIC OPTICS

John N. Latta

Ronald C. Fairchild

Environmental Research Institute of Michigan

P. O. Box 618, Ann Arbor, Michigan 48107

(Formerly - Willow Run Laboratories, The University of Michigan)

ABSTRACT

Conventional optics normally includes only two types of elements: refractive and reflective. Holographic optics encompasses a third type of element; one whose properties are diffractive in nature. The focus of this paper is to outline the properties of a general computer-based analysis and design tool that is directed to holographic optics. This tool is called the Holographic Optics-Analysis and Design (HOAD) program. The program has been designed to be both user oriented and flexible. Four sections are covered in the paper. They are directed towards (1) the operating system (MTS) used to support the HOAD program, (2) the hologram ray tracing programs which form the basis of the program, (3) a general discussion of the HOAD program, and (4) an outline of the techniques of using HOAD. The last section of the paper is directed towards an assessment of where HOAD presently stands and the direction it is going.

INTRODUCTION

The design of conventional optical systems normally includes only two types of components: refractive and reflective. For approximately the past four years we have studied the inclusion of a third type of element within the domain of optics. In a broad sense this is a diffractive element, however, our examination has largely been directed to holographic elements.

Programs such as POSD and others have incorporated an analysis of diffractive structures for many years. Our approach is considerably different in that no assumptions are

made about the pattern of the fringes on the surface of the element and that this pattern may be created by a recording process, i. e., holography. This new type of general diffractive structure greatly extends the domain of optics by including a third class of elements. We call this area holographic optics.

Before considering the design aspects we should first inquire; why is holographic optics of interest? The properties of diffractive structures are in contrast to reflective and refractive elements. First, in a diffractive element the surface shape plays a negligible role in the properties of the elements. Thus, these types of elements have seen application in what we call conformal optics (Ref. 1,2). That is, optical systems in which the elements conform to a given surface and yet whose properties are invariant with the surface. Examples include automotive windshields and face masks. Another difference is that these elements may be made with arbitrary phase wavefronts and can thus have an effect on a propagating wavefront similar to a lens which has an arbitrary surface shape. In principle, holographic optical elements would not require mechanical fabrication in the same sense as conventional optics. The basic construction process is the exposure of a photographic emulsion or photoresist. Thus, multiple copies are no more than a step and repeat process. The potential for automation is obvious. In less than near term one can easily visualize rolled optics which are made on rolls of film and unrolled when needed. Further, with some of the materials that are a read-write-erase type required for holographic memories one can visualize an optical system which is optically alterable. That is, the elements themselves could be made by two optical beams, erased by one beam, and

Presented at: SPIE Seminar-in-Depth on "Applications of Geometrical Optics,"
August 27-28, 1973, San Diego, California (to appear in Proceedings).

then made to look like another element with different properties by again exposing it with two light beams. This could be done *in situ* and potentially in a relatively short period of time.

These rather interesting prospects for holographic optics also include some attendant drawbacks. One of the first is the sensitivity of the elements to wavelength. Because the structures are diffractive, the light rays which exit from the elements change in direction as a function of wavelength. We have examined in some detail the design of a two element holographic lens that has low chromatic aberrations. In brief, the image quality from such a system is unacceptable and the design problem quite difficult (Ref. 3). Additional elements may provide a means for improving the image quality. In fact, a seven element achromatic lens was designed and built by Rose (Ref. 4,5). The light efficiency of these elements is another drawback. Using thick materials (Ref. 6), 100% efficiency is theoretically possible. However, when applying elements with such efficiencies to either light distributed over a waveband or an angular extent, apodization of the beam takes place. This problem has been discussed by Latta (Ref. 7). Another approach to recording the element is to make it with a material which results in surface relief as the diffracted structure. Unless blazing methods are used the efficiency is normally limited to 33%. These types of elements have the advantage of operating outside the visible spectrum when overcoated with a reflective material. Thus, as long as the element has been designed to operate with a wavelength shift from construction to reconstruction of say, 5145 Å to 1.06 μ , the reflective overcoated element is a means of implementing such an IR element. At this point we have provided some rationale for why holographic optics is of interest. Let us now examine the need for an analysis and design capability.

It is quite clear that holographic optics has some unique attributes. Many of these are in contradistinction to conventional optics. Further, present glass and mirror technology has solved many optical problems quite well. In general, holographic optics should be viewed as complementary to present optical systems rather than as a competitor. For this reason and others it has

been quite apparent throughout our work in holographic optics that flexible and general optical analysis and design tools must be available. The only means through which these tools can be realized is with the aid of a high-speed general purpose digital computer.

In this paper we will describe recent developments in the tools used to design holographic optics. We have simply called our programs - Holographic Optics - Analysis and Design (HOAD). The discussion will be divided into five sections: Michigan Terminal System (MTS), Hologram Ray Tracing Programs, HOAD Programs, HOAD Program Usage, and Comments and Conclusions.

Michigan Terminal System (MTS)

In any large program either the user or program must be cognizant of the operating system. Preferably, as the program becomes more oriented toward the user he need know less about the operating system. These statements are especially true in a time sharing environment. The HOAD program makes use of its operating environment extensively. This is known as the Michigan Terminal System (MTS). In this section we will give a brief overview of MTS and how it is used by the HOAD program. For additional details on MTS the reader is referred to the system documentation (Ref. 8) and Alexander (Ref. 9).

When writing any large set of computer programs (Ref. 10) one is confronted with the dichotomy of maximum flexibility and portability. Obviously the most flexible system could be written in the system assembly language. The portability then is restricted to machines of the same class or type. On the other hand, one can write the programs in ANSI Fortran and realize a highly portable program but one whose operational use changes from machine to machine. Thus, most programs are somewhere in between. The HOAD program uses to considerable advantage the environment provided by MTS. To be able to effectively discuss the features in HOAD it will be necessary to describe briefly the characteristics of interest within MTS.

MTS is a virtual memory time sharing and batch operating system on a duplex IBM 360/67 computer. This system was developed by the Computing Center staff at The

University of Michigan. Indicative of its flexibility and advantages over other similar operating systems, it is in use at several other institutions in the U.S. and the world. The MTS system provides support for remote batch, batch, and time sharing from terminals. There is no distinction between these environments, i.e., the time sharing and batch commands are identical. Further the batch mode, or remote batch station can be accessed via the time sharing mode. For example, a user may create a batch job from the time shared terminal, submit it to the batch stream, and direct the output to a remote batch station.

From a programmer's standpoint, MTS provides an environment for program development that is nothing less than excellent. Three factors contribute to this assessment: virtual memory, the file system, and the text editor. In the four years of program development we have not used any program overlays. We have not been cognizant of the memory required to solve a design problem because such an awareness was not required. The second and third factors are equally as significant. Within MTS a file is a set of data located on the disc system. In general, the location of data is immaterial and transparent to the user. No distinction is made as to the type of data. Any file may contain object, source, or alphanumeric data. The names assigned to a file are determined only by the user; except in the case of system files. For many files, especially source code and input data, line files are normally used. This scheme assigns a line number to every record in the file. These line numbers allow the file user to access any line or set of lines. In fact, in MTS every file can be constructed as a subset of any other file or a concatenation of files or subfiles. In the context of the HOAD program a file can mean literally any collection of data. In MTS, however, the meaning is actually much broader. A file may be accessed in many ways. One method uses the text editor. This is a powerful, fast, and flexible string oriented editor. In keeping with the general nature of files the editor may also operate on any set of data. For our purposes here we will be most concerned with its application to input data and its modifications. This brief overview provides some insight to the flexibility that MTS provides the individual doing program devel-

opment. Of more direct concern to us here is the environment in which the user finds himself. Before examining this we must discuss the use of MTS to handle interrupts.

Interrupts are simply a break in the normal events of processing. These may be caused by the program user or the programs. A user generated interrupt is normally initiated in a time sharing mode at the terminal by hitting the break key. In normal MTS operation this allows the user to return to the system level and consequently leave the programs he was in when processing was underway. The result is then one where the user must restart or reload the programs that were operating when the break key was hit. It should be made clear that it is not an unusual event that the program user finds an error and wishes to correct that error and restart operation. From our perspective the goal of a good operating environment is that it be both interactive and allow the user complete control of the analysis and design process and one where he has little concern with the system (MTS) environment. Thus, the terminal interrupt function only allows us to meet this problem partially. The program is under the control of the user, however, he must exercise this control at the expense of having to restart the program. Within MTS a capability exists to intercept these interrupts and allow the program to process them in any way it desired. The implementation of this technique will be discussed later in this paper.

The second level of interrupts is a program caused break in processing. Such events are typically the result of unexecutable machine code and consequently always catastrophic. Examples of an interrupt include divide by zero, exponent overflow, and addressing exceptions. In a program as large as HOAD it is very difficult to protect the user from every potential interrupt condition. Our approach has been one where the interrupts are intercepted by the program and the user is allowed to proceed. This again avoids the problem of a failure which brings the user to the system level. The details of this method will also be discussed later in the paper.

The basic operating steps for accessing and using the HOAD program are very simple. These steps are the same from a terminal or batch mode. Once the user is signed on a

terminal or enters a set of cards into the card reader he is ready to access the program. This is simply a run command.

\$RUN < FILE >

where < FILE > is the name where the load modules for HOAD currently reside. This file may be associated with the user's identification number, i.e. ID, or another such number. In any case the accessing is very simple.

Once the HOAD program is resident in virtual memory, the user may perform analysis or design tasks at will and in any order. In addition, the output may be directed to any location including the terminal, a file, a remote batch station, or a printer at the computer site. Further, the HOAD program user may re-enter the system level without unloading the programs and then return to the programs. Thus, the approach outlined here is one of a subsystem which has its own user environment.

With this brief overview of MTS and its relationship to the HOAD program we will examine the ray tracing programs which form a basis of the HOAD program.

Hologram Ray Tracing Programs

In any ray tracing program there must be a kernel from which the program is built. In the HOAD program this is the module which is referred to as the hologram ray tracing program. This section of the paper will focus on the mechanics of the program in a block diagram form rather than a detailed description of the ray tracing technique. For this information the reader is referred to Latta (Ref. 11) and Latta and Champagne (Ref. 12).

The complexity permitted in the analysis is shown in Fig. 1. Several types of holograms can be analyzed:

- Transmission
- Reflection
- Reflective Overcoated

In addition the holograms may be either forward or backward illuminated and reconstructed using an order of $\pm n$ or zero. One hologram is located with respect to another using six variables: x, y, z separation

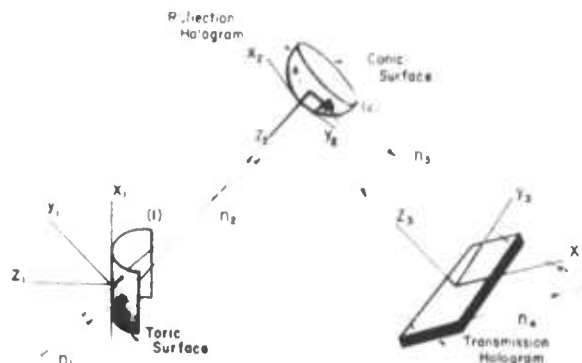


Figure 1. General Hologram and Optical System Geometry

between the elements and the set of three euler angles α, β, γ , from one coordinate system to the next. In addition, the holograms may be on substrates of conic, toric, or aspheric types.

In performing an analysis of a holographic optics system the rays are kept in an array which contains the x, y, z location of the last point on the ray, the direction cosines, the phase, and amplitude. The phase plays an important role in this analysis because most of our present results are expressed in terms of wavefront aberrations. The amplitude is included because the rays undergo attenuation when propagating through the emulsion as a result of a hologram efficiency which is less than 100%.

The analysis of a system when a set of rays is propagated through it is best illustrated with the aid of Fig. 2. This analysis is initiated when a reconstruction phase surface is incident on the first hologram. This plane surface is the result of one point in reconstruction space, i.e. object space in conventional optics terminology. This phase surface is actually a set of rays. The set can be defined by the program user or the programs. Normally, we use a set of two orthogonal fans of rays with sufficient density to sample the wavefront. This set of rays propagates to the first hologram. At this point in the program the hologram ray tracing operation is begun; we will examine this block in more detail later. For the time being let us assume that this set of rays has been propagated through the hologram. If we are considering a single element the ray analysis

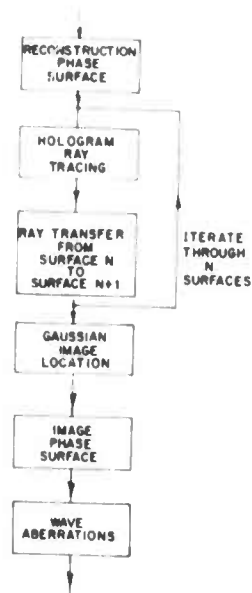


Figure 2. HOAD Program Hologram Module

proceeds to the image location routine. In a multiple element system, the rays are transferred from one element to the next. The ray bundle is then incident on the next hologram and the analysis proceeds as before until the set of rays have propagated through all the holograms.

Once all the rays exit the last hologram they are analyzed to determine the location of the Gaussian image. This is accomplished using an algorithm suggested by Hopkins (Ref. 13) and discussed by Titian (Ref. 14). After the image is located, the rays are propagated from the hologram to a constant phase surface. This phase surface is then compared against the reference sphere that is centered at the Gaussian image point. This comparison calculates the wavefront aberrations. The results of the ray tracing analysis is then complete. Let us now return to the earlier discussion of the hologram ray tracing section shown in Fig. 2.

Illustrated in Fig. 3 is a block diagram of that section of the analysis program which does the actual ray tracing. Initially the ray set is located on the tangent plane of the hologram surface. The function of this section is to propagate that ray to the actual surface. Once the x, y, z point is determined, two routines are called which calculate the

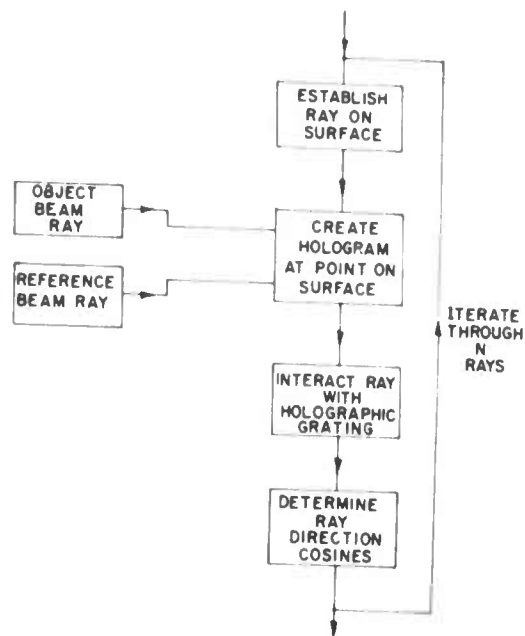


Figure 3. Hologram Module Ray Tracing Block Diagram

direction cosines of the two rays originating from the object and reference beams. These are the two beams which were used in the original construction process to make the hologram. The interaction of these two rays results in interference fringes and thus the hologram. Once the property of the interference fringes at this location is determined the grating equation (Ref. 12) can be used to find the direction cosines of the ray which exits from the hologram. The actual cosines are also dependent on the type of hologram, i.e., reflection or transmission. This process of iterating the rays from the tangent surface to the point where they exit from the hologram proceeds until all rays have been propagated through the hologram.

In this section we have established an overview of the basic module for tracing rays in the holographic system. We will now combine this module into a system which not only includes the features discussed earlier in the MTS description but also a design section in the HOAD program.

Holographic Optics - Analysis and Design (HOAD) Program

The HOAD programs are very flexible

and directed towards a high level of user interaction. Such objectives are not accomplished without some penalty, in this case the relative length of the programs. The statistics are given in Table 1. Each of the modules are shown on the left and will be discussed in this section. The total number of lines is 14,845 for a total of 144 subroutines and the mainline. The load module size for HOAD is 330 K bytes.

Table 1. HOAD Program Statistics

<u>MODULE</u>	<u>LINES</u>
CONTRO.	4165
HOLOGRAM	2565
OPT	3433
SINGLE	1115
UTILITY	3567
TOTAL	14,845
FORTTRAN	: 91%
ASSEMBLER	: 9%
SUBROUTINES	: 144
ENTRY POINTS	: 179
LOAD MODULE SIZE	: 330 K Bytes

The module interaction is best illustrated with the aid of Fig. 4. MTS is accessible through the control module. Such access allows the user to input most system level commands and then re-enter the HOAD program. Of most interest to a normal user is the availability of the file system. Two levels of files are shown in Fig. 4; user and public. We have discussed the user file system in an earlier section and will therefore direct our attention to the public files. These include the pseudo-devices, i.e., files, where data either originates from and/or is sent to. For example, *PRINT* is a file which in actuality is the high speed printer at the computer site. HASP is the spooling system which serves as a buffer of input or output data. It is the normal interface to the remote batch stations. Examples of public and user file usage will be given in the next section. We will now examine the various modules and their functions.

The control module provides the user-program interface. Its functions are as follows:

- a) input line parsing to permit a free field format and syntactical error diagnostics
- b) input command decoding
- c) input command error checking and diagnostics
- d) generation of a table to define a hologram system
- e) global checking of input data to determine if a minimum system has been specified
- f) conversion of the table generated in d) above to the common blocks in the hologram module
- g) attention, program, and I/O interrupt handling
- h) dumping of table and common blocks as error diagnostics
- i) remote station printing of files
- j) input/output file maintenance i.e., opening and closing of files
- k) issuing of MTS commands
- l) trace of subroutine entry and exits.

Aside from these functions the control module calls the appropriate modules when a solution to a given system is requested.

The hologram module has been discussed previously. It is simply invoked by a request or command

SOLVE RAY

which is interpreted by the control module to obtain a solution. At this point the tables which were generated by the previous commands are entered into the common block of the hologram modules. The passing of parameters is not necessary; only a call to the entry point for a solution of the system.

The design of a system is implemented via the optimization module. This module has a set of variables defined for its use in the optimization process. The currently defined hologram system is used as a beginning point. The optimization module is invoked by a command

SOLVE OPT

which is decoded by the control modules. The optimization process and module will be discussed in more detail later in this section.

Single holographic elements can be studied using either the complete hologram ray tracing

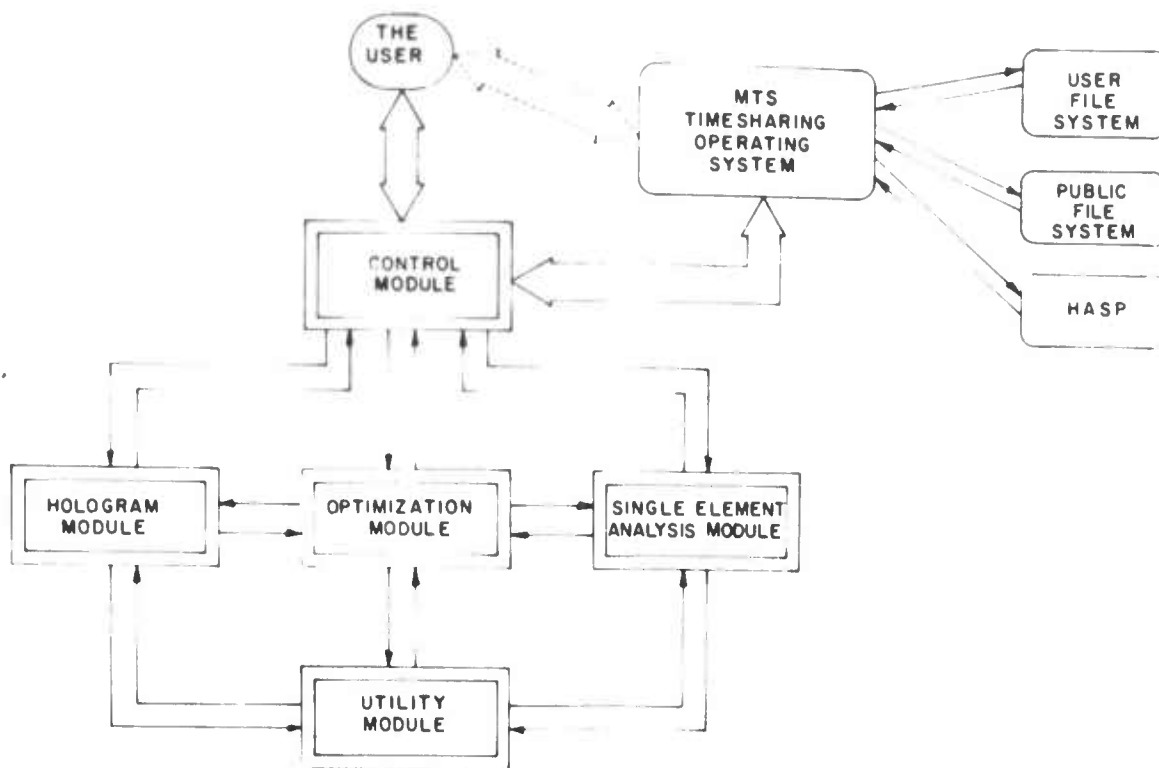


Figure 4. HOAD Program Module Interaction Block Diagram

module or the single element analysis module. In the latter case, this module is used to obtain quick answers. The single element analysis program will complete the same level of solution as the larger hologram module.

The utility module is a set of low level mathematical subroutines that may be used in any of the other modules. All the routines are called by argument and have no common blocks. In general, these routines call no other routines. Examples of the functions performed include: coordinate conversion, coordinate transformation, and surface intercepts.

We have briefly discussed some of the functions of the control module. Now consider Fig. 5 which illustrates in a block diagram the various functions. It is important to note that one of the main purposes of this module is as an interpreter. That is, it analyzes each input line and takes appropriate action based on the contents of the line. This is normally done while the user is at a term-

inal. Input may also originate from a user file on disk. Once the command has been decoded the necessary action is initiated. For nearly all commands, once the required steps are complete the program returns to the command level mode and awaits further input. Consider the case where the command specifies parameters associated with the hologram. These parameters are decoded and their variables identified and then placed in a table. This process continues until the user requests a solution. It is important to note here the role that the table plays in the operation and organization of the programs. The table essentially provides a decoupling of the control modules from the modules which are called. Generally, there is only one routine which handles the table to common block conversion. Thus, either the input command format or the ray tracing programs may be changed without a severe impact on the other module. Although a technique which uses both common blocks and tables may appear bulky we feel it has the distinct advantage of a more modular program construction.

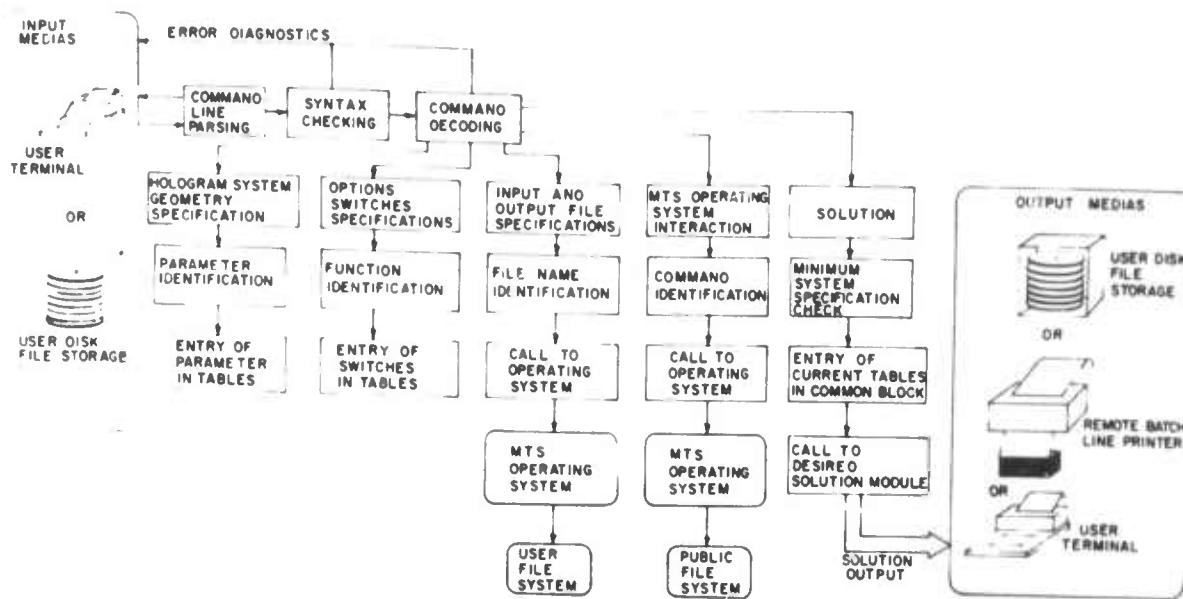


Figure 5. HOAD Program Control Module

The program user may specify any of the five general classes of commands:

- a) system parameters or variables
- b) options
- c) files
- d) MTS
- e) solutions

In (a) the input may include both data for the hologram or optimization module. As with any optical analysis and design program the user has a set of options he may select. Examples in the case of HOAD include the method of image determination, selection of output data, etc. The file related commands allow the user to direct output to a file or request input from a file. The end goal of the program is to provide the user with a solution to his problem. Be it analysis or design this is requested by the SOLVE command. The output can be directed to various devices or files. Upon completion of the solution, control is returned to the command level.

The optimization module is shown in Fig. 6. The parameters which are passed to this module include a table of variables, their initial values, the range over which they can vary, and a selection of merit function and search method. Upon entry to the module the variables are initialized and the hologram

module is called for an initial solution. These programs are also written in a modular fashion so that additional merit functions and search methods can be incorporated quite easily. When the program proceeds to the search method the selected technique essentially takes over control of the programs by making repeated calls to the hologram module and calculating the merit function selected earlier. The search method library presently includes four methods, however, others can be added quite easily. One of the parameters in the initial call to the optimization method is a count of the number of steps permitted. The number of iterations will not exceed this value. Further, if the program user finds that the optimization is not reaching a satisfactory conclusion he can abort the design by simply hitting either the break or attention key at the terminal. The programs then return to the command level. When the search is completed the best result is placed into the common block and the tables. The optimization module provides a flexible environment in which to access and vary virtually any variable in the system and evaluate the performance of the system using whatever merit function is required.

With a program as large as HOAD it can be quite difficult to locate an error. From a user's viewpoint it is also quite convenient to have an indication where an error has occurred.

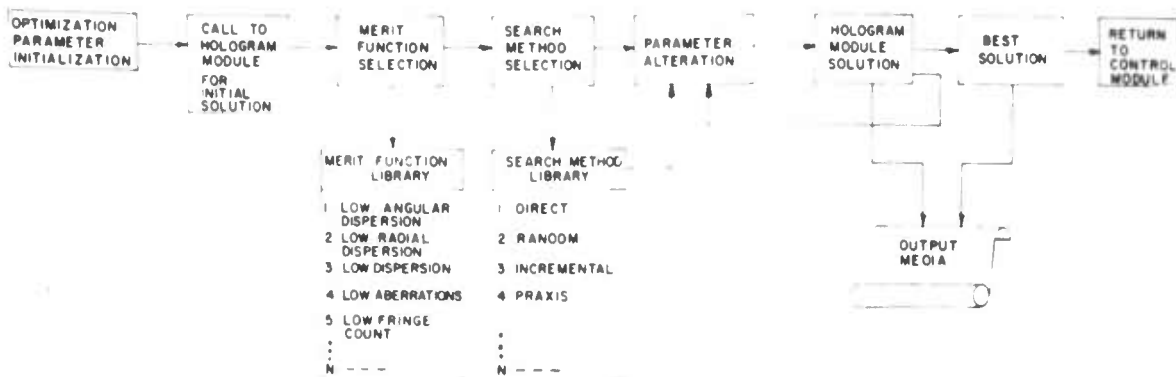


Figure 6. HOAD Program Optimization Module

In our experience such information can readily lead the user to suspect a specific type of input error. To implement a traceback facility we have included a first in last out stack within the total HOAD program. This stack is accessible by every subroutine and is best illustrated with Fig. 7. At entry to the subroutine the stack is pushed down with a unique code which designates the particular routine currently being processed. If, in this routine, another routine is called it will also enter the stack. Upon exit the stack is pushed up and the code for the specific module is erased from the stack. Thus, if an abort should take place within a module, one only need examine the stack to determine all the modules called to reach the specific routine which aborted. We have found this technique introduces only a small overhead and in return it provides a valuable diagnostic tool for both the program user and developer.

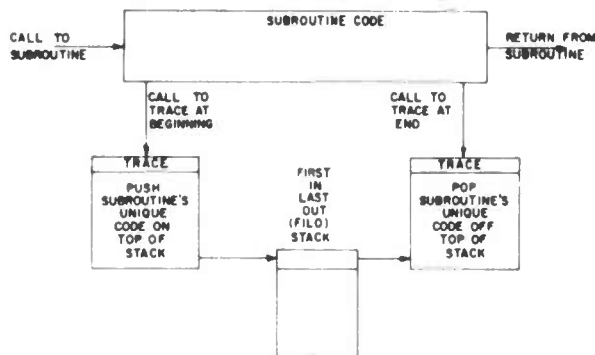


Figure 7. Subroutine Tracing Technique

As illustrated in an earlier description the attention interrupt feature of the HOAD programs provides a means for the user to have complete control. This, however, is only implemented by using system level routines in MTS and non-standard FORTRAN returns. Figure 8 illustrates the process by which these techniques are implemented. In (a) the HOAD programs initiate a call to MTS to request that when any interrupt occurs that the transfer of control be directed to a designated location. This call to MTS takes place early in the main line control program. When an interrupt occurs MTS intercepts the break in processing and returns control to the interrupt handling code originally designated in (a). As part of the interrupt handling module the traceback routine is called to examine the first-in-last-out stack. This provides data on where the interrupt occurred. The processing step is shown in d) where the interrupt trap shown in (a) is reestablished in the event another interrupt should occur. The final step is shown in e) where control is returned from the interrupt handling code to the control module. This concept of interrupt handling provides the user with full control of his analysis and design session from the terminal.

HOAD Program Usage

Up to this point the discussion has largely centered on the implementation details and little on the actual user interface to the program and its usage. We will now direct our attention to this area. Rather than discuss

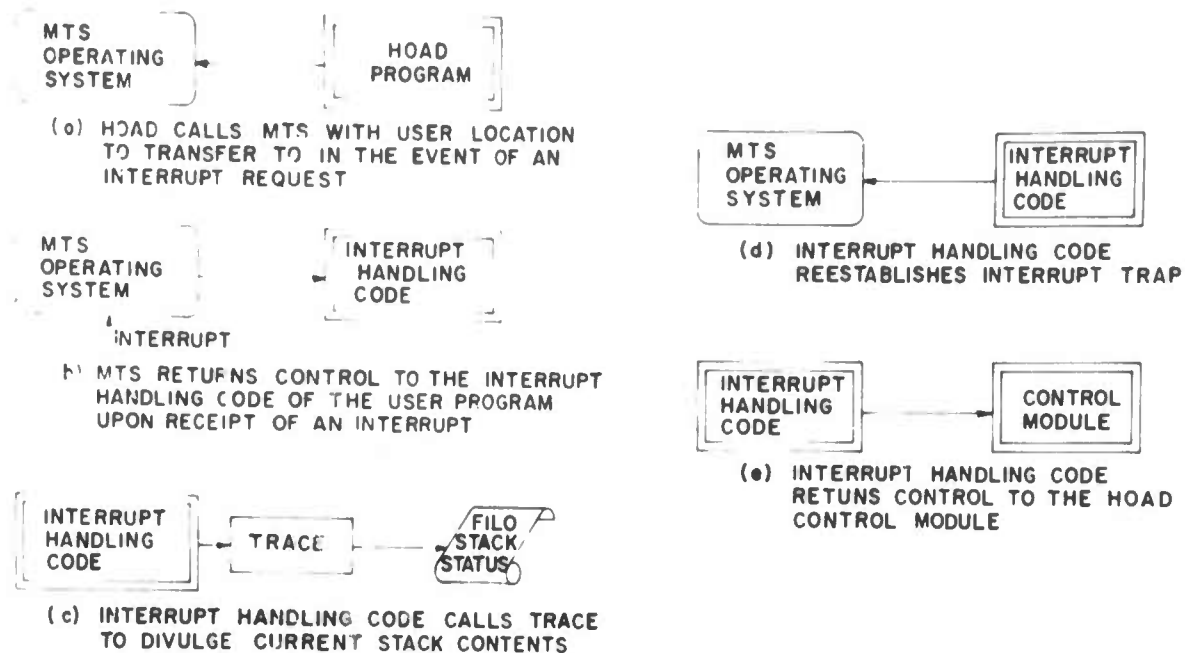


Figure 8. Interrupt Handling in MTS and the HOAD Program

the various program commands in detail here we have included a summary of them in an appendix.

To illustrate the correspondence between an element and its input description let us first consider Fig. 9. Shown here is an infrared optical element which is designed to operate with a wavelength shift from $\lambda_0 = 5145 \text{ \AA}$ to $\lambda_C = 1.06 \mu$. In other words, this element is constructed using an argon laser wavelength and reconstructed using a NdYAG laser. The parameters used to specify the system follow Champagne (Ref. 15) and Latta (Ref. 16). These are summarized in Table 2. All dimensions as input to the program are in meters. A list of the input commands for this system is given in Table 3.

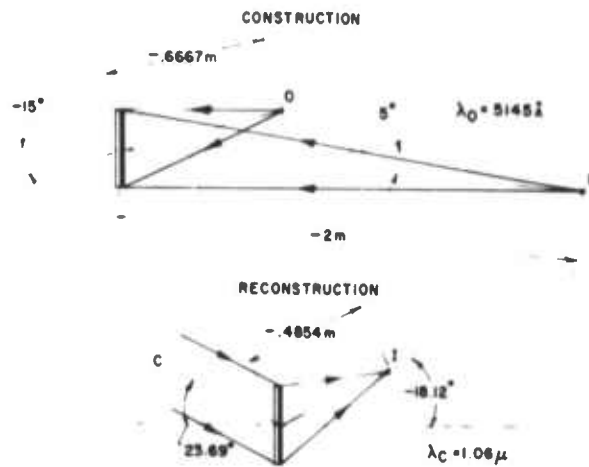


Figure 9. Infrared Optical Element

Table 2. Infrared Optical Element Parameters

CONSTRUCTION	RECONSTRUCTION
$\alpha_0 = -15^\circ, R_0 = -.6667\text{m}$	$\alpha_C = 23.691^\circ, R_C \rightarrow \infty$
$\alpha_R = +5.0^\circ, R_R = -2.00\text{m}$	$\alpha_I = -18.119^\circ, R_I = -.485\text{m}$
$\lambda_0 = 5145 \text{ \AA}$	$\lambda_C = 1.06 \mu$
$D = .1016 \text{ m}$	$D = .1016 \text{ m}$

Table 3. Infrared Optical Element Input Description to the HOAD Program

```

REC A 23.691 P
LAMC .1060D-05
HOL 1
OBJ A -15. R -.667 D
REF A 5. R -2. D
LAMO .5145 D-06
DIA .1016
ORDER -1
FAN PTS 21
FAN PTS 21 THETA 90
    
```

One of the primary objectives of these programs is to make the input as closely related to the actual parameters as possible. This can be seen by comparing tables 2 and 3. For example, the reconstruction beam is simply specified as REC and a trailing list of those parameters associated with it. There are default assignments also which ease the input task. In this case $\beta_0 = 0^\circ$ is assumed because no input was specified. The general rule to follow is that a qualifier proceeds the specification of a variable. In the case of the object beam A for α proceeds -15 for $\alpha_0 = -15^\circ$ and likewise R in front of .6667 for $R_0 = .6667$ m. Also included on the three commands which specify beams, i.e., O, R, and C, are trailing modifiers P and D. These are from the set where P and M are for plane waves that come from plus and minus infinity respectively and D and C which represent spherical wavefronts which are diverging and converging. The command HOL 1 simply indicates that the next set of commands applies to the first hologram. The ORDER -1 is used because this is a hologram which is backward illuminated as can be seen in Fig. 9. The two fan commands set up two sets of fans on the surface of the hologram which are along the y-axis ($\theta = 0^\circ$) and x-axis ($\theta = 90^\circ$). The DIA command applies for both construction and reconstruction. When the input shown in Table 3 is used the output illustrated in Fig. 10 results. The output, however, can only be generated once a SOLVE RAY command is issued. This output example is quite simple and illustrates two aspects. The

first is an echo of the input data and the second is the output which was calculated by the program. The output includes both the image location denoted by beam I and the aberration. The two tables of coordinate and actual are a listing of the wavefront aberrations associated with each ray in the two fans for the image point given earlier. The two measures of aberration indicate the relative performance of the system. The one which we use most frequently is DELTA G or the maximum to minimum wavefront deviation from the reference sphere. One option which can be included in the output is a curve fit to determine the contribution of the various aberrations at this image point.

This example represents approximately the simplest level of analysis that can be required of the HOAD program. Let us now move on to a more complex system. Consider Fig. 11 which illustrates a three element 5X holographic optics telescope. The system parameters are described in Table 4 and the corresponding HOAD program input in Table 5. This system differs from the previous one in that multiple elements are present. These elements are indicated by a SEP command for separation. We again use the α , β , R coordinate system. In this case α_{12} is the angle from hologram 1 to 2. Note that from hologram 2 to 3 that there is an Euler angle β of -24.877° . This is also shown in Fig. 11. Our Euler angle geometry follows that of Korn and Korn (Ref. 17).

The input or command decoding portion of the control module in the HOAD program is essentially an interpreter. Thus, each command is read one at a time. Little in the way of rules are imposed on the input other than to follow the command syntax. For example, a numerical value may be specified as integer or floating point and it is automatically converted to the proper format. The input format is free form and the values may occur any place within a command. Blanks have no meaning except for the HEAD command. In addition, HOL 2, for example, may be specified before HOL 1. The only condition is that HOL 1 be eventually specified before issuing a SOLVE command. Within any given input set, any command may be multiply specified and the last value is always used.

Reproduced from
best available copy.

HOLOGRAM NUMBER = 1, HOLOGRAM TYPE = TRANSMISSION, HOLOGRAM ORDER = -1

HOLOGRAM SHAPE = ROUND, DIAMETER = 1.160000E-01

BEAM	ALPHA	BETA	R	X	Y	Z	C,D,+,-
O	-15.000000E-01	0.0					
R	0.000000E-01	0.0	-0.067000E-01	1.7554457E-01	0.0	-6.45522748D-01	E
C	23.691000E-01	0.0	-2.000000E-01	-1.75311465E-01	0.0	-1.5523540E-01	D
I	-16.11945794E-01	0.0	0.0	0.0	0.0	0.0	+
			-4.6540221E-01	1.50556487E-01	0.0	-4.6133259D-01	C

WAVELENGTH (O,R) = 5145.000000D-10, (C,I) = 1060.000000E-06

RECONSTRUCTION = REAL IMAGE

TOTAL RMS WAVEFRONT DEVIATION = 6.3294653528390420E-01

TOTAL WAVEFRONT DEVIATION FROM REFERENCE SPHERE (DELTA G) = 2.5919453907176590E-01

FAN NUMBER = 1. FIRST RAY IN FAN HAS THE FOLLOWING PARAMETERS
 X = 8.20202362E-04, Y = 5.05207020E-04, Z = -2.50575100E-03
 L = 3.09352417D-01, M = -1.04216122D-01, N = -9.45206500E-01

COORDINATE	ACTUAL
5.0524659D-C2	1.5270001D-C0
4.5540595E-C2	5.9542851E-C1
4.0533540D-C2	0.15222351E-C1
3.5526228E-C2	3.5456175E-C1
3.0450158D-C2	1.86052622E-C1
2.5373954D-C2	6.53179112D-C2
2.0306654E-C2	3.15410354E-C2
1.5224365D-C2	7.65410645E-C3
1.01563312E-C2	1.87525253E-C4
5.07575157D-C3	-4.35520545D-C4
5.81507767E-17	0.0
-5.07575157D-C3	-4.35520545D-C4
-1.01563312E-C2	1.87525253E-C4
-1.5224365D-C2	7.65410645E-C3
-2.0306654E-C2	3.15410354E-C2
-2.5373954D-C2	6.53179112D-C2
-3.0450158D-C2	1.86052622E-C1
-3.5456175E-C2	3.54561759E-C1
-4.0533540D-C2	0.15222351E-C1
-4.5540595E-C2	5.9542851D-C1
-5.0524659D-C2	1.52700021D-C0

FAN NUMBER = 2. FIRST RAY IN FAN HAS THE FOLLOWING PARAMETERS
 X = 4.79722612E-02, Y = 0.0, Z = 1.50154706E-02
 L = 2.12244662E-01, M = 0.0, N = -9.7721655E-01

COORDINATE	ACTUAL
4.97075856D-C2	-1.45570287D-C0
4.46212176E-C2	-1.0815154E-C0
3.95578334E-C2	-7.6935614E-C1
3.45185078E-C2	-5.17388936D-C1
2.95042800D-C2	-3.225625E-C1
2.45181570D-C2	-1.81426755D-C1
1.9551125E-C2	-1.62653440E-C2
1.46220876D-C2	-2.97640527D-C2
9.71798641E-C3	-3.07277921E-C3
4.84567923D-C3	3.45156255E-C3
5.81507767E-17	0.0
-4.81225358E-C3	-3.45140676D-C3
-5.59432252E-C3	3.06361154E-C3
-1.4334831D-C2	3.4373835D-C2
-1.90530511D-C2	3.46796631E-C2
-2.37323605D-C2	1.94570934D-C1
-2.83768639D-C2	3.43519456E-C1
-3.29699390D-C2	5.47190366D-C1
-3.75550566D-C2	6.11530029D-C1
-4.20557510D-C2	1.14049204E-C0
-4.6455559D-C2	1.53624252D-C0

Figure 10. Sample HOAD Program Output

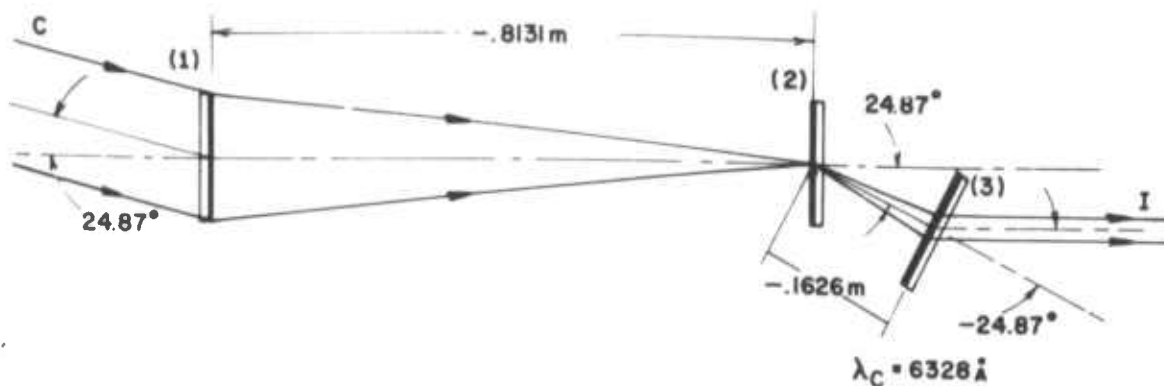


Figure 11. Three Element 5X Telescope

Table 4. Three Element 5X Holographic Optics Telescope Parameters

Hologram 1	Hologram 2	Hologram 3
$\alpha_0 = 0^\circ, R_0 = -1 \text{ m}$	$\alpha_0 = 0^\circ, R_0 = .4 \text{ m}$	$\alpha_0 = 0^\circ, R_0 = .2 \text{ m}$
$\alpha_R = 20^\circ, R_R \rightarrow \infty$	$\alpha_R = 20^\circ, R_R = 4 \text{ m}$	$\alpha_R = -20^\circ, R_R \rightarrow \infty$
$\lambda_0 = 5145 \text{ \AA}$	$\lambda_0 = 5145 \text{ \AA}$	$\lambda_0 = 5145 \text{ \AA}$

SYSTEM

$$\alpha_{12} = 0^\circ, R_{12} = -.81305 \text{ m}$$

$$\alpha_{23} = 24.877^\circ, R_{23} = -.16261 \text{ m}$$

$$\beta = -24.877^\circ$$

$$\lambda_C = 6328 \text{ \AA}$$

Consider a more representative example of the use of HOAD in Fig. 12. This is an output from a terminal session. We notice a series of 0* and 1* at the beginning of a line. These are known as the prompting characters sent by MTS to the terminal to indicate MTS is ready for input. A typical character is a # or \$ sign. However, for the HOAD program we chose to modify this character and to use the current hologram number. In this manner the program user always knows what elements he is specifying parameters for. As can be seen following the SOLVE RAY command, the output example shown in Fig.

10 can be suppressed. In the example shown here, the values of interest were simply requested with a display command. The image parameters are shown and then the aberrations present in the image. An interesting example of the use of an MTS function from the HOAD program is shown when the command

MTS /DISPLAY COST/

is given. The portion of the command DISPLAY COST is then issued to MTS and then control is returned to HOAD. The cost shown here is for the complete terminal

Table 5. Three Element 5X Holographic Optics Telescope Input Description to HOAD

```

REC A 24.877, P
LAMC 0.6328D-06
HOL 1
OBJ A .0, R -1., D
REF A 20., M
LAMO 0.5145D-06
DIA .1016
SEP A .0, R -.81305
ORDER -1
HOL 2
OBJ A .0, R .35, D
REF A 20., R 4., D
LAMO 0.5145D-06
SEP A 24.877, R -.16261
EULER B -24.877
ORDER -1
HOL 3
OBJ A .0, R .2, D
REF A -20., P
LAMO 0.5145 D-06
ORDER -1
FAN PTS 21
FAN PTS 21, THETA 90

```

section up to this point and includes the loading of the HOAD program. The next set of commands down to OUT illustrate the use of the MTS file structure. In this example we have simply emptied a file on this ID known as PRINT. The output from HOAD is then directed to PRINT by the OUT /PRINT/ command. To put data into the PRINT file we simply issue a command DISPLAY IMAGE, ABER. To examine the output an MTS command LIST PRINT is issued and the results are then listed. In the next section of the run we illustrate an example of an optimization using only one variable with a direct search and merit function for low aberrations. The command REC A ... requests that the variable α_C be varied from a lower bound of -20° to an upper bound of -5° . When the MERIT

command is given we request FUNC 4, i.e., low aberrations, and with only 20 steps and a direct, i.e., DIR, search procedure. The table which results after the SOLVE OPT command shows in the first column the merit function value, in this case $|\Delta_G|$, and then the variable or variables which are being changed by the optimization technique. When either a specified level of performance is reached or the number of steps permitted is exceeded the optimization procedure stops. At the end of the run the best evaluation is printed out. As a last exercise we request that the output be sent to PRINT. Then a SOLVE RAY command is issued. We should be careful to note that since the completion of the optimization run the variables now resident in the common blocks are those of the best optimization solution. Thus, by giving the command SOLVE RAY a complete analysis is performed on the best system that resulted from the optimization command. This command then issues a set of MTS commands to direct the contents of the file delimited by /.../ to the station. These examples illustrate the relative ease with which the programs can be used. It is difficult to provide any type of exhaustive example because the number of possibilities is virtually infinite. What we have attempted here is an overview of the typical kinds of problems that can be solved.

Comments and Conclusions

The HOAD program has proved to be an extremely valuable tool in the design of holographic optics systems. Earlier versions used the conventional FORTRAN approach of fixed field inputs with typical FORMAT statements. The numerical results from using such a program are essentially the same as the current version of the HOAD program. However, the difference in productivity is very significant. We find that very productive terminal sessions up to four hours can readily be experienced. This is the total time that the program resides in virtual memory and is in use by the designer. On the basis of our experience with this version and the earlier fixed field version, the additional cost overhead is minimal. From our vantage point the added cost of the CONTROL module to implement a flexible interpreter of commands is insignificant compared to the marked increase in productivity.

THE ENVIRONMENTAL RESEARCH INSTITUTE OF MICHIGAN
HOLOGRAM RAY TRACING PROGRAM

```

PLEASE ENTER COMMANDS -
C> LANC 6, 100L-7
C> RAY A -10, F
10 LANC 5, 105L-7
10 QW A 0, R -1, D
10 RIB A -10, B
10 ORAN -1
10 DIA .5016
10
10 PAB PAB 21
10 PAB PAB 20, ITS 21
10 SWIT TIME, RIB, CFAL
10
10 SOLVE RAY
10
10 DISPLAY IMAGE
IMAGE# A=0.22854D C1 B=0.0          R=-.81240D C0 C
10
10 DISPLAY ABERRATIONS
TOTAL 3RD ORDER ABERRATIONS* S= 8.6658E-01 C= 1.2478E 01 A= 3.99549D 00
TOTAL WAVEFRONT DEVIATIONS* PWE= 2.15115D C0 C= 1.22263E 01
10
10 WTE (/DISPLAY COST/
*DISPLAY COST
*COST = 81.42
10
10 WTE (/EMPTY PRINT OK/
*EMPTY PRINT OK
*OK=1.
10
10 OUT /PRINT/
10 DISPLAY IMAGE, AMBER
10 WTE (/LIST /RIBS/
*LIST /RIBS/
. 1 IMAGE# A=0.22854D C1 B=0.0          R=-.81240D C0 C
. 2 TOTAL 3RD ORDER ABERRATIONS* S= 8.6658E-01 C= 1.2478E 01 A= 3.99549D 00
TOTAL WAVEFRONT DEVIATIONS* PWE= 2.15115D C0 C= 1.22263E 01
*END OF FILE
10
10 OUT
10 /END MA WILL INITIALIZE GR MAC. A FOR RIB. ABERRATIONS/
10
10 RIB A, LON -2, UP -5
10 RIBS PWB 4, STEPS 20, DIA
10
10 SOLVE OPT
INITIAL EVALUATION OF FUNCTION
1.22263E 01 -1.0000E 01
BEGIN EFFECT SEARCH
1.1700E 01 -1.0100E 01
1.1710E 01 -1.0200E 01
1.1720E 01 -1.0300E 01
5.0714D 00 -1.0600E 01
2.5461E 00 -1.0700E 01
4.2741E 00 -1.1400E 01
4.5267D 00 -1.1500E 01
3.4832D 00 -1.2400E 01
2.5462D 00 -1.2500E 01
1.1710E 01 -1.2600E 01
2.4412E 00 -1.2800E 01
1.5474E 00 -1.2700E 01
1.5707E 00 -1.2400E 01
8.5434D-01 -1.2300E 01
8.5434D-01 -1.2300E 01
3.5000E 00 -1.1700E 01
2.5462E 00 -1.2500E 01
2.5462E 00 -1.2500E 01
2.5462E 00 -1.2500E 01
2.5462E 00 -1.2500E 01
*END EVALUATION OF FUNCTION
8.5434D-01 -1.2300E 01
10
10 DISPLAY IMAGE, AMBER
IMAGE# A=0.68049D C2 B=0.0          R=-.81240D C0 C
TOTAL 3RD ORDER ABERRATIONS* S= 8.25317D-01 C= 3.7510E-02 A= 1.68400D-02
TOTAL WAVEFRONT DEVIATIONS* PWE= 3.22674E-01 C= 8.28875D-01
10
10 OUT /PRINT/
10 SWIT RAY
10 SOLVE RAY
10
10 PRINT /PRINT/
*SET "PRINT"
**PRINT* ASSIGNED RECEIPT NUMBER 63576
*READY.
*SCALE *RIBS* ROUTE=BRIN
**PRINT *PRINT*
*END.
**PRINT* 63576 RELEASABLE, 5 PAGES
10 ERASE ALL
C> END
**FUNCTION TERMINATED

```

Figure 12. Sample Terminal Session Using the HOAD Program

We feel that in a program as complex as a major optical analysis or design system the designer and user must be taken into account. In fact, the program design and implementation for ease of use should play a critical role in the overall system development.

As with any large program it is never finished. One can ask where does HOAD go from here? This can best be stated by discussing a few of the current version's

limitations. First, conventional optics are not explicitly treated. They can be included in an analysis by setting the hologram order to zero. However such a technique is indirect at best. The next major revision must include the full range of conventional optics. The coordinate system transformations can also be improved. Presently a hologram is specified from one element to the next. Any future revisions should include the ability to assign arbitrary reference coordinate systems which are either local or global. Additional improvements can also be made in the areas of aberrations, spot diagrams, pupils, transfer functions, and hologram thick media.

The HOAD program is a reflection of a new aspect of optics. That is, it is an implementation of the diffractive optical element within the set of conventional optical components. We feel its potential can only be effectively explored with general analysis and design tools such as the HOAD program.

REFERENCES

1. McCauley, D. G., Simpson, C. E., and Murbach, W. J., "Holographic Optical Element for Visual Display Applications," *Applied Optics*, Vol. 12, No. 2, pp. 232-242, Feb. 1973.
2. Latta, J. N. and Champagne, E. B., "General Vector Analysis of Ray Tracing in Holography," *J. Opt. Soc. Am.*, Vol. 63, No. 4, p. 486A, April 1973.
3. Latta, J. N., "Evaluation of Hologram Optical Elements," Final Report 197400-1-F, Willow Run Laboratories, The University of Michigan, August 1973. (Available from DDC).
4. Rose, H. W., "Holographic Lens Systems," Ph.D. Thesis, Dept. of Electrical Engrg. Ohio State University, Columbus, Ohio, 1972.
5. Rose, H.W., "Broad-band Characteristics of Zone-Plate Holographic-Lens Systems," *J. Opt. Soc. Am.*, Vol. 62, No. 11, p. 1345A November 1972.
6. Kogelnik, H. "Coupled Wave Theory for Thick Hologram Gratings," *Bell System Tech J.*, Vol. 48, No. 9, pp. 2909-2947 November 1969.

7. Latta, J. N., "Holograms as Optical Elements," in Proceedings of the Engineering Applications of Holography Symposium, pp. 345-359, Feb. 16-17, 1972, Los Angeles, California, Society of Photo-Optical Instrumentation Engineers, 1972.
8. "MTS: The Michigan Terminal System," 3rd Ed., Ten Volumes, The University of Michigan Computing Center, Ann Arbor, Michigan.
9. Alexander, M., "Organization and Features of the Michigan Terminal System," AFIPS Proceedings, Vol. 40, pp. 585-591, 1972.
10. Chan, L., "Better Techniques for Developing Large Scale Fortran Programs," Proc. of 1971 Annual Conf., Association for Computing Machinery, pp. 520-537, Aug. 3-5, 1971, Chicago, Ill.
11. Latta, J. N., "Computer-Based Analysis of Holography Using Ray Tracing," Applied Optics, Vol. 10, No. 12, pp. 2698-2710, December 1971.
12. Latta, J. N. and Champagne, E. B., "Evaluation of Holographic Optical Elements in a Heads-up Display," Final Report 11057-3-F, Willow Run Laboratories, The University of Michigan, Ann Arbor, Michigan, March 1973 (AD 758 057).
13. Hopkins, H. H., "The Wave Aberration Associated with Skew Rays," Proc. Phys. Soc. B, Vol. 65, pp. 934-942, December 1, 1952.
14. Tatian, B., "A Comment on the Wave Aberration Formula of H. H. Hopkins," Optica Acta, Vol. 19, No. 1, pp. 79-83, January 1972.
15. Champagne, E. B., "A Qualitative and Quantitative Study of Holographic Imaging," Ph.D. Thesis, Ohio State University, Columbus, Ohio, July 1967, (U. Microfilms, No. 67-10876).
16. Latta, J. N., "Computer-Based Analysis of Holography," Ph.D. Thesis, University of Kansas, Lawrence, Kansas, December 1970 (U. Microfilm No., 71-27,168).
17. Korn, G. A. and Korn, T. M., "Mathematical Handbook for Scientists and Engineers," 2nd Ed., McGraw Hill, New York, 1968.

APPENDIX

The following is a list of the commands available in the HOAD program:

HEAD /< HEADING -----> /

The heading command will be printed at the beginning of the run output. If no heading is entered, the last header line entered is deleted.

LAM < >

LAMC < >

LAMO < >

When LAM is input the variable it is assigned to is determined by its context in the input group. For example if it is the first command specifying LAM the variable is assumed to be LAMC. Any occurrence of LAM within a HOL set is assumed to be LAMO for that hologram set. If LAMC or LAMO is specified it is directly assigned to the respective variables.

REC A < > B < > R < > < C,D,P,M > or X < > Y < > Z < > < C,D,P,M >

OBJ A < > B < > R < > < C,D,P,M > or X < > Y < > Z < > < C,D,P,M >

REF A < > B < > R < > < C,D,P,M > or X < > Y < > Z < > < C,D,P,M >

IMAGE A < > B < > R < > < C,D,P,M > or X < > Y < > Z < > < C,D,P,M >

IMREF A < > B < > R < > < C,D,P,M > or X < > Y < > Z < > < C,D,P,M >

SEP A < > E < > R < > or X < > Y < > Z < >

EULER A < > B < > G < >

By specifying a partial list of only one or more variables and their associated aberrations the remaining unspecified variables default to zero. Note, on those input commands requiring C,D,P, M one of these characters must appear. The parameters are:

A = alpha

B = beta

R = radial distance

X = coordinate

Y = coordinate

Z = coordinate

D = diverging source

C = converging source

P = plane wave coming from + infinity

M = plane wave coming from - infinity

The OBJ and REF commands are applied to the current hologram number, i.e. last HOL < > command. If none is present the first hologram is assumed.

POINT R < > THETA < > or X < > Y < >

FAN LFAN < > THETA < > PTS < > XCTR < > YCTR < >

ARRAY MAXX < > MAXY < > PZ < > PY < > SCTR < > YCTR < >

HEX RHEX < > PHEX < > XCTR < > YCTR < >

These commands define a set of points on the first hologram. More than one command may be used in the input. Each command is cumulative on the next. The total number of points should not exceed 100. The parameters are:

R = radial distance to center point
 THETA = angle of center point with X-axis (degrees). (default = 0)
 X = coordinate of point
 Y = coordinate of point
 LFAN = length of fan. (default = diameter of hoiogram #1)
 THETAX = angle of fan with X-axis (degrees). (default = 0)
 PTS = number of points on fan. (default = 7)
 XCTR = X coordinate of center point. (default = 0)
 YCTR = Y coordinate of center point. (default = 0)
 MAXX = length of array in X direction
 MAXY = length of array in Y direction
 PX = number of points in X direction
 PY = number of points in Y direction
 RHEX = radius of hexpolar array
 PHEX = number of points along radius including center point

HOL < >

This command indicates the hoiogram set associated with the next group of commands. It is in effect until another HOL command is entered. This command is optional only if one hoiogram is analyzed.

DIA < >

This command specifies the diameter of the current hoiogram. If no parameter is given, the default value is set.

PAGE

This command provides a skip to top-of-page on the current output device.

COMMENT / < TEXT > /

This command causes the text field to be printed on the current output device.

CDUMP

This command causes a dump of the current common blocks on the currently defined output unit.

SURFACE CC < > CV < > CR < > AD < > AE < > AF < > AG < >

This command specifies the hologram surface parameters. The command is optional with the default of zero for all parameters. The parameters are:

CC = conic constant
 CV = curvature at vertex
 CR = curvature of revolution (torics only)
 AD = 4th order aspheric coefficient
 AE = 6th order aspheric coefficient
 AF = 8th order aspheric coefficient
 AG = 10th order aspheric coefficient

If no parameters are given the default values for all parameters are set.

ORDER < +N, -N, or 0 >

This command specifies the hologram order. It is optional with the default of +1.

TYPE < TRANS OR REFL >

This command forces the hologram type to that specified. In general, it is optional as the program automatically determines the hologram type.

EULER = EULER angle parameters for current hologram
REC = reconstruction beam parameters
IMAGE = image beam parameters
IMREF = image reference beam parameters
ABER = aberrations of image for current solution
INDEX = index parameters for current hologram
EMUL = emulsion parameters of current hologram
DIA = diameter of current hologram
LAMC = reconstruction wavelength
LAMO = construction wavelength of current hologram
SURFACE = surface parameters of current hologram
ORDER = order of current hologram
TYPE = type of current hologram

SOLVE < RAY, OPT, SINGLE >

This command affects a ray, optimization or single hologram solution. If no solution type is specified, the previous solve command solution type is used. The solution type is initialized to ray upon entry of the program.

STOP

This command terminates the program and returns control to MTS. The program cannot be restarted.

END < RAY, OPT, SINGLE >

This command terminates a command reading and halts program execution after analysis of preceding commands. The program cannot be restarted. The options available are the same as for the solve command.

ERASE < OPTION > ... < OPTION >

This command permits a completely new specification for those command types given in < OPTION >. If no new specification is later given in the following input commands the default value is used. The option list may include the following:

POINT = this eliminates any previous specification of points on the first hologram with the commands - POINT, FAN, ARRAY, and HEX
OPT = all previously defined optimization parameters are deleted plus FUNC, STEPS, SEARCH TYPE, and all optimization switches
RAY = all previously defined hologram specifications are deleted. Default values are set where applicable
HEAD = erases the header lines
ALL = delete all previous specifications including POINT, OPT, RAY, and HEAD.
This command essentially resets the input for new commands.

If no options are specified, ALL is assumed.

IN / < FILENAME > /

This command initiates reading of commands from the file < FILENAME >. At an end-of-file on < FILENAME > reading returns to the first command after the file command. This command may appear anywhere in the input. Note: Any valid MTS file or subfile may be entered, e.g., IN /INFILE(1,10)/ IN /-IN/

OUT / < FILENAME > /

This command redirects all raytracing and optimization output to the file specified. If no filename is specified, the output destination will default to *SINK*. Note: Any

EMUL NB < > NA < >

This command specifies the index of refraction of the emulsion before and after processing. The command is optional and the default is EMUL NB 1.5 NA 1.5. If neither parameter is specified, both parameters are set to their default value.

INDEX N1 < > N2 < > N3 < > N4 < >

This command specifies the index of refraction for the following:

N1 = index in +Z space during construction
N2 = index in -Z space during construction
N3 = index in +Z space during reconstruction
N4 = index in -Z space during reconstruction

Default values for all variables are 1.0. If no parameters are specified, the default values for all parameters are set.

SWITCH < OPTION > ... < OPTION >

This command sets switches for program operation, the switches are as follows:

ALL = the following switches are set: CFAB, PFAIL, PSAG, PRAIN, PIMPH, PRSIN, and PHGEN

* RFAIL < > = total number of rays that may fail before abort of analysis
* CFAB = curve fit and determine aberrations
PTAB = print total aberrations only. Suppress curve fit.
NOAB = no aberration curve fit
* PFAIL = print output when rays fail
NPFAIL = no printing of output when rays fail
PSAG = print SAG data for each ray
* NPSAG = no printing of SAG data for each ray
PRAIN = print ray intercepts
* NPRAIN = no printing of ray intercepts
PIMPH = print image phase surface intercepts
* NPIMPS = no printing of image phase surface intercepts
PRSIN = print reference sphere intercepts
* NPRSIN = no printing of reference sphere intercepts
PHGEN = print hologram generation data
* NPHGEN = no printing of hologram generation data
FIMA < > = determine image from fan number < >
* AFIMAG = all fans used to determine image
* RAY = print ray trace output
* DECK = print deck output
NDECK = no deck output
SRAY = print short ray trace output
* NSRAY = no short ray trace output
* IMAGE = compute image
NIMAGE = no image computation (note: image must be defined using the 'image' command in order to compute aberrations)
DEFAULT = the following switches are set (*)
RFAIL 5, CFAB, PFAIL, NPSAG, NPRAIN, NPIMPS, NPRSIN, NPHGEN, AFIMAG.

DISPLAY < OPTION > ... < OPTION >

This command allows the user to display selected hologram parameters. The valid options are:

OBJ = object beam parameters for current hologram
REF = reference beam parameters for current hologram
SEP = separation parameters for current hologram

valid MTS file or subfile may be entered, e.g., OUT /OUTFILE (LAST +1)/
OUT /-OUT/, OUT /* PRINT*/

MTS / < MTS COMMAND > /

This command allows the user to momentarily cease execution of the program and issue an MTS command. Upon completion of the MTS command, the program is restarted in command mode. If no MTS command is entered, execution of the program will be halted and control will be returned to MTS, however the program may be restarted using the \$RESART command. Note: Any valid MTS command may be entered, e.g., MTS /\$CREATE OUTFILE/, MTS /\$EMPTY OUTFILE OK/. However, some commands, such as \$RUN and \$SIGNOFF will not return control to the program upon completion.

.PRINT / < FILENAME > /

This command will cause the file specified by < FILENAME > to be printed at the ERIM remote batch station.

D---

This command permits the deviation of one hologram set specification to another. It is formed by simply placing a "D" in front of the appropriate command. An example is DREC A -.01. Where the new reconstruction beam angle alpha is less by .01 from the previous value. To use this command its context in the original input set must be defined. For example a "LAM" command may appear anywhere in the input as "LAMC" or "LAMO". If "DLAM" alone is specified it is assumed to be "DLAMC". For example, if the command is specified after a HOL < > command such as

```
HOL 1          HOL 1
DLAM -10D-6   or   DLAMO -10D-6
```

which designates the construction wavelength for the first hologram. The following commands permit a "D" prefix: LAM, LAMC, LAMO, OBJ, REF, SURF, EMUL, INDEX, SEP, EULER, IMAGE, IMREF.

MERIT FUNC < N > STEPS < > < DIR, RAN, INC, PRA >

This command specifies the merit function to be used for the optimizations where N corresponds to the merit function number as listed below. This function is selected from the library. The library includes the following:

- 1 LAD = low angular dispersion
- 2 LRD = low radial dispersion
- 3 LD = low angular and radial dispersion
- 4 LA = low aberration
- 5 LDSR = low dispersion with solve for RO2
- 6 LD2 = special low angular and radial dispersion
- 7 LDME = low dispersion with modification of EULER angles
- 8 LASR = low aberrations over a band and solve for RR
- 9 LDR3 = three element solve for RO3 and low dispersion
- 10 PD = parameter determination
- 11 LFNG = low fringe count minimization
- 12 CVAB = curved surface aberrations

The steps parameter specifies the number of iterations to be performed in the optimization before control is returned to the user. The search type parameter selects one of the following search procedures -

- DIR = direct search
- RAN = random search
- INC = incremental search
- PRA = praxis search

MSWITCH RAY < > DECK < > LIST < > MERIT < > DEFAULT

This command selects the various merit function switches. The options include:

- RAY = N generate no ray tracing program output
- = E generate ray tracing program output on every iteration
- = I generate ray tracing program output at initial evaluation
- = B generate ray tracing program output at best evaluation
- = IB generate ray tracing program output at initial and best evaluation
- DECK = N generate no output deck
- = E generate output deck on every iteration
- = I generate output deck at initial evaluation
- = B generate output deck at best evaluation
- = IB generate output deck at initial and best evaluation
- LIST = N generate no parameter list output
- = E generate parameter list output at every evaluation
- = I generate parameter list output at initial evaluation
- = B generate parameter list output at best evaluation
- = IB generate parameter list output at initial and best evaluation
- MERIT = N no output from merit function
- = E output from merit function at every evaluation
- = I output from merit function at initial evaluation
- = B output from merit function at best evaluation
- = IB output from merit function at both initial and best evaluation
- DEFAULT = RAY, DECK and MERIT are set to N, LIST is set to E

< VARI > BEGIN < > LOW < > UP < > < LOG OR LIN > DR < > FR < > INCR < >

This command specifies the variable to be changed in the optimization. The list of variables < VARI > include the following:

OBJ A, OBJ B, OBJ R,
REF A, REF B, REF R,
REC A, REC B, REC R,
SEP A, SEP B, SEP R,
EULER A, EULER B, EULER G,
IMAGE A, IMAGE B, IMAGE R,
IMREF A, IMREF B, IMREF R,
LAMC, LAMO, SURF CV,
SURF CC, SURF CR, SURF AD,
SURF AE, SURF AF, SURF AG

Note: OBJ, REF, SEP, EULER, LAMO and SURF are hologram dependent and as such will use the last HOL command hologram number.

The parameters on the command are as follows:

BEGIN < > = initial value for the variable < VARI >. If not specified the default is the current value of < VARI >:

LOW < > = lower limit that is permitted for the variable < VARI >

UP < > = upper limit that is permitted for the variable < VARI >

< LOG OR LIN > = for incremental or random searches this variable denotes the mode.

DR < > = in a direct search this parameter assigns the initial value for delta

FR < > = in a direct search this parameter assigns the final value of delta. If FR is equal to delta, the search process is terminated

INCR < > = in an incremental search this parameter specifies an increment value for this variable.

REFERENCES

1. Latta, J. N., "Evaluation of Hologram Optical Elements," Final Report 197400-1-F, Willow Run Laboratories, The University of Michigan, August 1973. (Available from DDC).
2. Champagne, E. B., A Qualitative and Quantitative Study of Holographic Imaging, Ph.D. Thesis, Ohio State University, Columbus, Ohio, July 1967 (Univ. Microfilms No. 67-10876).
3. Latta, J. N., Computer-Based Analysis of Holography, Ph.D. Thesis, The University of Kansas, Lawrence, Kansas, December 1970.